TNO-report

97-CMC-R0290

SHOCK TRANSMISSION, RESPONSE CALCULATION OF A COMPARTMENT OF A FRIGATE WITH DISCRETE MASSES AND RAYLEIGH DAMPING

TNO Building and
Construction Research

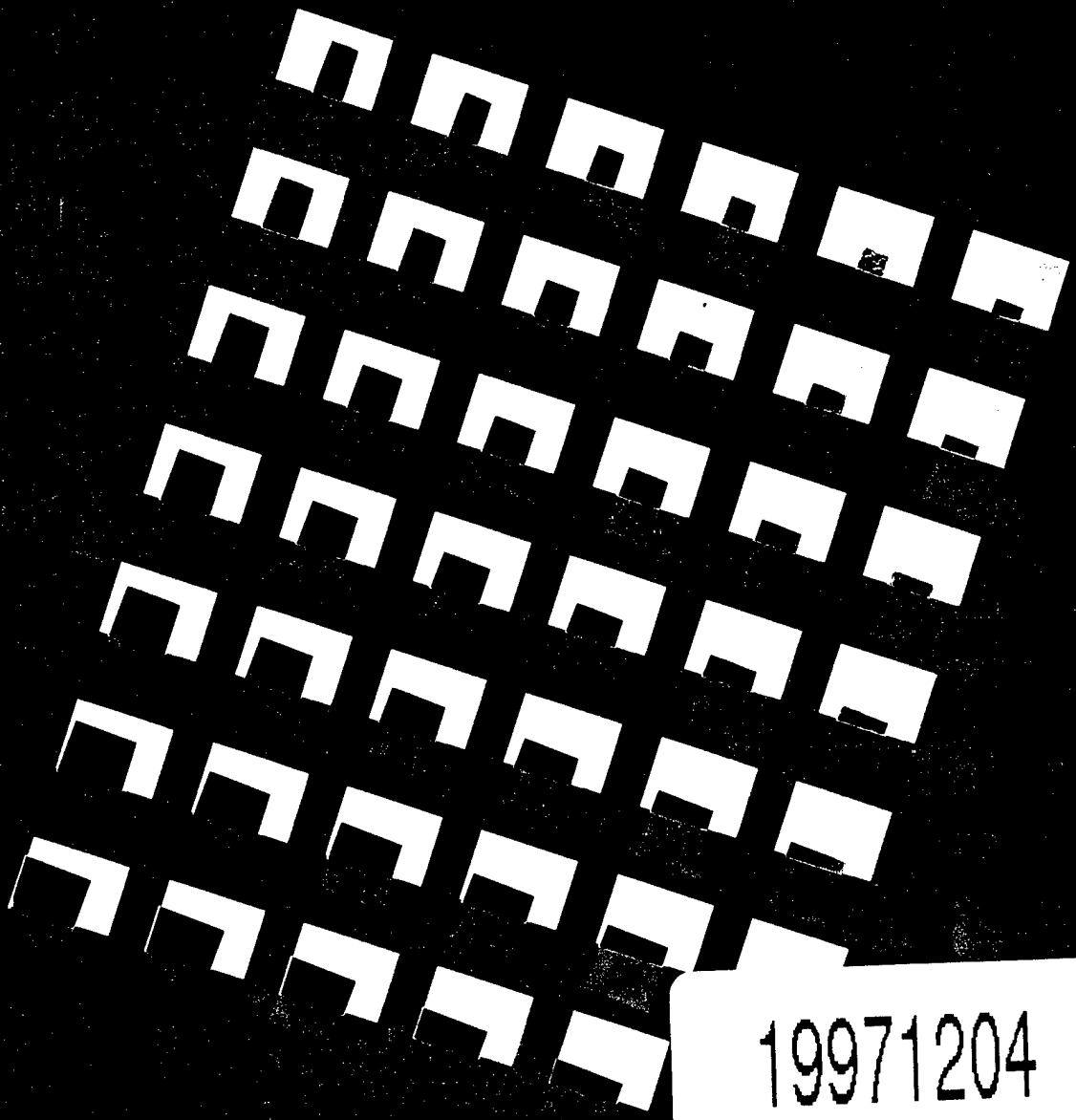

TNO

ONGERUBRICEERD

TNO-report

97-CMC-R0290

SHOCK TRANSMISSION, RESPONSE CALCULATION OF A COMPARTMENT OF A FRIGATE WITH DISCRETE MASSES AND RAYLEIGH DAMPING

TNO Building and Construction Research

Lange Kleiweg 5, Rijswijk
P.O. Box 49
2600 AA Delft
The Netherlands

Phone +31 15 284 20 00
Fax +31 15 284 39 90
Telex 38270

Date 3 July 1997

Author(s) ir. W. Trouwborst

Sponsor: Ministry of Defence
Directie Materieel Koninklijke Marine
Afdeling Maritieme Techniek
Postbus 20702
2500 ES 's-Gravenhage

Monitoring agency: TNO Defence Research

Security Classification
Classified by : ir. T.N. Bosman
Classification date : 11 April 1997

Title : ONGERUBRICEERD
Managementuittreksel : ONGERUBRICEERD
Report text : ONGERUBRICEERD
Figures : ONGERUBRICEERD

The classification designation 'ONGERUBRICEERD' is equivalent to 'UNCLASSIFIED'.

Project name : Shock transmission
Project nr. : 62375617 - A95/KM/117
Approved : ir. R. Regoord
Visa : ir. G.T.M. Janssen

Pages : 92 (incl. figures, excl. RDP & distribution list)

ONGERUBRICEERD

Netherlands Organization for Applied Scientific Research (TNO)

TNO Building and Construction Research provides a comprehensive research and development service specifically geared to the needs of the construction and engineering industry.

The Standard Conditions for Research Instructions given to TNO, as filed at the Registry of the District Court and the Chamber of Commerce in The Hague, shall apply to all instructions given to TNO.

MANAGEMENTUITTREKSEL

Titel : Shock transmission, response calculation of a compartment of a frigate with discrete masses and Rayleigh damping

Auteur : W. Trouwborst

Datum : 3 Juli 1997

Opdrachtnr. : A95/KM/117

Rapportnr. : 97-CMC-R0290

Het doel van dit onderzoek is om na te gaan of aanstoting van een scheepsconstructie met de snelheidspuls zoals die volgt uit het 'kick-off velocity' concept resulteert in dekresponsies die redelijk voldoen aan de standaardpulsvormen zoals gedefinieerd in het Shock Handbook. Uit eerdere berekeningen bleek deze overeenstemming vrij slecht te zijn. Het gebruikte model bestaat uit een kwart van een compartiment van een fregat met symmetrie randvoorwaarden, met drie dekken (F-, G- en H-dek). Berekeningen zijn uitgevoerd met het eindige-elementen programma DIANA. Als belasting is de 'kick-off' puls zoals bepaald met het programma SWISS aangebracht op de halve diepgang van het fregat.

Dit rapport geeft de resultaten van onderzoek naar mogelijke oorzaken van de eerder gevonden verschillen tussen de berekende dekresponsies en de standaard pulsvormen. Hiertoe is het bij de voorgaande berekeningen gebruikte model als volgt aangepast:

- de equivalent verdeelde massa's voor de dekken zijn vervangen door discrete puntmassa's op een steek van 1.2 m, gedeeltelijk verend opgesteld (met demping), en gedeeltelijk vast opgesteld.
- Rayleigh demping (4 - 8 procent van de kritische demping) is ingevoerd in de constructie.
- aanstoting door de kick-off puls vindt nu alleen op het schot plaats, en niet op de huid.

Daarnaast zijn berekeningen uitgevoerd voor analyse van de effecten van de afzonderlijke modelwijzigingen en met andere waarden voor de Rayleigh demping.

De belangrijkste conclusie is dat de dekresponsies nu verrassend goed overeenstemmen met de standaardpulsvormen, voornamelijk veroorzaakt door de op veren gemonteerde discrete massa's in plaats van equivalent verdeelde massa's, en door de Rayleigh demping. Demping van de veren en aanstoting van de huid hebben nauwelijks effect. Vast gemonteerde discrete massa's resulteren in een slechtere overeenstemming. Een en ander wordt uiteraard wel bepaald door (verhoudingen van) stijfheden en massa's van de afzonderlijke dekdelen.

TABLE OF CONTENTS

LIST OF SYMBOLS

a_0, a_1	Rayleigh damping coefficients	
c	Damping	[Ns/m]
c_{cr}	Critical damping	[Ns/m]
c	Velocity of sound	[m/s]
C_x	Damping matrix	
E	Young's modulus	[N/m^2]
I	Unit matrix	
k	Stiffness	[N/m]
K_x	Stiffness matrix	
m	Mass	[kg]
M_x	Mass matrix	
t	Time	[s]
v	Velocity	[m/s]
ξ_i	Modal damping coefficient of eigenmode i	
Ξ	Diagonal matrix of ξ_i	
Φ	Matrix with eigenmodes	
ρ	Density	[kg/m^3]
ν	Poisson's ratio	
ω_i	Eigenfrequency of eigenmode i	[1/s]
Ω	Diagonal matrix of ω_i	

1. INTRODUCTION

The aim of this project is to investigate whether the deck responses as calculated using a finite element model of a compartment of a frigate, excited by a pulse as derived from the kick-off velocity concept, do fit within the standard pulse shapes as defined in the Shock Handbook (ref. [3]). In ref. [1], these analyses were carried out using the maximum allowable deck masses (equally distributed). It was found that quite large differences occurred between the calculated deck responses and the standard pulse shapes. Therefore, in ref. [2] these analysis were repeated using more realistic deck masses (approximately one third of the maximum allowable deck masses, still equally distributed). Stresses were also investigated in ref. [2]. These stresses were considerably larger than the yield stress, and therefore analyses were carried out including plasticity for the material model. Due to full yielding of the flanges of the stiffeners, a failure to converge occurred, or in other words, the structure showed a plastic collapse.

This report gives the results in case that some other physical effects are included in the model, such as (Rayleigh) damping and discrete deck masses (either mounted on springs or fixed) in stead of equally distributed masses. Chapter 2 discusses the modifications of the model, chapter 3 gives the results for the modified model, chapter 4 gives results of some additional analyses to investigate the largest effect on the responses. Finally, in chapter 5 results are discussed for both the modified model and the original model from ref. [2], both for different values of the Rayleigh damping coefficients, and chapter 6 discusses the propagation of the shock wave for the three decks.

2. DESCRIPTION OF MODIFIED MODEL

2.1 Model description

First some general (unchanged) quantities of the model will be summarized (see ref. [1] for an extensive model description):

- length of the compartment is equal to 14.4 meter.
- maximum breadth of the compartment is equal to 18.8 meter, at G-deck.
- height of the compartment is equal to 13.2 meter.
- model describes one quarter of the compartment with symmetry conditions.
- hybrid model using plate elements and beam elements. Beam elements are used for the HP-profiles in length direction, for the flanges of the heavy stiffeners in length direction and for the flanges of the hull stiffeners and the deck stiffeners within the cross section of the compartment.
- the material model used is linear elastic.

In ref. [1], the maximum allowed masses on the decks (500 kg/m^2, 1000 kg/m^2 and 700 kg/m^2 for F-, G- and H-deck respectively) were incorporated within the model using a modified density for the plate elements of the decks, resulting in a total mass of 173 tonnes. In ref. [2], an analysis was carried out for a model with more realistic but still equally distributed deck masses, such that the mass of the model (74.2 tonnes) was approximately equal to one third of the displacement. Both in ref. [1] and in ref. [2], the kick-off pulse was applied at all nodes at y=-11.17 meter, so both at the bulkhead and at the hull section of the model.

The following modifications are incorporated into the model:

- the kick-off pulse is now only applied at the nodes at y=-11.17 m at the bulkhead, and not at the hull nodes.
- the payload of the decks is now modelled by discrete masses in stead of by an increase of the density of the decks (equally distributed). The discrete masses are either mounted at springs or fixed at the deck. The total mass of the model is still 74.2 tonnes. These discrete masses are located at distances of 1.2 m, and its values are still based on deck masses of 160 kg/m^2, 310 kg/m^2 and 220 kg/m^2 for F-, G- and H-deck respectively (mass of model equal to one third of water displacement). The discrete masses have only a vertical degree of freedom. If discrete masses are mounted on springs, these springs have a damping equal to 15 percent of the critical damping, see the next section. Table 2.1 summarizes the values as used for the masses and the springs, see also fig. 2.1. In this table, the small part of a deck denotes the part between longitudinal corrugated plate and centreline, and the large part denotes the part between longitudinal corrugated plate and hull. With respect to fig. 2.1, it is noted that the discrete masses at Y=-11.17 m are unchanged with respect to the previous analyses from ref. [1] and [2], except of course for the hull part (removed, no excitation). These (extremely large) masses are used to introduce the kick-off pulse using nodal forces as function of time.

Region	Method	Mass [kg]	Spring [N/m]
Small part F-deck	Spring, 4 Hz	283.891	1.79321E5
Large part F-deck	Spring, 4 Hz	283.891	1.79321E5
Small part G-deck	Fixed	586.876	-
Large part G-deck	Spring, 6 Hz	586.876	8.34081E5
Small part H-deck	Fixed	396.554	-
Large part H-deck	Spring, 6 Hz	396.554	5.63591E5

Table 2.1 Type of mounting, masses and spring stiffnesses

- Rayleigh damping is used to model structural damping, see the next section.

2.2 Determination of damping values

Ref. [4] will be followed here to determine the Rayleigh damping, so to calculate the values a_0 and a_1 of the following equation:

$$C_x = a_0 M_x + a_1 K_x \qquad (2\text{-}1)$$

with C_x, M_x and K_x the damping matrix, mass matrix and stiffness matrix respectively. If eigenmodes Φ are normalized on the mass matrix, applying a transformation from physical degrees of freedom to modal degrees of freedom results in:

$$\phi^t M_x \phi = I \; ; \; \phi^t K_x \phi = \Omega^2 \; ; \qquad (2\text{-}2)$$

with Ω^2 the diagonal matrix with eigenvalues ω_i^2. In case of modal damping, the modal damping matrix becomes:

$$\phi^t C_x \phi = 2 \Omega \Xi \qquad (2\text{-}3)$$

with Ξ the diagonal matrix with modal damping coefficients ξ_i (as fraction of the critical damping, $\xi_i = c/c_{cr}$). Combining eq. 2-1 to 2-3 results in:

$$2 \Omega \Xi = a_0 I + a_1 \Omega^2 \qquad (2\text{-}4)$$

For an individual mode this equation becomes:

$$2 \omega_i \xi_i = a_0 + a_1 \omega_i^2 \qquad (2\text{-}5)$$

The general approach is then that for two eigenmodes the values for the eigenfrequencies and the desired damping coefficients are inserted in eq. 2-5, resulting in two equations with two unknowns,

namely a_0 and a_1. Damping coefficients for other eigenmodes are then of course determined by eq. 2-5.

For the present problem, as a first guess it was desired to have damping values of 4 to 8 percent of the critical damping. Choosing several pairs of frequencies and damping values, and solving the resulting set of equations 2-5, finally leads to the choice of frequencies of 0.5 and 60 Hz, each with a damping coefficient equal to 22 percent of the critical damping. The corresponding values for a_0 and a_1 are 1.3709 and 0.0011575 respectively. The damping coefficient as function of the frequency is shown in fig. 2.2, showing that for frequencies between approximately 1.5 and 20 Hz the damping coefficient has a value between 4 and 8 percent of the critical damping.

The discrete springs have a damping equal to 15 percent of the critical damping. According to ref. [4], the critical damping can be calculated using:

$$c_{cr} = 2\ m\ \omega = 2\ \frac{k}{\omega} = 2\ \sqrt{m\ k} \qquad (2\text{-}6)$$

A summary of damping values is given in table 2.2.

Finally, fig. 2.3 to 2.5 show the deck locations for which responses will be given. Locations A to F are unchanged with respect to ref. [1] and [2]. Additional locations are defined for the effects of the discrete masses, namely E-0, E-1 and G-0, G-1. Location E-0 and G-0 are located at the deck, so below the corresponding spring, and location E-1 and G-1 are located at the discrete mass, so above the corresponding spring.

Region	Method	Damping [Ns/m]
Whole structure	Rayleigh	$a_0 = 1.3709$, $a_1 = 0.0011575$
Small part F-deck	Spring, 4 Hz	2140.4913
Large part F-deck	Spring, 4 Hz	2140.4913
Small part G-deck	Fixed	-
Large part G-deck	Spring, 6 Hz	6637.4057
Small part H-deck	Fixed	-
Large part H-deck	Spring, 6 Hz	4484.9184

Table 2.2 Summary of damping values for the modified model

3. RESULTS FOR THE MODEL INCLUDING RAYLEIGH DAMPING

3.1 Effect of time step

For the modified model, an analysis was carried out using the current version 6.2 of DIANA (ref. [5]). It was found that the effect of the model modifications on the deck responses is quite large, and therefore a number of analyses were carried out to investigate which modification has the largest effects on the responses. However, while changing stepwise the modified model to the original model from ref. [2], the responses as calculated with version 6.2 remained different, even for the unmodified model. This was caused by a change in the required input data from version 5.2 to 6.2.

To check the responses from version 6.2, after modification of the beam eccentricity input the original model from ref. [2] has been analyzed again. Because it was desired that responses should be available for a larger end time, the effect of the time step size was also investigated. Fig. 3.1 to 3.6 show the displacements, velocities and accelerations as function of time for the original model from ref. [2] as calculated with version 6.2, for the most interesting locations B and E for all three decks, and for two different time step sizes, namely the original time step size of $2.5 \cdot 10^{-5}$ seconds as used in ref. [1] and [2], and for a time step size of $2.5 \cdot 10^{-4}$ seconds. Comparing the results for the original time step size with the responses from ref. [2] (fig. 4.2 - 4.4) shows that now indeed the responses from version 6.2 are equal to those as calculated with version 5.2. Furthermore, the results from fig. 3.1 to 3.6 show that the use of a time step of $2.5 \cdot 10^{-4}$ seconds results in a slightly lower response. The general response characteristics agree quite well and it was decided to perform all remaining analyses with the new and larger time step, thus taking advantage of a considerable decrease in CPU-times. However, one should keep in mind that the compression (forces) of low frequency shock mountings now is underestimated with some 10 percent.

3.2 Results for the modified model

Fig. 3.7 shows the deformed geometries at different time steps. Comparing these deformed geometries with fig. 3.1 to 3.3 of ref. [1], clearly show the effect of one of the modifications, namely the fact that now the kick-off pulse is not present at the nodes of the hull part at Y=-11.17 m. Therefore the front of the shock wave in the bulkhead becomes curved (hull has to be accelerated). For the same reason, compare fig. 3.8 with fig. 4.1 of ref. [2], the velocities and accelerations of the nodes at Y=-11.17 m in the hull part do not follow exactly the input pulse (constant acceleration 574.83 m/s^2 upto t=2.94 milliseconds, constant acceleration -36.219 m/s^2 for larger time values) but oscillate around the input pulse. Note the larger time scale in fig. 3.8, resulting in the linear decreasing velocity. Please note that in general the kick-off pulse approach includes a linearly decreasing velocity until zero. In this case this is at t=49.6 ms. In general after that point in time the velocity is kept at zero, thus maintaining the input displacement at a constant

value. Unfortunately in the present calculations the constant deceleration was maintained beyond t=49.6 ms, thus leading to very large downward velocities and displacements. For that reason displacement signals are not shown in this report.

In fig. 3.9 to 3.11 the velocities and accelerations for locations A to F at all three decks for the modified model are shown. These figures can be compared with fig. 4.2 to 4.4 of ref. [2]. Firstly it is noted that responses become very smooth functions, which is caused by the relatively large damping for higher frequencies. This effect is of course most clear for the accelerations. In fact, having in mind measured deck motions in general, these analysis results seem to be overdamped. Secondly, while responses (both velocities and accelerations) in ref. [2] are considerably larger than the standard pulse shapes C and D, especially for locations B and E which are the most interesting locations (other locations are at connections between deck and bulkhead, hull or corrugated plate, B and E are real deck locations), for the modified model the responses do fit quite well within the standard pulse shapes (especially the velocity of location E). All amplitudes are smaller than the amplitude of the standard pulse shape. Some responses, especially the velocities for locations C and the accelerations for locations B of G- and H-deck, have a duration of the positive pulse which is considerably larger than that of the standard pulse shapes.

Because only the original location B is located at a discrete mass of the modified model, the additional locations E-0, E-1 and G-0, G-1 are introduced in the previous chapter, see fig. 2.3 to 2.5. Locations E-0 and E-1 are close to location E, but at a node with a discrete mass (E-0 at deck below spring, E-1 at discrete mass above spring), and locations G-0 and G-1 are at the centre of the largest deck part between hull and corrugated plate, again at a node with a discrete mass (G-0 at deck below spring, G-1 at discrete mass above spring). Fig. 3.12 to 3.14 give the accelerations for these additional locations. The effectiveness of the springs is quite clear, the accelerations of the discrete masses with some 50 m/s^2 are relatively small (locations B-1 (only for F-deck), E-1 and G-1). Again, the responses for the additional locations below the springs do fit remarkably well within the standard pulse shapes.

Finally fig. 3.15 to 3.17 compares the velocities and accelerations of locations B, E and G for the three decks. For the locations corresponding with a deck region with masses mounted on springs (location E and G), the responses of the three decks are quite close to each other. The response for these locations at the F-deck is less damped then for these locations at the G- and the H-deck, compare the damping values of table 2.2. Quite remarkable are the results for location B, having a fixed discrete mass at the G- and H-deck and a discrete mass mounted on a spring for the F-deck, see fig. 3.15. The fixed mass at the G- and H-deck causes a 'cut-off' of the acceleration pulse (fig. 3.15 c)), but also a considerable larger duration for this maximum acceleration, necessary to accelerate the fixed mass. Large differences do also exist between the responses for location B at G- and H-deck for the current model and for the original model, see ref. [2], while both models have fixed masses at this location, either equally distributed or fixed. The reason for these

differences will be discussed in chapter 5. It is clear that, as for the original model, see ref. [2], the results still do not confirm the idea that the pulse decreases for higher deck levels.

Summarizing, differences in the responses for the original model and for the modified model are quite large. Opposite to the original model, responses for the modified model do fit within the standard pulse shapes. In the next chapter it will be investigated which of the modifications, namely:

- including Rayleigh damping,
- replacement of equally distributed mass by discrete masses, either fixed or mounted on springs including damping,
- kick-off pulse only applied at bulkhead, and not at the nodes,

has the largest effect on the responses, and so the largest effect on the correspondence between calculated responses and standard pulse shapes.

4. EFFECTS OF MODEL CHANGES ON RESPONSES

4.1 Effect of Rayleigh damping

A new analysis has been carried out using the modified model from the previous chapters, but now without Rayleigh damping. Velocities as function of time for locations A to F of the three decks, for the original model from ref. [2], for the modified model including Rayleigh damping, and for the modified model without Rayleigh damping are shown in fig. 4.1 to 4.3. Differences for location A between the results of the three analyses are quite limited, and slightly larger for locations D and F. This can be understood considering that these responses are mainly determined by the input shock wave moving through bulkhead, hull and corrugated plate, and hardly by the decks. Therefore differences between the three models do not appear in these responses, except for some relatively small oscillations (caused by presence or absence of damping, and by different reaction forces from the decks (different mass modelling) at bulkhead, hull and corrugated plates). By far the largest differences are found for the real deck locations B and E. Comparing the maximum amplitudes of the velocities, the absence of Rayleigh damping results in an increase from approximately 2.0 m/s to 3.0 - 3.5 m/s, while the original model from ref. [2] (no Rayleigh damping, equally distributed mass, kick-off pulse at both bulkhead and hull) results in even larger maximum velocities. So the effect of Rayleigh damping is significant, but one of the other model differences must also have a considerable effect, otherwise responses for the original model and for the modified model without Rayleigh damping should have been close to each other.

In the next section one of the other model changes, namely the effect of including the kick-off pulse at the hull nodes at Y=-11.17 m is investigated.

4.2 Effect of excitation at hull

Fig. 4.4 to 4.6 show the accelerations of a selected number of locations of the three decks, for the modified model from the previous chapter, but now the kick-off pulse is applied to both hull and bulkhead at Y=-11.17 m. The other modifications with respect to the original model from ref. [2] are still present, so discrete masses are used, either fixed or mounted on springs including damping for the springs, and Rayleigh damping is applied. As expected, these results show that the larger the distance from the location to the hull (location A, B), the smaller the differences in the responses. For locations relatively close to the hull (location E) or even at the connection of the deck to the hull (location F), the effect of the hull excitation is slightly larger, but these differences are still such small that this model change can not be responsible for the large difference in the correspondence between calculated responses and standard pulse shapes as found for the original model from ref. [2] on the one hand and the modified model from the previous chapter on the other hand.

4.3 Effect of damping for discrete springs

Fig. 4.7 to 4.10 show the accelerations as function of time for the modified model without spring damping. The remaining modifications with respect to the original model from ref. [2] are still present, so discrete masses in stead of equally distributed masses, either fixed or mounted on springs, no kick-off pulse for the hull, and Rayleigh damping included. Firstly, it is noted that damping of the spring has of course its effects on the responses for both the location at the deck (below the spring) and at the discrete mass (above the spring). At the discrete mass the effect becomes more clear for larger time values, because the velocity has to be built up before the damping becomes a significant term in the equations of motion. Amplitudes of the acceleration at the deck locations becomes slightly larger, but, compare fig. 3.12 to 3.14, it is clear that these responses will still fit within the standard pulse shapes. Secondly, comparison of fig. 4.7, 4.8 and 4.9 again show that these results do not confirm the idea that the pulse decreases for higher deck levels, neither for locations below the spring nor for locations above the spring. Thirdly, as expected the absence of spring damping has also its (small) effects for locations far away of the discrete springs, simply because the energy that is not dissipated by the discrete springs if the spring damping is removed remains in the structure, see fig. 4.10 a) and b).

Finally, comparing the responses for location B of the three decks as shown in fig. 4.10, it is clear that the application of a spring for a discrete mass has a large influence on the response of both the deck and the mass.

So thus far it can be concluded that the difference in the correspondence between calculated responses and standard pulse shapes as found for the original model from ref. [2] and for the modified model is mainly caused by:

- the application of Rayleigh damping,
- the use of discrete masses on springs in stead of equally distributed masses,

while the effect of the hull excitation and the damping of the discrete springs is very limited. In the next chapter the effect of the magnitude of Rayleigh damping is investigated, both for the modified model and for the original model from ref. [2] with equally distributed mass.

5. EFFECTS OF MAGNITUDE OF RAYLEIGH DAMPING

5.1 Results for the modified model

Fig. 5.1 shows three curves with the damping as fraction of the critical damping as function of the frequency. As in chapter 2, the frequencies used are still 0.5 and 60.0 Hz, while for these frequencies the desired damping ratio is reduced from 22 percent to 11 and 5.5 percent respectively. The resulting values for the Rayleigh damping coefficients a_0 and a_1 are:

- ratio 22 percent $a_0 = 1.37088$ $a_1 = 0.00115750$ denoted as: modified
- ratio 11 percent $a_0 = 0.68544$ $a_1 = 0.00057875$ denoted as: 0.5 times modified
- ratio 5.5 percent $a_0 = 0.34272$ $a_1 = 0.00028937$ denoted as: 0.25 times modified.

Fig. 5.1 shows that the last Rayleigh damping coefficients result in a damping ratio less than 2.0 percent for a quite large frequency range.

As discussed in section 4.1, the effect of Rayleigh damping on the responses of locations A, D and F is limited. Therefore, fig. 5.2 to 5.7 give the velocities and accelerations as function of time for the 'real' deck locations B, C, E-0 and G-0, as calculated for the modified model with the Rayleigh damping coefficients from chapter 2, 0.5 times these damping coefficients, 0.25 times these damping coefficients and for the case without Rayleigh damping. For the case without Rayleigh damping, accelerations are not shown (higher frequencies).

It is quite interesting to draw conclusions with respect to the location of the response:

- if the location is at the position of a discrete mass at the deck (below a spring, location E-0, G-0 for all decks), a relatively small amount of Rayleigh damping is sufficient to get a good fit with respect to the standard pulse shapes, see also fig. 3.12 to 3.14. Velocities require a larger Rayleigh damping than accelerations.
- if the location is at a deck between a number of discrete masses on springs, e.g. location E from fig. 3.9 to 3.11, the correspondence between calculated velocities and accelerations with the standard pulse shapes is quite good.
- if the location is at a fixed mass, or at the deck between a number of fixed masses (location B, C for G- and H-deck), the amplitudes of both velocity and acceleration do fit within those of the standard pulse shapes, but the duration of the positive pulse becomes much larger. Again, velocities require a larger Rayleigh damping than accelerations.
- comparing locations B and C at the F-deck (fig. 5.6 a), b) and 5.7 a), b), mass at discrete spring) with locations B and C at the G- and H-deck (fixed mass) show that:
  - the accelerations of location B at the F-deck show a considerably better correspondence with the standard pulse shapes than the accelerations of location B at the G- and H-deck, corresponding with the conclusions above. However, the velocity of location B at the F-deck has more or less the same shape as those of location B at the G- and H-deck,

including the larger duration of the positive pulse.

- both the velocity and the acceleration of location C at the F-deck (between discrete masses mounted on springs) are more or less of the type as found for location C at the G- and H-deck (between fixed discrete masses), which does not correspond with the conclusions above.

So it can be concluded that the calculated responses fit quite well within the standard pulse shapes, as long as the location is at a deck part with discrete masses that are mounted on springs. A small amount of Rayleigh damping has to be available to reduce the amplitudes, while the velocities require a slightly larger Rayleigh damping than the accelerations. The last conclusion above shows that only the responses for the small part of the F-deck between corrugated plate and centreline do not satisfy this main conclusion. This will be discussed in the next chapter.

5.2 Results for the original model including Rayleigh damping

Fig. 5.8 to 5.13 show the effect of Rayleigh damping on the original model from ref. [2], so with the equally distributed mass. Although the correspondence between calculated responses and standard pulse shapes becomes better, the correspondence is still worse than that of the previous section:

- although the correspondence between maximum amplitudes is better, several responses show a larger duration of the positive pulse than the standard pulses, see for example fig. 5.10 c).
- the correspondence between the accelerations is worse than in fig. 5.2 to 5.7. The time to the maximum amplitude for locations B and E is larger than that of the standard pulses, see fig. 5.9, 5.11 and 5.13 a) and c).
- the equally distributed mass requires a larger Rayleigh damping than the model with discrete masses for a correct amplitude of the velocity. Comparing the velocities for location E from fig. 5.8, 5.10 and 5.12 with those for location E-0 from fig. 5.2, 5.4 and 5.6, show that for the Rayleigh damping values of the modified model, the velocity amplitudes of the model with the equally distributed mass are more or less equal to that of standard pulse shape C, while the velocity amplitudes for the model with the discrete masses are more or less equal to that of standard pulse shape D.
- the velocities for location C for all three decks are more or less comparable with those as calculated for the model with the discrete masses (larger duration of positive pulse).

So although the responses as calculated with a model with equally distributed masses show a better correspondence with the standard pulse shapes if Rayleigh damping is applied, by far the best correspondence is obtained for a model with discrete masses mounted on springs including only a small amount of Rayleigh damping.

Finally the differences as found for the responses at location B at G- and H-deck for the modified

model on the one hand (section 3.2), and for the original model from ref. [2] on the other hand, while both models have fixed masses at this location, either equally distributed or discrete, will be discussed. Fig. 5.8 to 5.13 show that this is caused by the presence of Rayleigh damping.

6. SHOCK WAVE PROPAGATION

This chapter discusses the problem that responses for the small part of the F-deck between centreline and corrugated plate (locations B, C, larger duration of positive pulse) are quite different from those at the large part of the F-deck between corrugated plate and hull (locations E, G), and therefore correspond less with the standard pulse shapes, while these deck parts are quite comparable (same stiffeners, same masses mounted on springs and so on).

Fig. 6.1 to 6.12 show the propagation of the shock wave for F- and H-deck along several lines, namely for the lines in length and transverse direction through location B and through location G. Accelerations are shown for the locations with discrete masses. These figures show that:

- For the large deck parts, shock wave propagation for the H-deck and the F-deck are similar, compare fig. 6.2 with 6.8, 6.3 with 6.9, and 6.5 with 6.11.
- Fig. 6.2 and 6.8 show the shock wave propagation from bulkhead through location G to location E. Responses start with the location at x = 1.2 m (first discrete mass, x = 0 is bulkhead), followed by x = 2.4 m, but the remaining responses for larger x-coordinates start at the same time value. This is caused by the fact that for larger x-coordinates, the response is initiated by the shock wave propagating through hull and longitudinal corrugated plate, in stead of through the deck, see fig. 6.3 and 6.5 (6.9, 6.11). These figures show that the shock wave reaches the connections between hull and deck and between corrugated plate and deck at more or less the same time. Then the shock waves propagates from both sides to the centre (location G) of the large deck part.
- At the small deck parts (fig. 6.1, 6.7) the shock wave propagation is quite different. Only the responses for the discrete masses at a stiffener start at the same time as for the large deck part, while the responses for the remaining locations start at a considerably later time value, compare fig. 6.1 and 6.7 with fig. 6.2 and 6.8. The shock wave propagation in transverse direction of the small parts along the stiffeners corresponds with the expectations (fig. 6.4, 6.6, 6.10 and 6.12), starting at the corrugated plate and travelling to the centreline.

Fig. 6.13 shows that the differences for the shock wave propagation for the large deck part and for the small deck part is caused by a less stiff deck at the centreline, resulting in half a sine between two stiffeners. It was found that no stiffener was present at the centrelines of the deck. Due to symmetry conditions, half a profile HP 100x7 has to be present at the decks at the centreline in length direction, see the model description in ref. [1]. Therefore, the analysis for the modified model including the Rayleigh damping has been repeated, but now with a full HP 100x7 profile in length direction at the centreline of the decks. Fig. 6.14 shows that indeed the half sine between the cross-sectional stiffeners has disappeared.

Fig. 6.15 to 6.20 show the shock wave propagation for the small deck parts of H- and F-deck, for the modified model including the additional HP 100x7 profile at the centrelines of the deck. It is

noted that the results for the large deck part are unchanged. Comparison of fig. 6.16 with 6.4, 6.17 with 6.6, 6.19 with 6.10 and 6.20 with 6.12 shows that the shock wave propagation in transverse direction through the cross-sectional stiffeners is not influenced by the additional HP profile. Comparison of fig. 6.15 with 6.1, and especially fig. 6.18 with 6.7, shows the effect of the additional HP profile. The shock wave propagation of the small deck part of the F-deck is now comparable with that of the large part of the F-deck, compare fig. 6.18 with 6.8.

Fig. 6.21 and 6.22 compares the velocities and accelerations of locations B and C of H- and F-deck with the standard pulse shapes. The results are comparable with fig. 3.9 and 3.11. Fig. 6.23 compares the velocities and accelerations for a location at the centreline of the F-deck with the standard pulse shapes, both for the case with and without additional HP profile. This location has been chosen because here the effect of the additional HP profile is quite large, compare fig. 6.7 and 6.18. For the case without HP profile (fig. 6.23 c) and d)), the acceleration is of the type as found thus far for locations at the small part of the F-deck:

- positive half sine fitting quite well within the standard pulse shapes,
- negative half sine (nearly) absent,
- resulting in larger duration for positive half sine of velocity.

For the case without the HP profile (fig. 6.23 a) and b)), these differences have disappeared resulting in a quite good correspondence between calculated responses and standard pulse shapes. So the correspondence with the standard pulse shapes is largely determined by the stiffnesses (only HP 100x7 added at centreline).

The discussion above leads to the conclusion that the worse correspondence with the standard pulse shapes as found for the small part of the F-deck, when compared with the large part of the F-deck, is caused by the smaller stiffness of the small deck part (width of large F-deck part is 5.2 m, width of small F-deck part (symmetry) is 7.2 m, same stiffening and masses). This is confirmed by the deformed geometry as shown in fig. 6.14. So whether calculated responses and standard pulse shapes do correspond, is strongly determined by (ratio's between) stiffnesses and masses ($\sqrt{k/m}$, $\sqrt{E/\rho}$).

7. CONCLUSIONS

- The calculated responses for the modified model (including Rayleigh damping, discrete masses either on springs or fixed, no hull excitation) correspond quite well with the standard pulse shapes, especially for the deck parts between longitudinal corrugated plate and hull. For the deck parts between centreline and corrugated plate, the correspondence is worse, as the response of this part of the deck is dominated by a vibration mode with a rather low natural frequency.

- With respect to the correspondence between calculated responses and standard pulse shapes, one should keep in mind that:
  - Rayleigh damping is a very simplified model of the damping behaviour of the real structure,
  - Rayleigh damping overestimates the damping for higher frequencies, as is clear when comparing the calculated responses with measured responses,
  - The kick-off pulse approach is an approximation for a very complex load transmission phenomenon,
  - The standard pulse shapes themselves are just average representations of rather widely diverging measured time signals. As well known, differences in amplitudes and time constants (T_1 and T_2) up to factor 2 may well occur.

- Removing or including the excitation of the hull by the kick-off pulse has a very limited effect.

- Removing or including the damping of the discrete springs has a very limited effect.

- The original value for the Rayleigh damping for the modified model (11 percent at 0.5 Hz and 60 Hz) can be considerably decreased, with still a correct correspondence between calculated responses for the deck parts between longitudinal corrugated plate and hull and the standard pulse shapes (section 5.1).

- The modelling of the mass as discrete masses mounted on springs has a large effect on the correspondence between calculated responses and standard pulse shapes. Including Rayleigh damping for the original model with equally distributed masses do increase the correspondence between calculated responses and standard pulse shapes, but this correspondence is still worse than that for the modified model including Rayleigh damping and discrete masses mounted on springs (section 5.2).

- These conclusions are strongly influenced by (ratio's between) stiffnesses and masses for the different deck parts. The response for each location is built up from the shock wave propagating through different paths (bulkhead - deck, bulkhead - longitudinal corrugated plate - deck, bulkhead - hull - deck), which is of course influenced by the stiffnesses and masses ($\sqrt{E/\rho}$,

$\sqrt{}$k/m). The discrepancy between calculated responses and standard pulse shapes for the F-deck part between corrugated plate and centreline with respect to the correspondence between calculated responses and standard pulse shapes for the F-deck part between corrugated plate and hull (same masses, stiffeners) is caused by the larger width of the F-deck part between centreline and corrugated plate (7.6 m versus 5.2 m, chapter 6).

- Finally, as in ref. [1] and [2], the results still do not correspond with the idea that smaller velocity and acceleration amplitudes occur for higher deck levels (transition from pulse C to pulse D). Including damping into the model, in that respect, makes no significant difference.

REFERENCES

[1] W. Trouwborst
Transmissie van schok, responsieberekening van een compartiment van een fregat
TNO-report 94-CMC-R1365, November 1994

[2] W. Trouwborst
Shock transmission, response calculation of a compartment of a frigate including plasticity effects
TNO-report 95-CMC-R1143, 29 January 1996

[3] Shock Handbook, part I, TNO-CMC, 1990
NSN 7610-17-104-1610

[4] Roy R. Craig
Structural Dynamics; An introduction to computer methods
John Wiley & Sons, 1991

[5] DIANA User Manual - Version 6.2
TNO Building and Construction Research

FIGURES

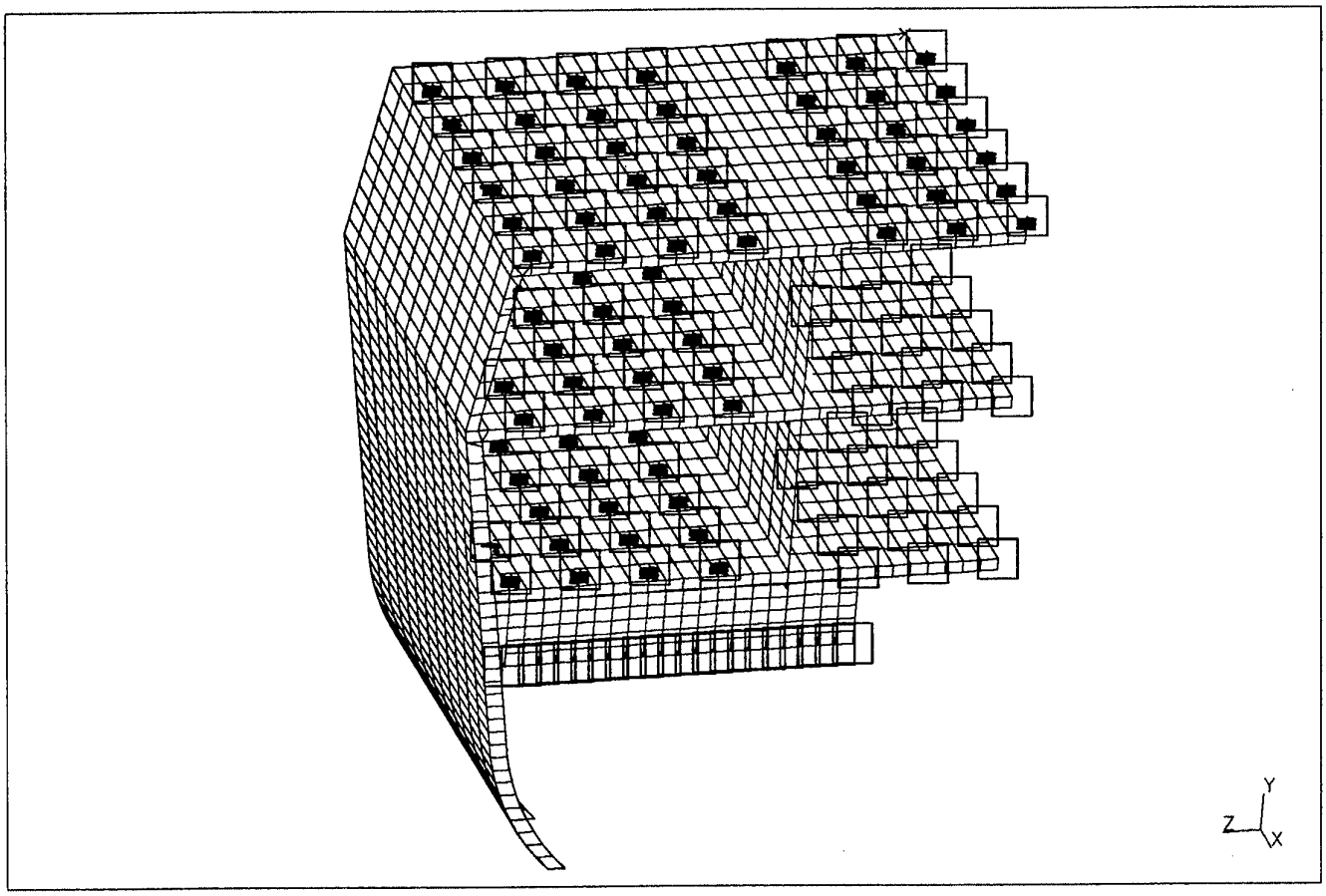

Fig. 2.1 a) Discrete masses and springs as present in the modified model

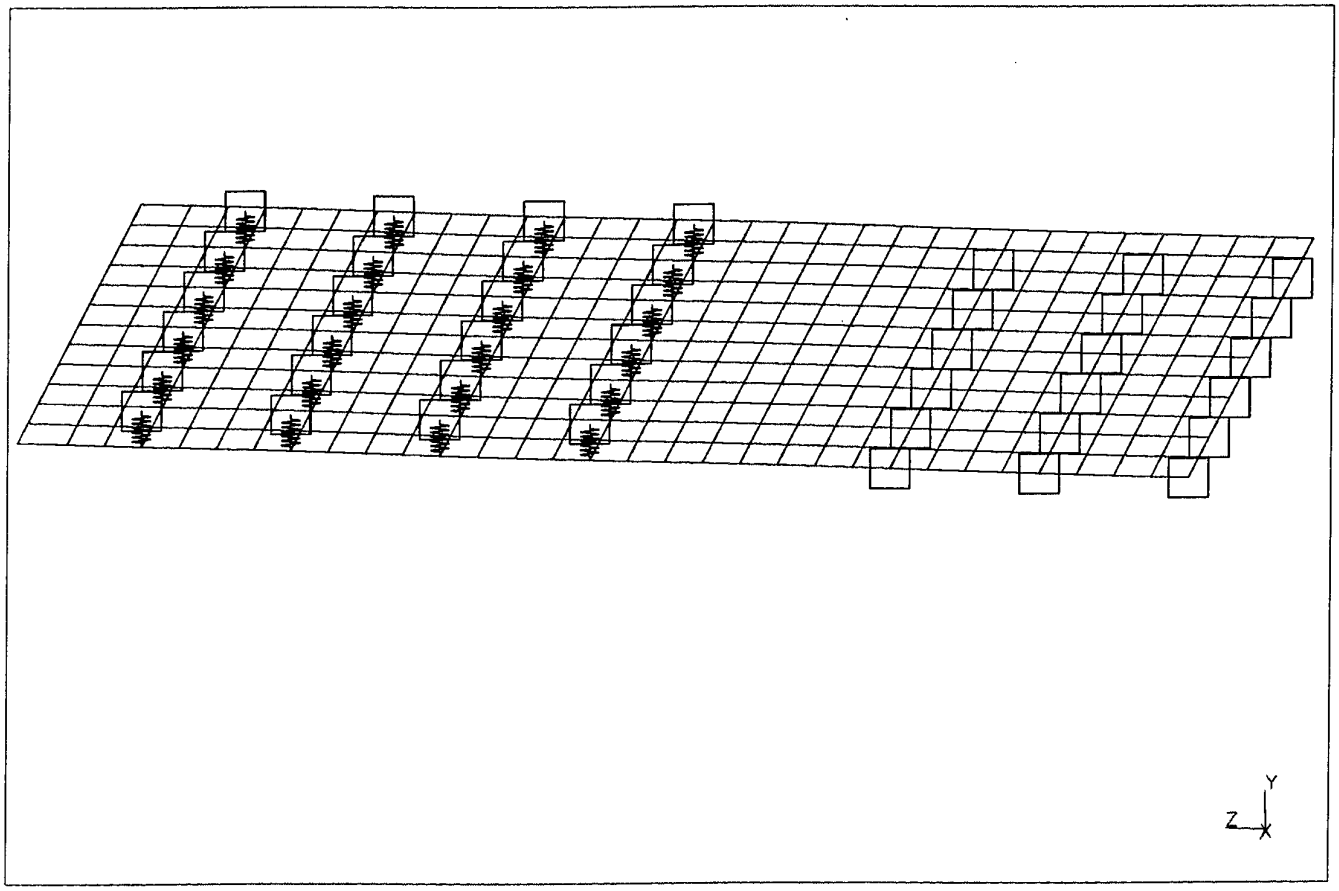

Fig. 2.1 b) Discrete masses and springs as present at the G-deck of the modified model

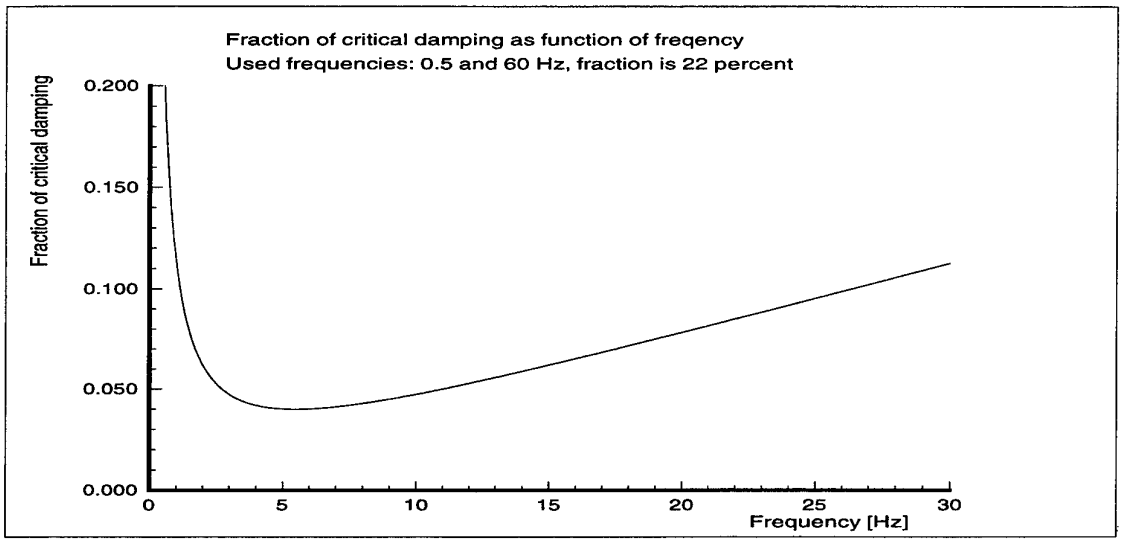

Fig. 2.2 Fraction of critical damping as function of frequency, calculated using 0.5 Hz and 60 Hz, both with 22 percent

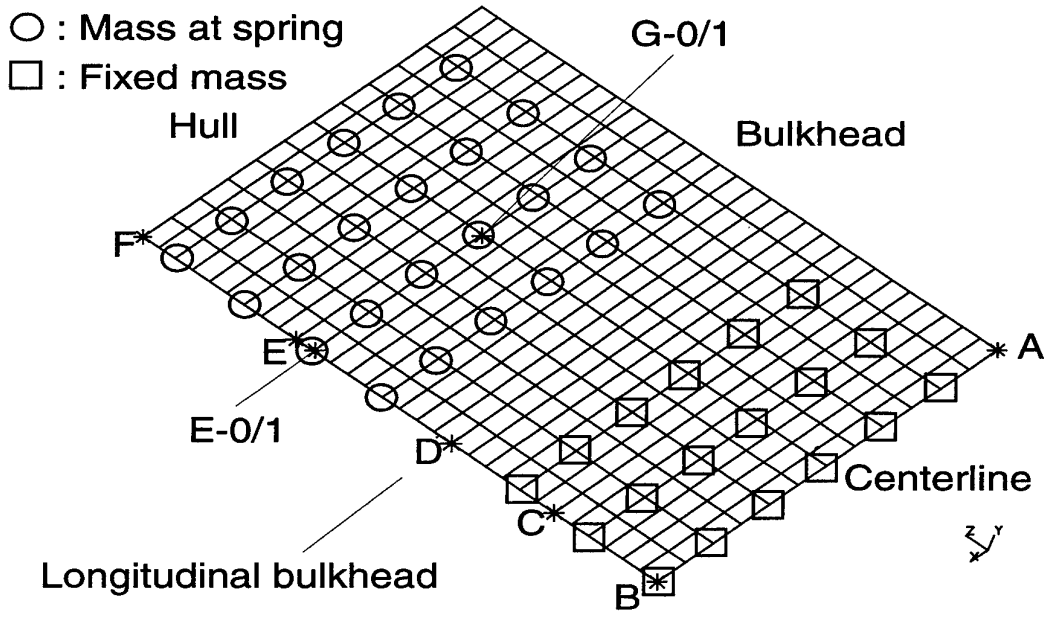

Fig. 2.3 Locations of H-deck used for time history plots (locations E-0/1 and G-0/1 are additional locations at nodes with discrete masses)

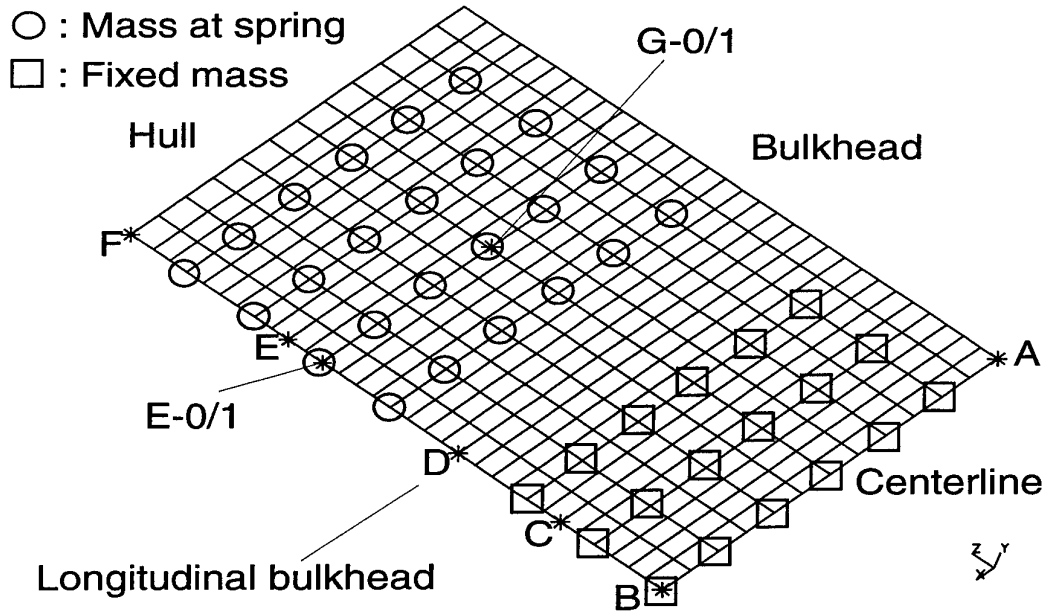

Fig. 2.4 Locations of G-deck used for time history plots (locations E-0/1 and G-0/1 are additional locations at nodes with discrete masses)

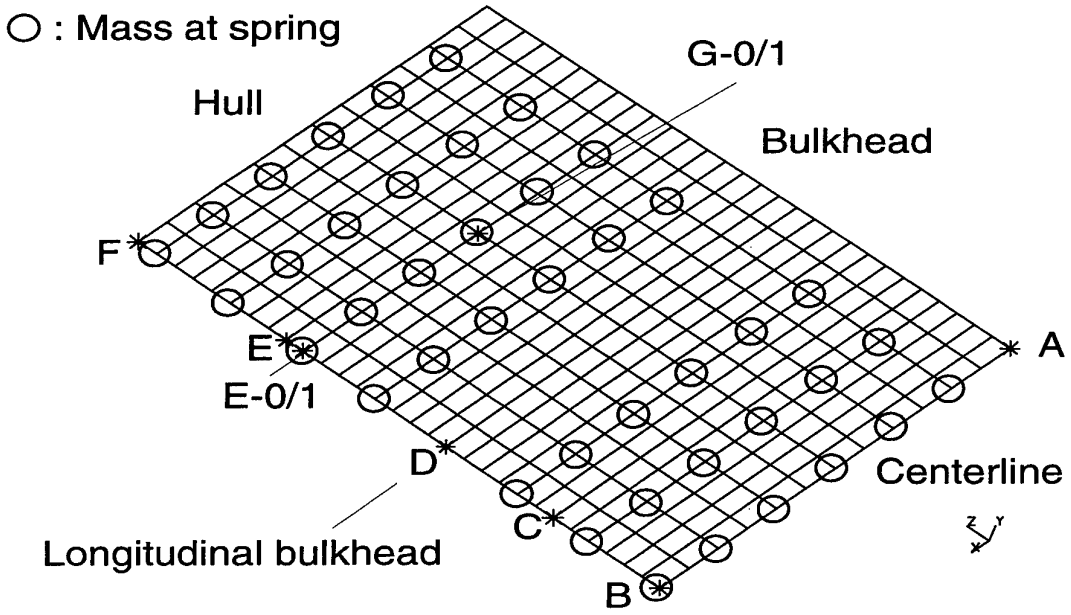

Fig. 2.5 Locations of F-deck used for time history plots (locations E-0/1 and G-0/1 are additional locations at nodes with discrete masses)

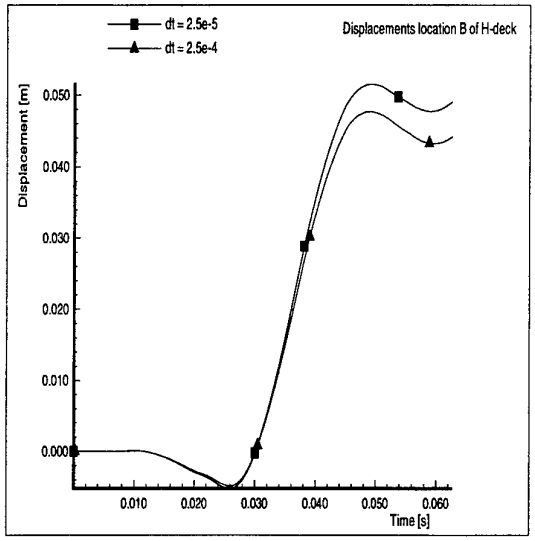

a) Displacements

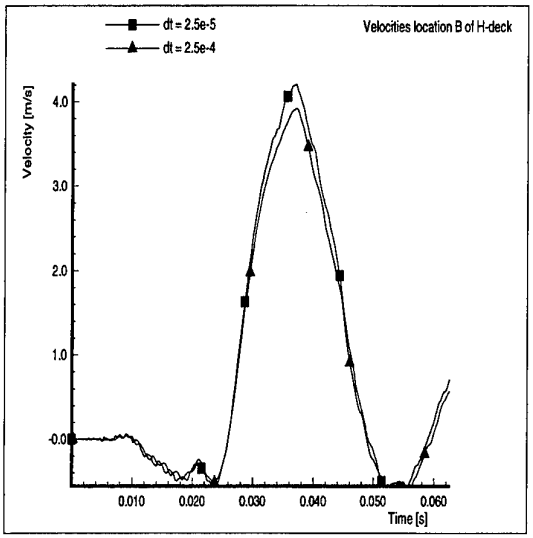

b) Velocities

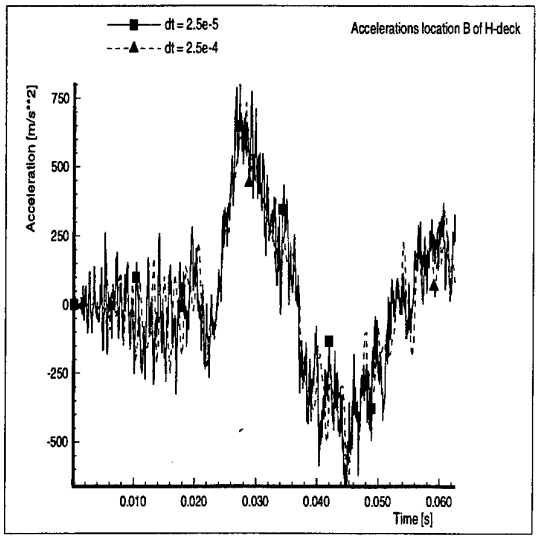

c) Accelerations

Fig. 3.1 Time histories for location B (centre of compartment) at the H-deck, both with version 6.2, effect of time step, original model with small deck masses, compare fig. 4.2 of ref. [2]

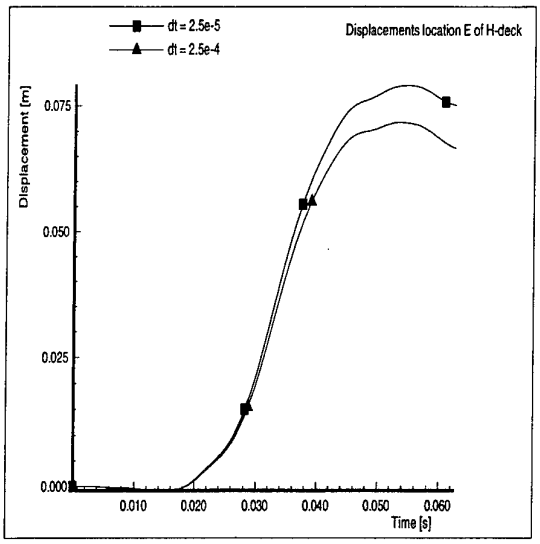

a) Displacements

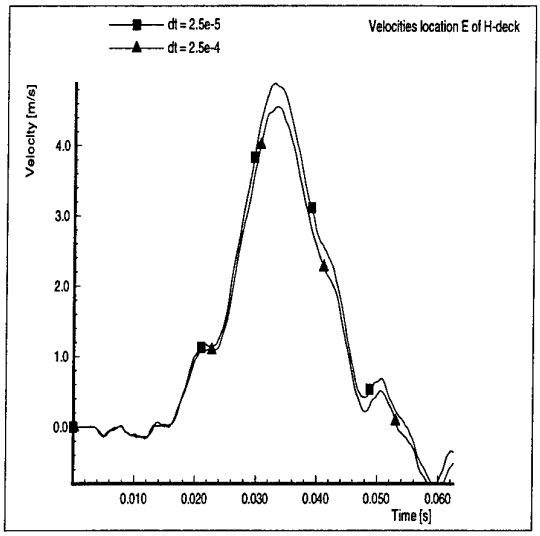

b) Velocities

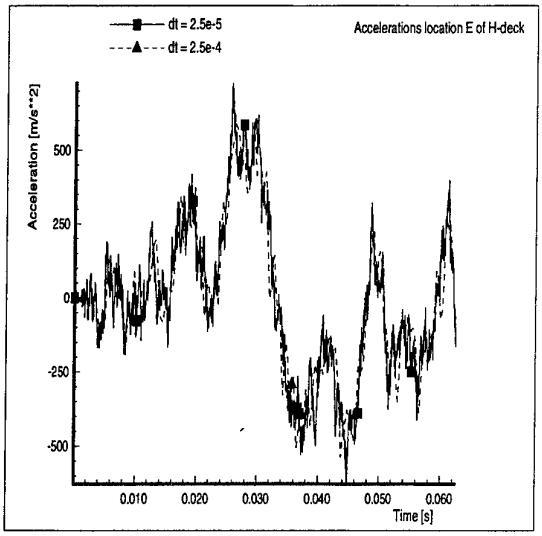

c) Accelerations

Fig. 3.2 Time histories for location E (midway between hull and longitudinal bulkhead (corrugated plate)) at the H-deck, both with version 6.2, effect of time step, original model with small deck masses, compare fig. 4.2 of ref. [2]

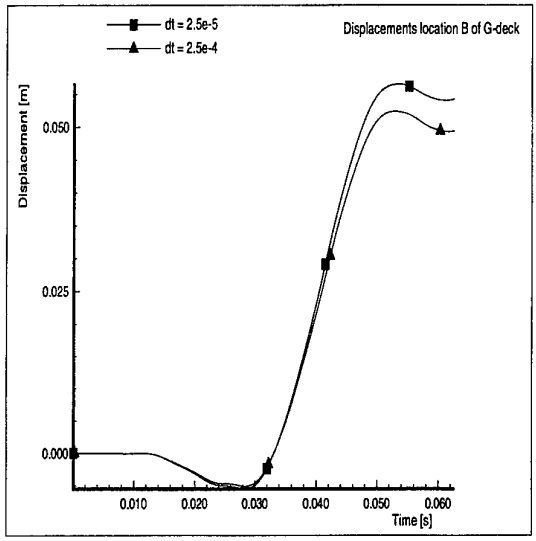

a) Displacements

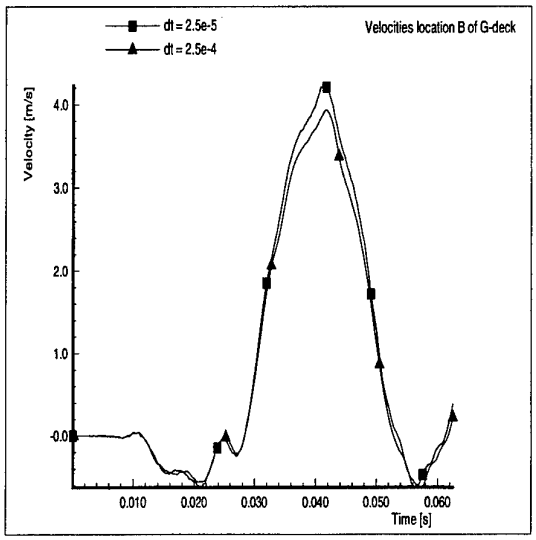

b) Velocities

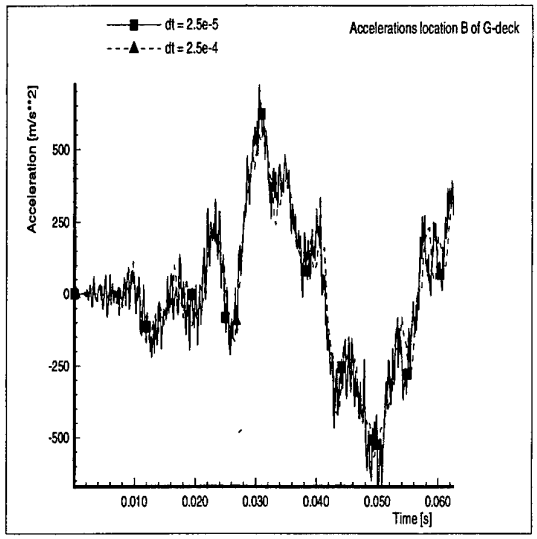

c) Accelerations

Fig. 3.3 Time histories for location B (centre of compartment) at the G-deck, both with version 6.2, effect of time step, original model with small deck masses, compare fig. 4.3 of ref. [2]

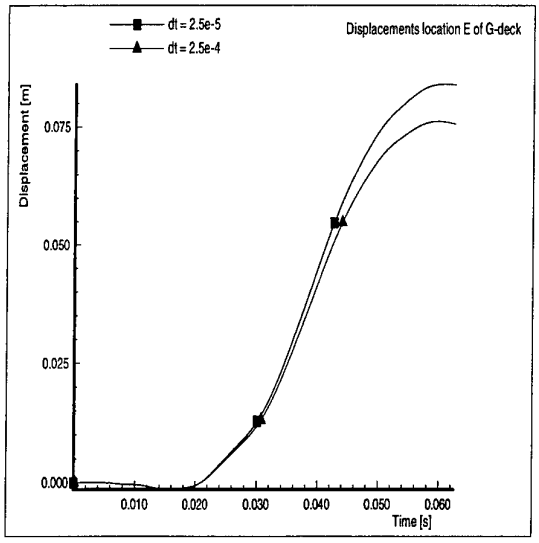

a) Displacements

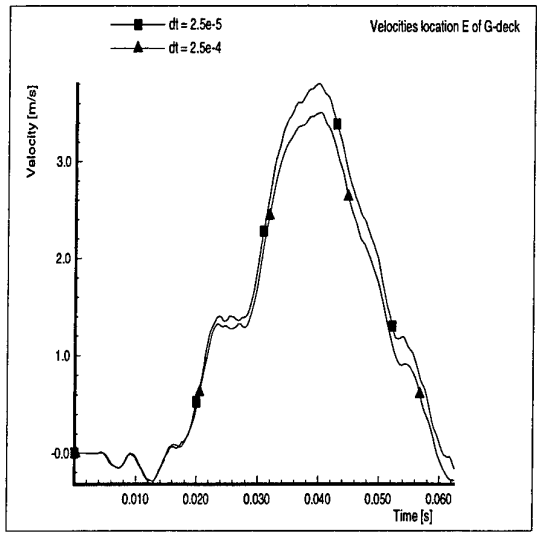

b) Velocities

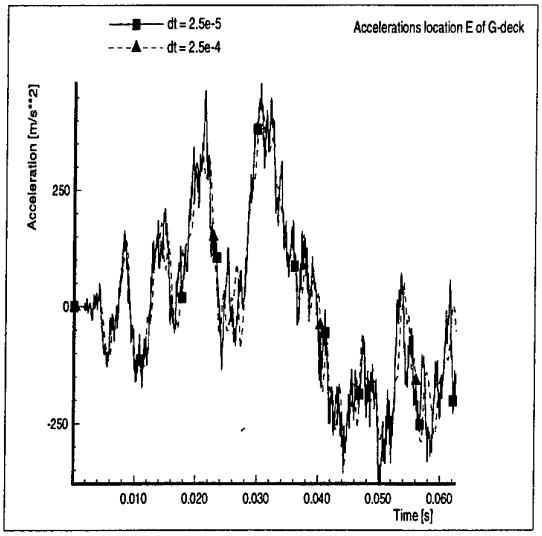

c) Accelerations

Fig. 3.4 Time histories for location E (midway between hull and longitudinal bulkhead (corrugated plate)) at the G-deck, both with version 6.2, effect of time step, original model with small deck masses, compare fig. 4.3 of ref. [2]

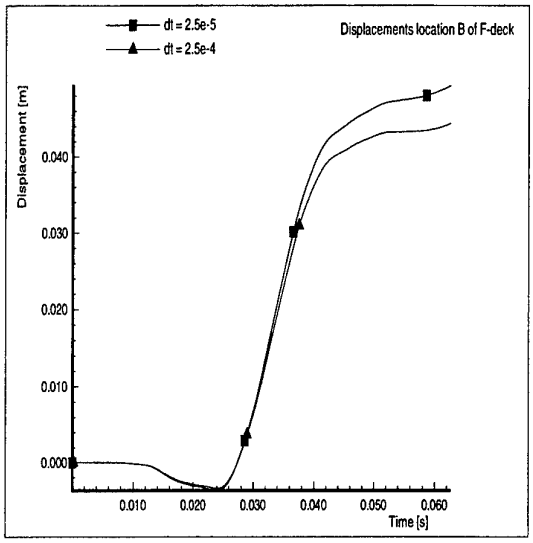

a) Displacements

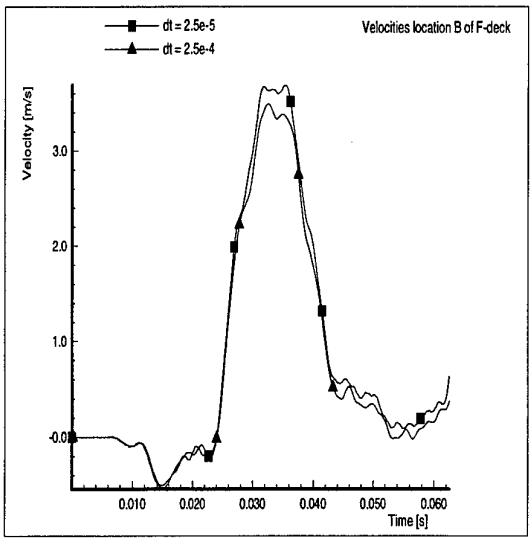

b) Velocities

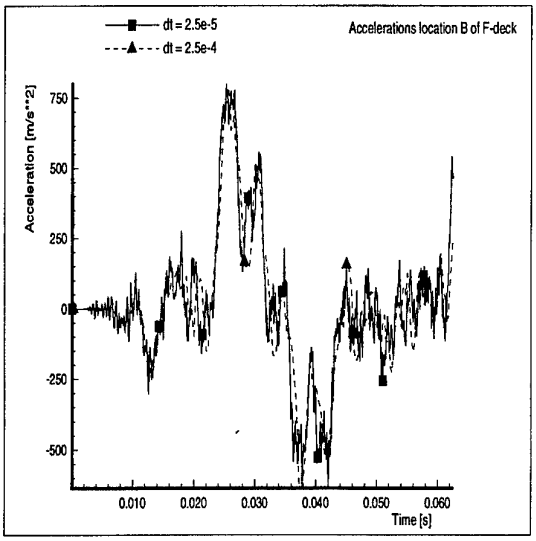

c) Accelerations

Fig. 3.5 Time histories for location B (centre of compartment) at the F-deck, both with version 6.2, effect of time step, original model with small deck masses, compare fig. 4.4 of ref. [2]

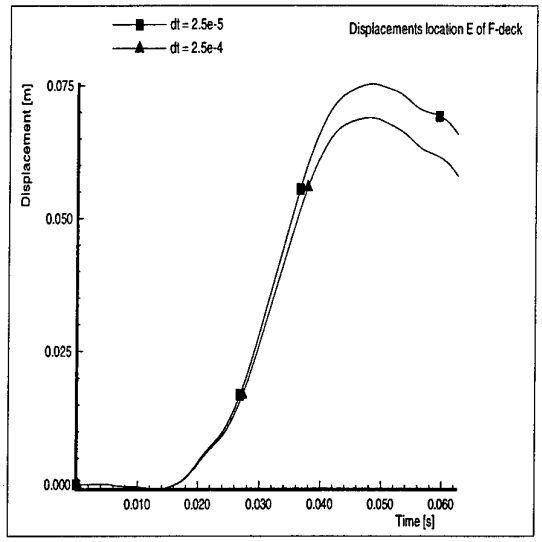

a) Displacements

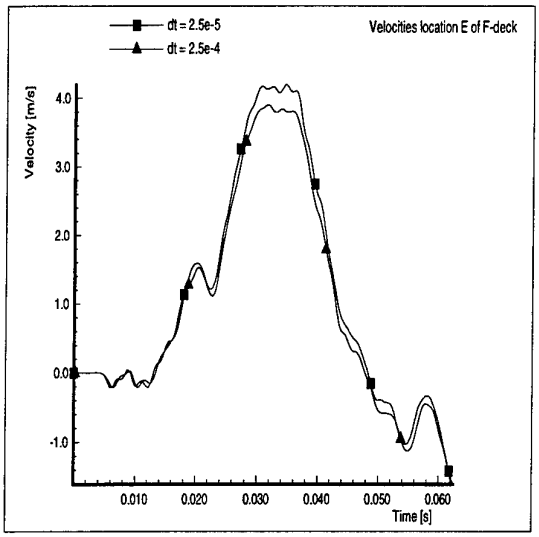

b) Velocities

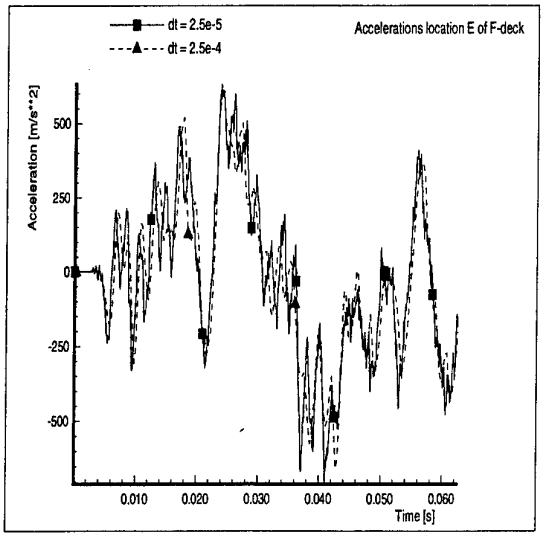

c) Accelerations

Fig. 3.6 Time histories for location E (midway between hull and longitudinal bulkhead (corrugated plate)) at the F-deck, both with version 6.2, effect of time step, original model with small deck masses, compare fig. 4.4 of ref. [2]

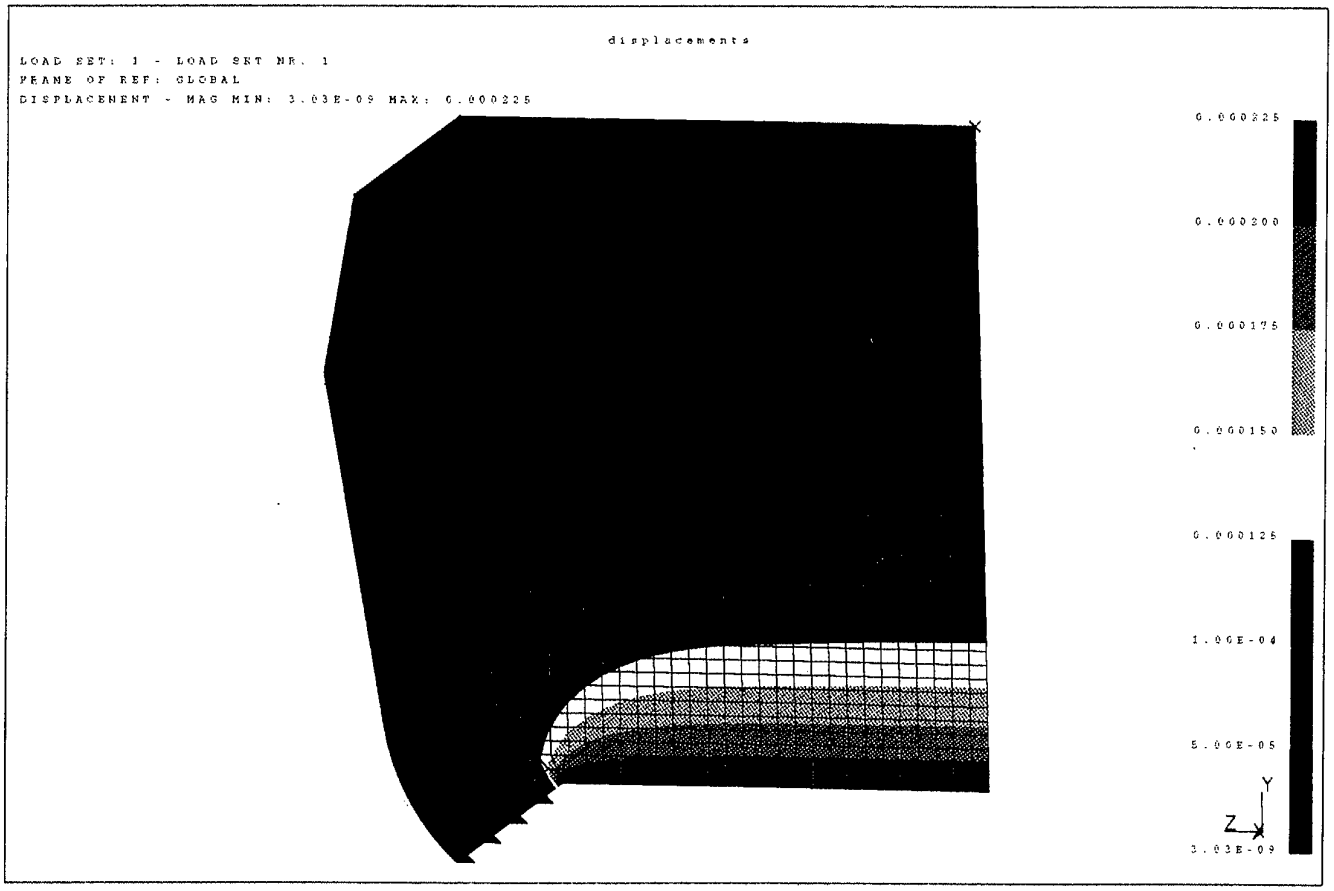

Fig. 3.7 a) Deformed geometry at time = 1.0 ms

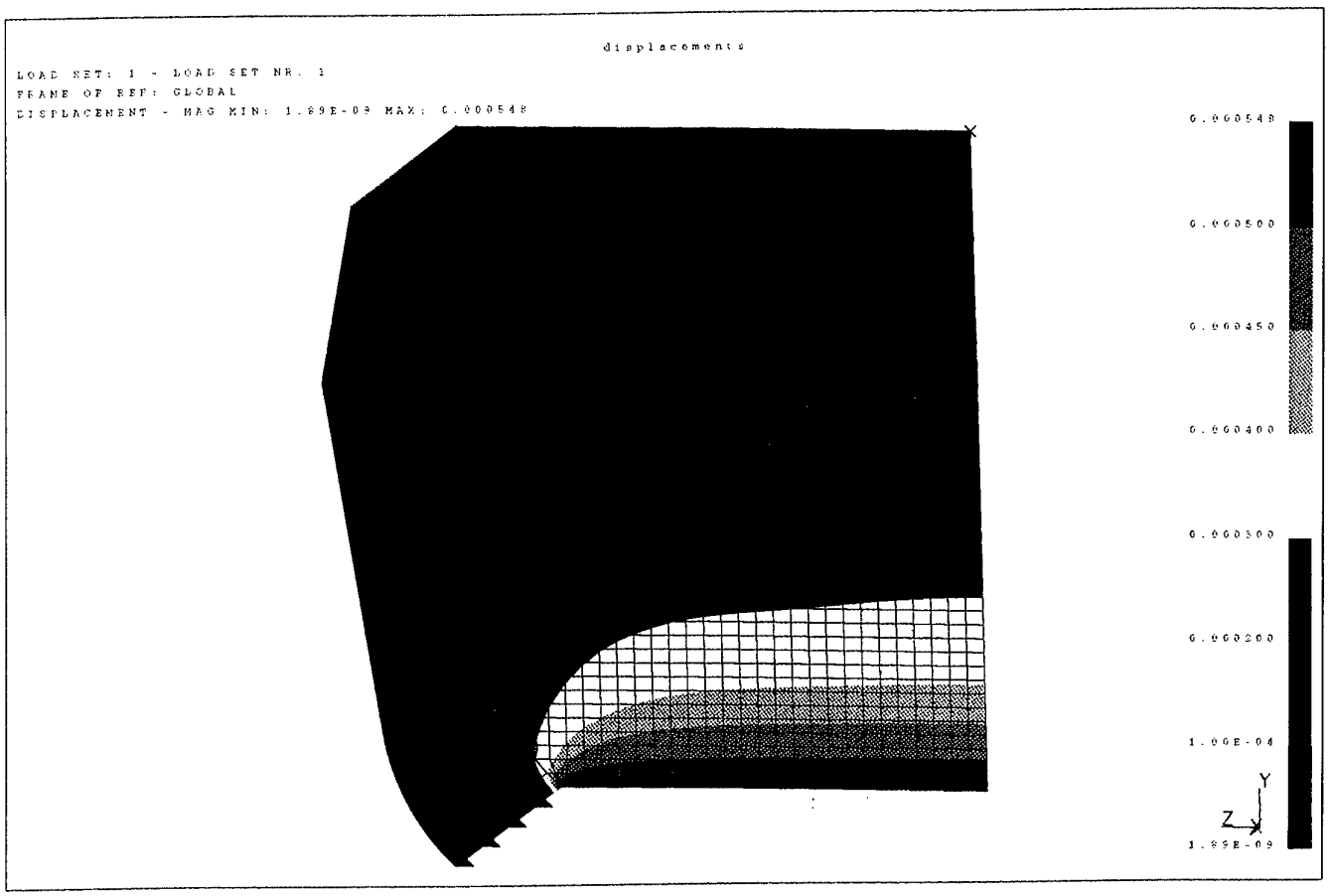

Fig. 3.7 b) Deformed geometry at time = 1.5 ms

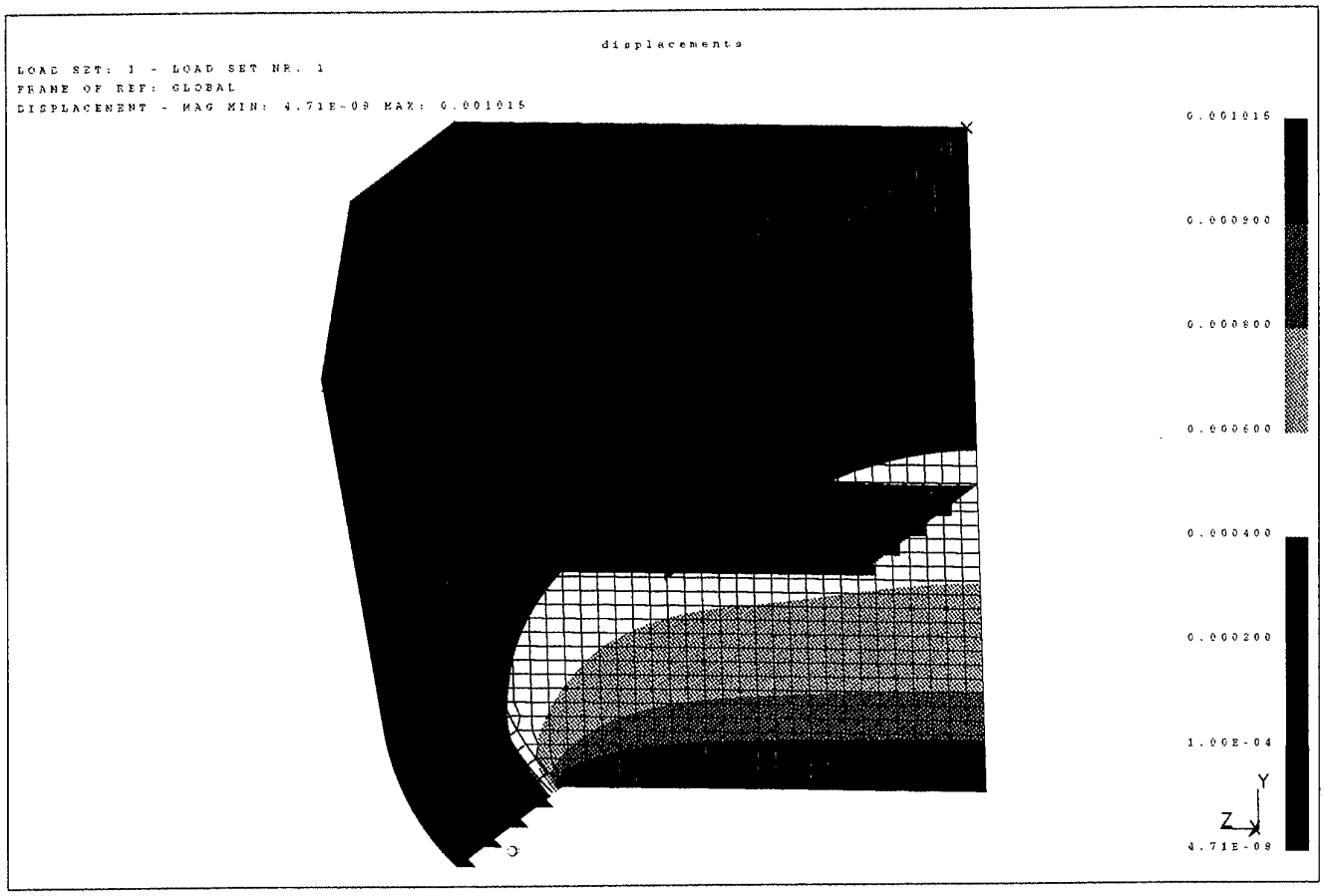

Fig. 3.7 c) Deformed geometry at time = 2.0 ms

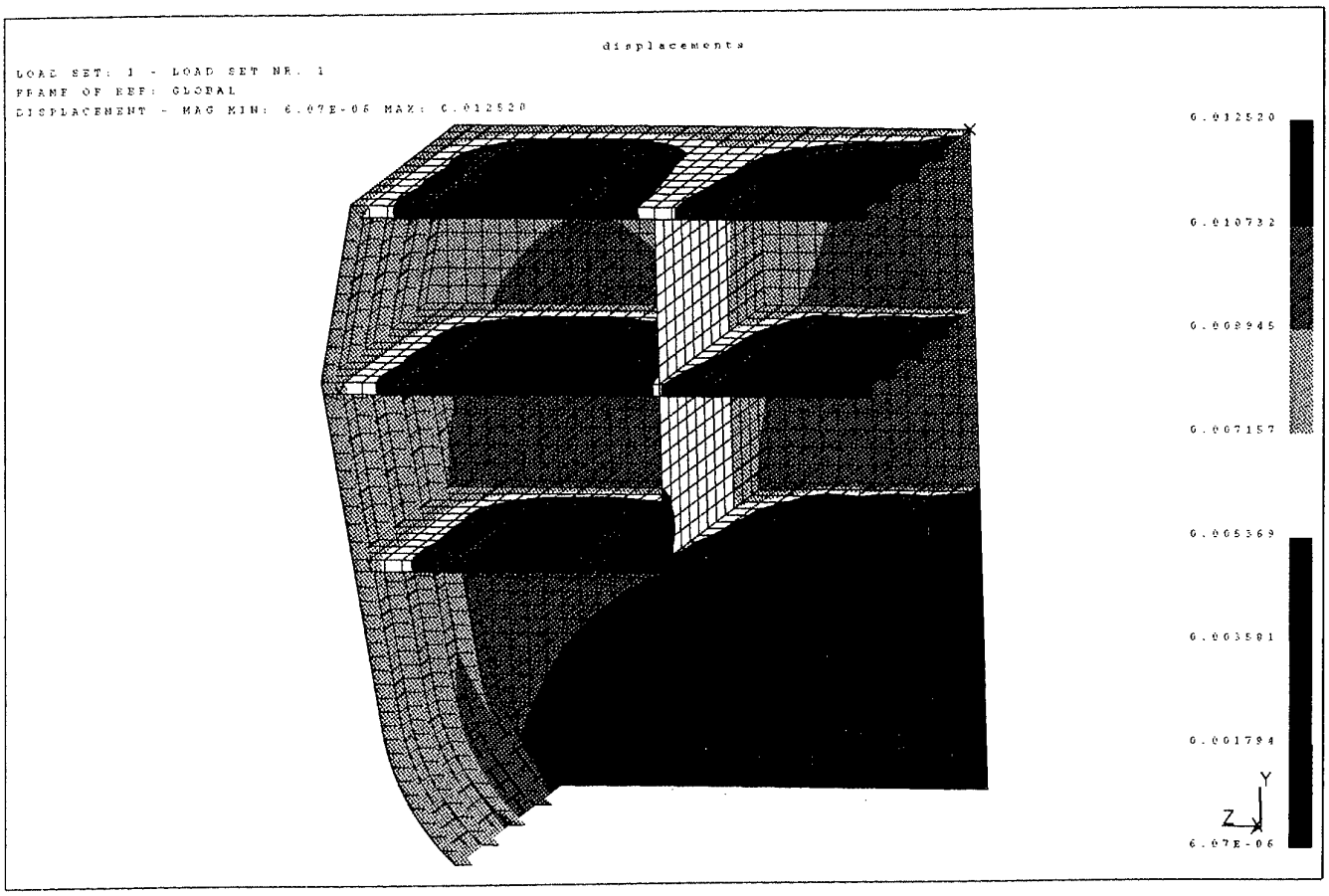

Fig. 3.7 d) Deformed geometry at time = 10.0 ms

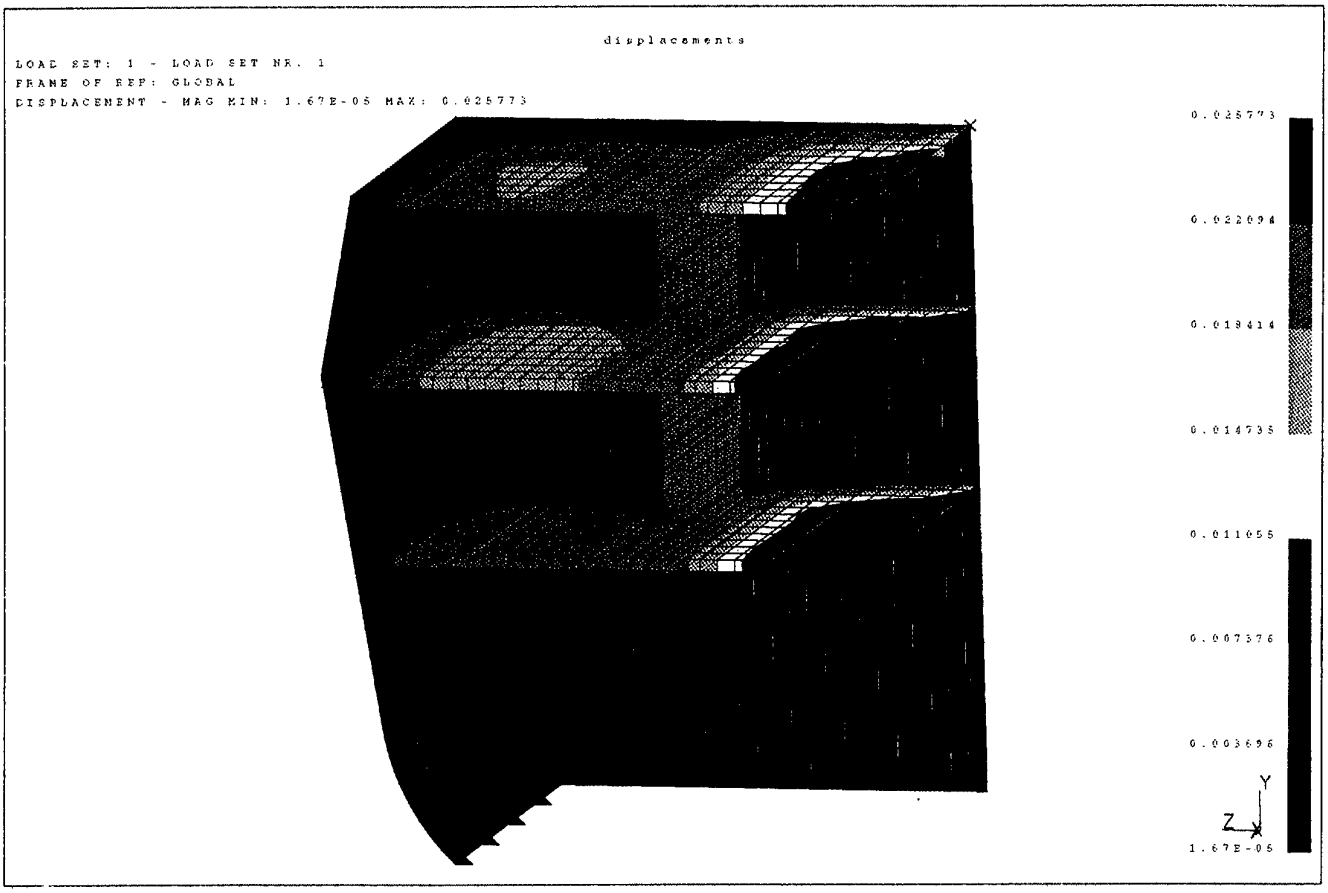

Fig. 3.7 e) Deformed geometry at time = 20.0 ms

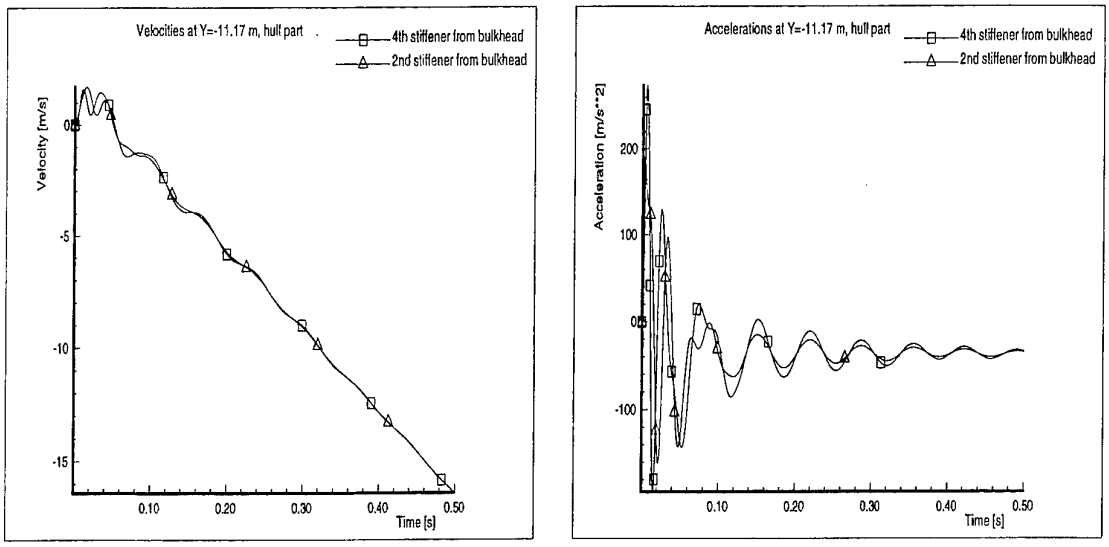

a) Velocities

b) Accelerations

Fig. 3.8 Velocities and accelerations for nodes at Y=-11.17 m, hull part (not excited), modified model including Rayleigh damping

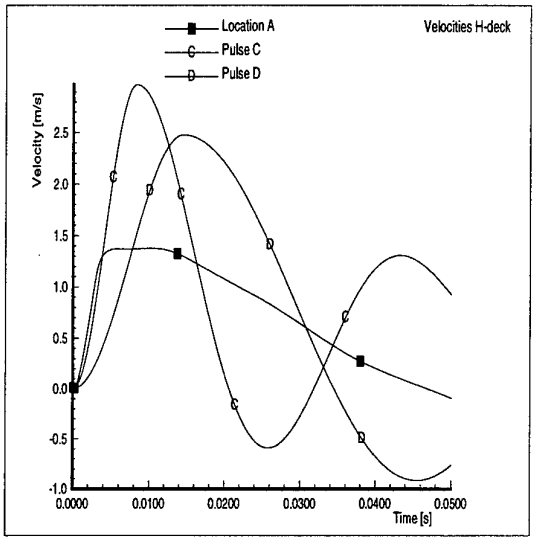

a) Velocities location A (centreline, at bulkhead)

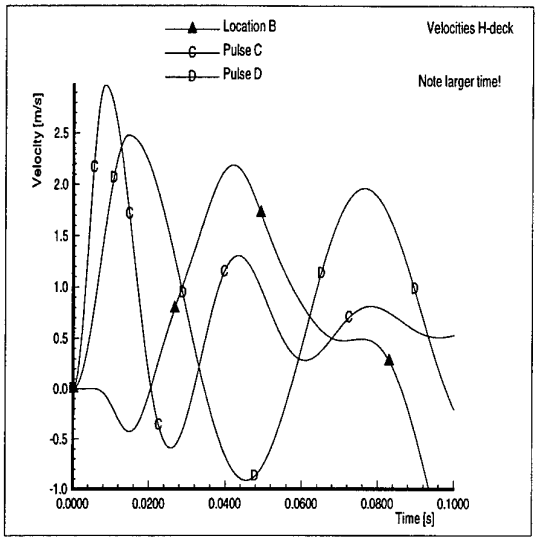

b) Velocities location B (centre of compartment)

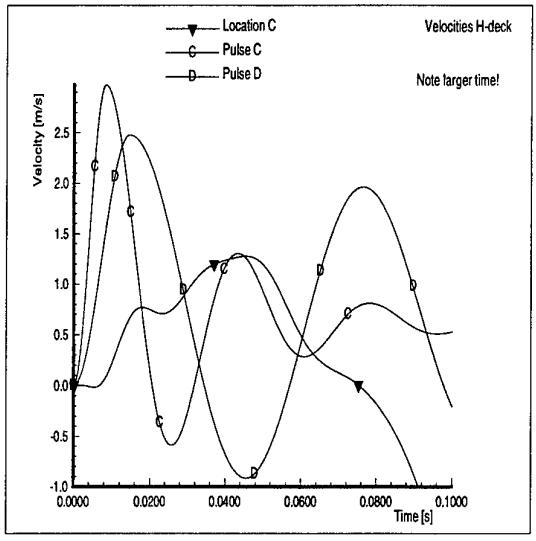

c) Velocities location C (between centreline and corrugated plate)

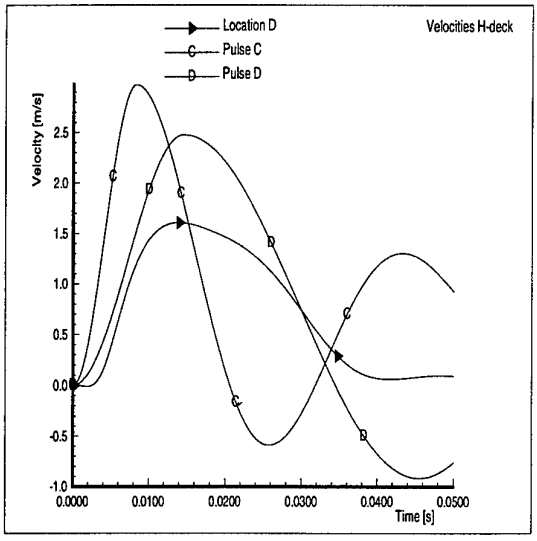

d) Velocities location D (midway compartment at corrugated plate)

Fig. 3.9 Velocities and accelerations as function of time for locations at the H-deck, modified model including Rayleigh damping, compare fig. 4.2 of ref. [2]

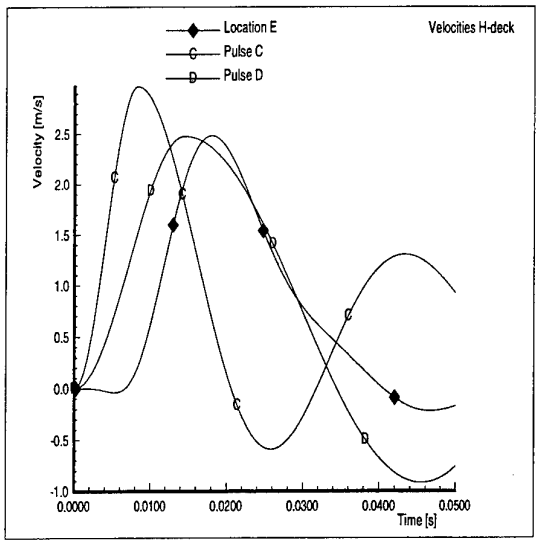

e) Velocities location E (midway between hull and corrugated plate)

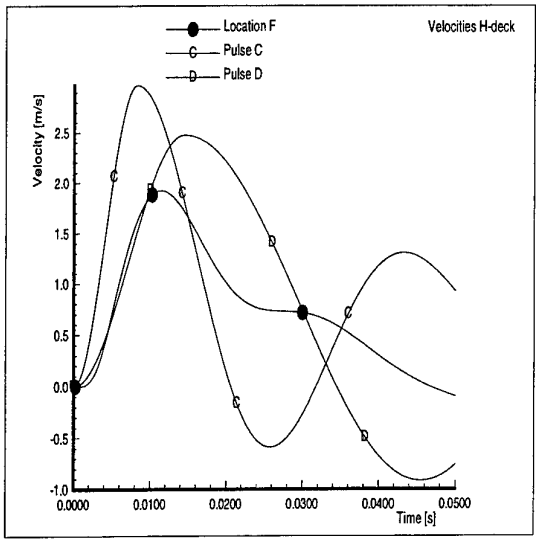

f) Velocities location F (midway compartment, at hull)

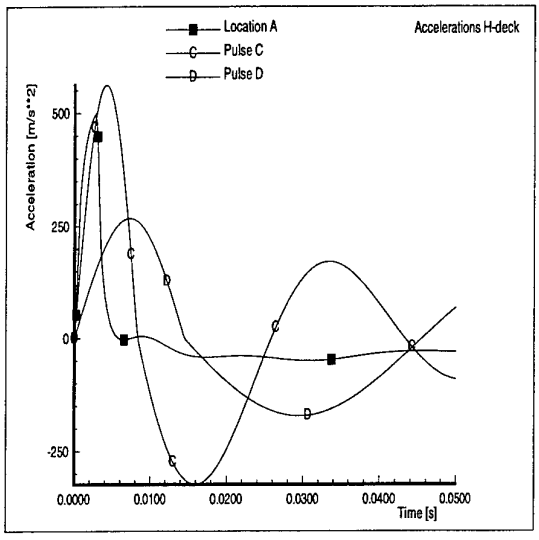

g) Accelerations location A (centreline, at bulkhead)

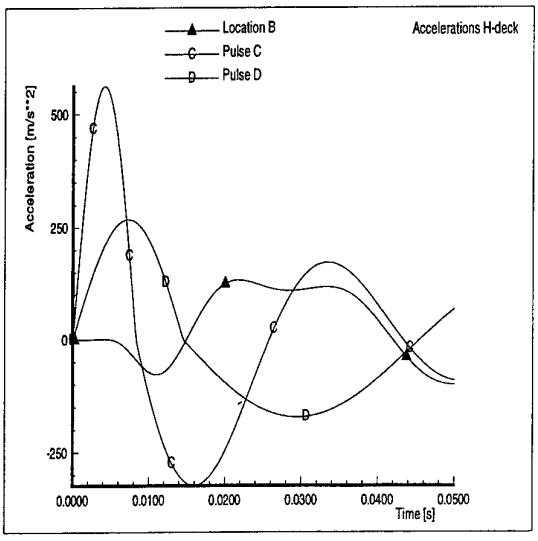

h) Accelerations location B (centre of compartment)

Fig. 3.9 Velocities and accelerations as function of time for locations at the H-deck, modified model including Rayleigh damping, compare fig. 4.2 of ref. [2]

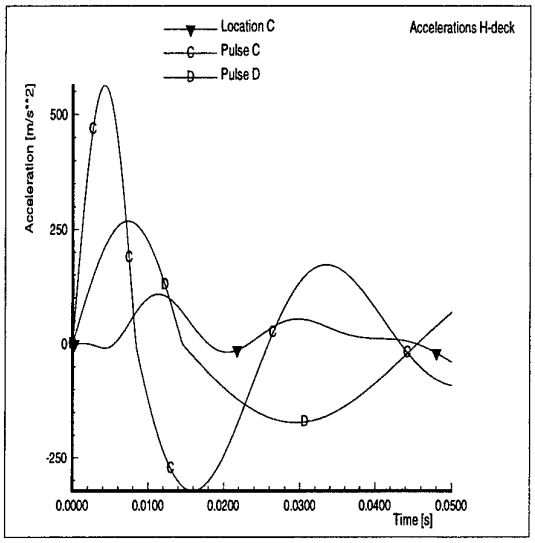

i) Accelerations location C (between centreline and corrugated plate)

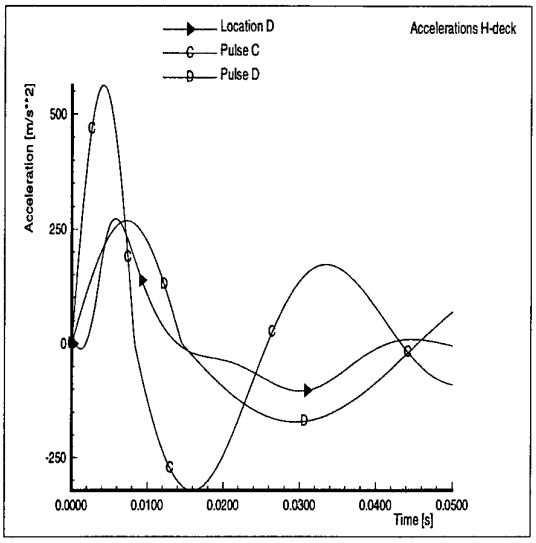

j) Accelerations location D (midway compartment at corrugated plate)

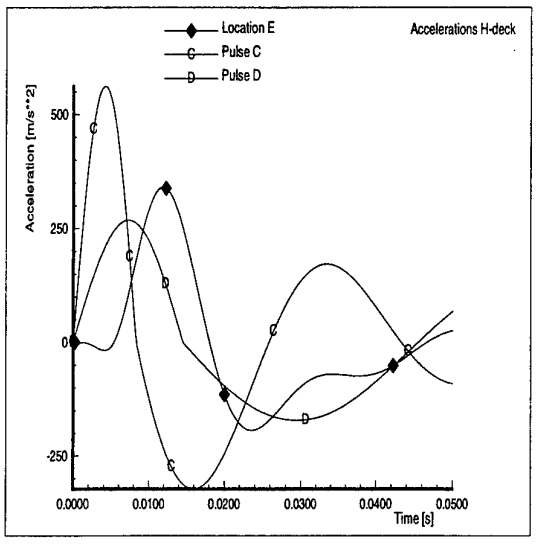

k) Accelerations location E (midway between hull and corrugated plate)

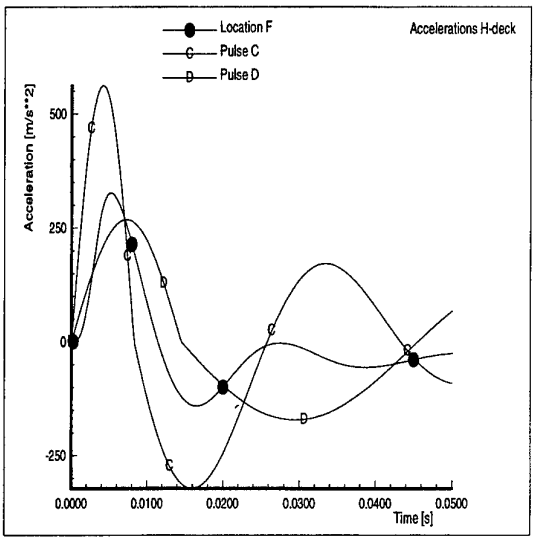

l) Accelerations location F (midway compartment, at hull)

Fig. 3.9 Velocities and accelerations as function of time for locations at the H-deck, modified model including Rayleigh damping, compare fig. 4.2 of ref. [2]

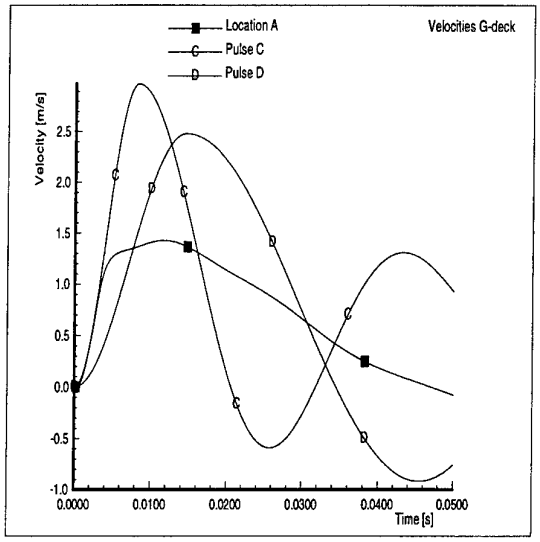

a) Velocities location A (centreline, at bulkhead)

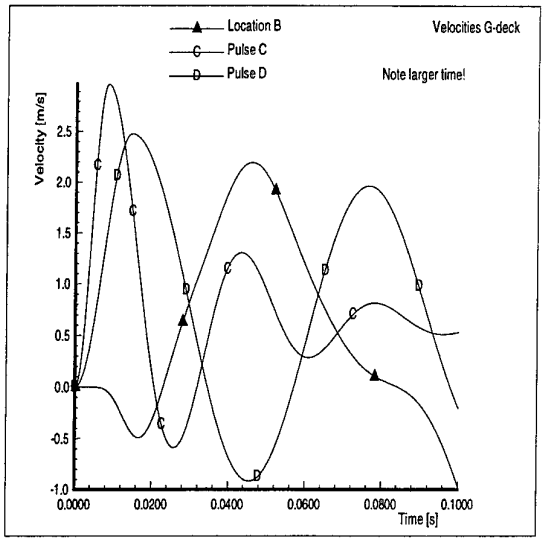

b) Velocities location B (centre of compartment)

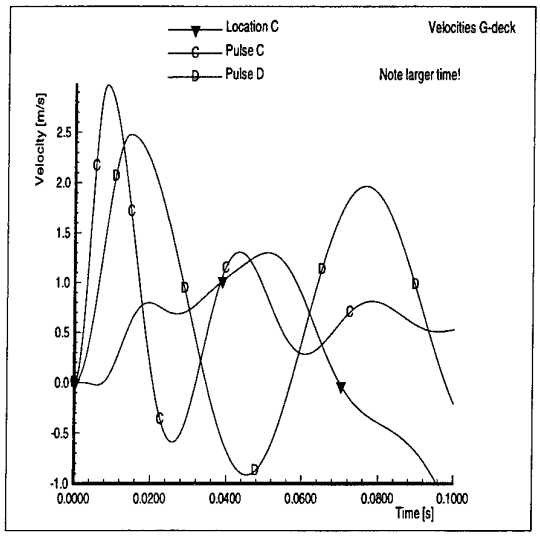

c) Velocities location C (between centreline and corrugated plate)

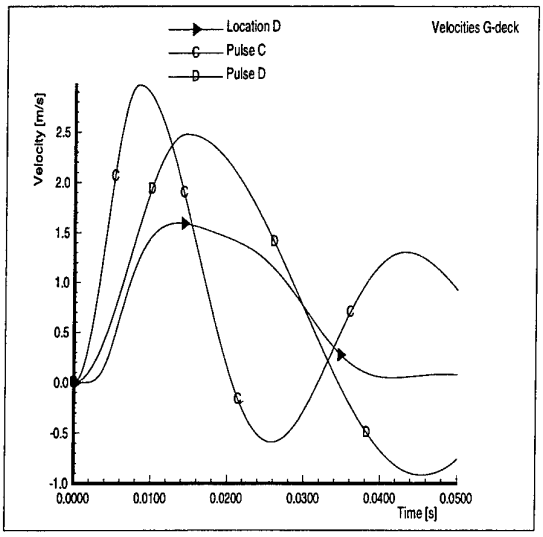

d) Velocities location D (midway compartment at corrugated plate)

Fig. 3.10 Velocities and accelerations as function of time for locations at the G-deck, modified model including Rayleigh damping, compare fig. 4.3 of ref. [2]

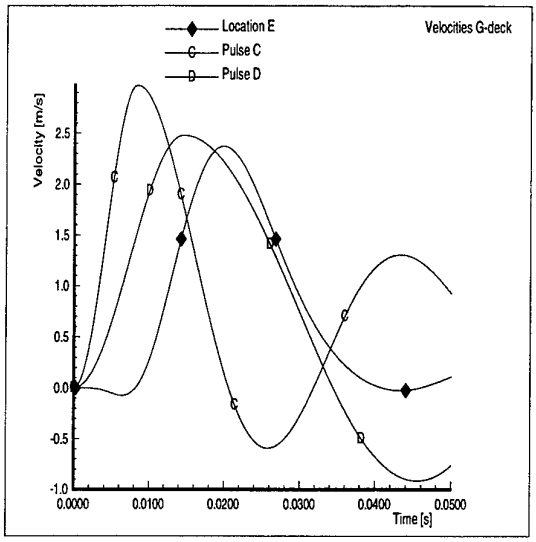

e) Velocities location E (midway between hull and corrugated plate)

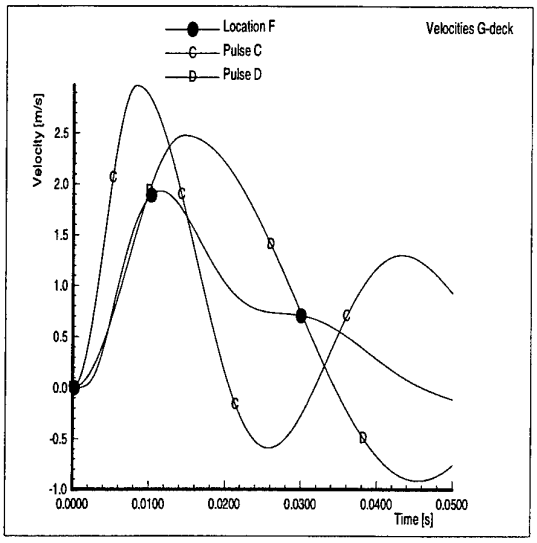

f) Velocities location F (midway compartment, at hull)

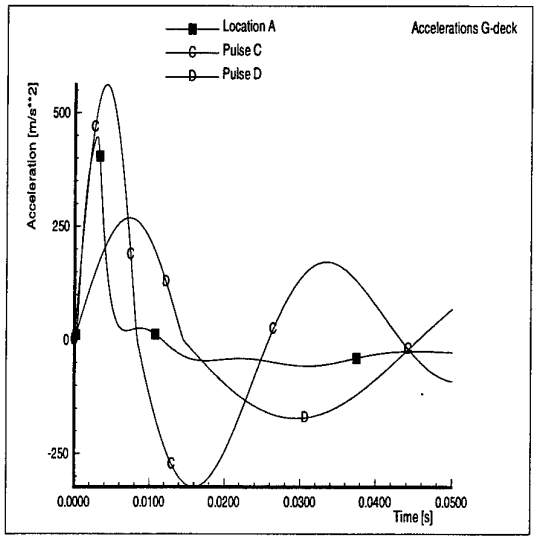

g) Accelerations location A (centreline, at bulkhead)

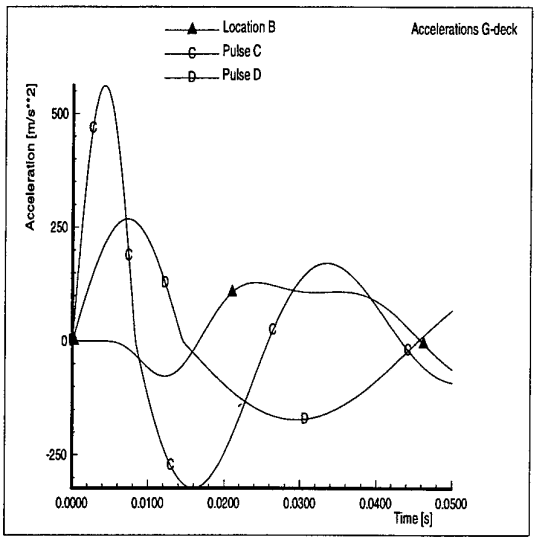

h) Accelerations location B (centre of compartment)

Fig. 3.10 Velocities and accelerations as function of time for locations at the G-deck, modified model including Rayleigh damping, compare fig. 4.3 of ref. [2]

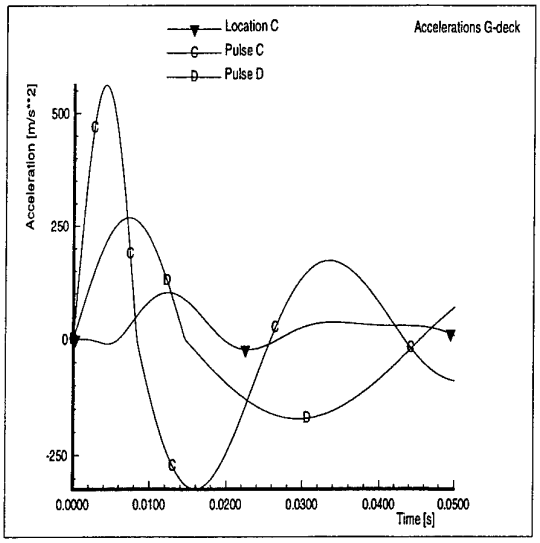

i) Accelerations location C (between centreline and corrugated plate)

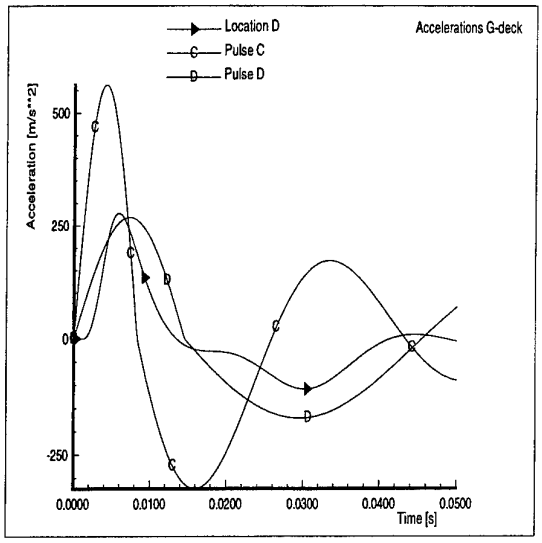

j) Accelerations location D (midway compartment at corrugated plate)

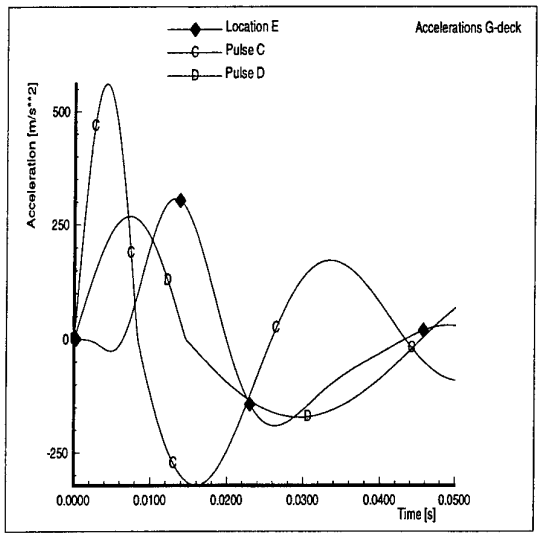

k) Accelerations location E (midway between hull and corrugated plate)

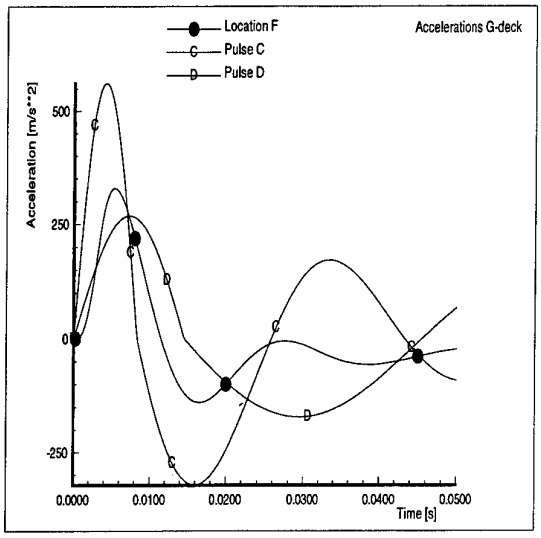

l) Accelerations location F (midway compartment, at hull)

Fig. 3.10 Velocities and accelerations as function of time for locations at the G-deck, modified model including Rayleigh damping, compare fig. 4.3 of ref. [2]

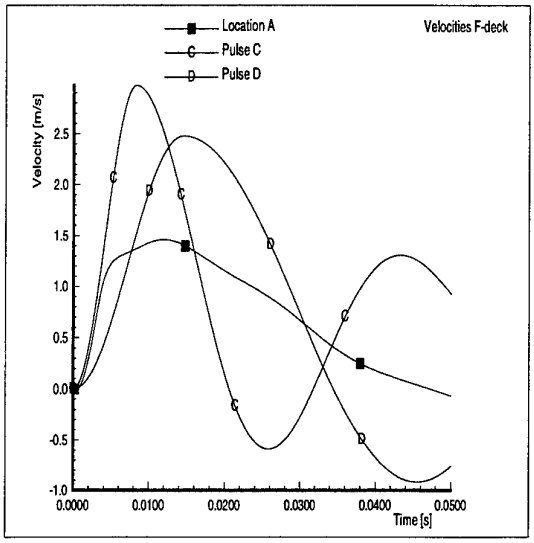

a) Velocities location A (centreline, at bulkhead)

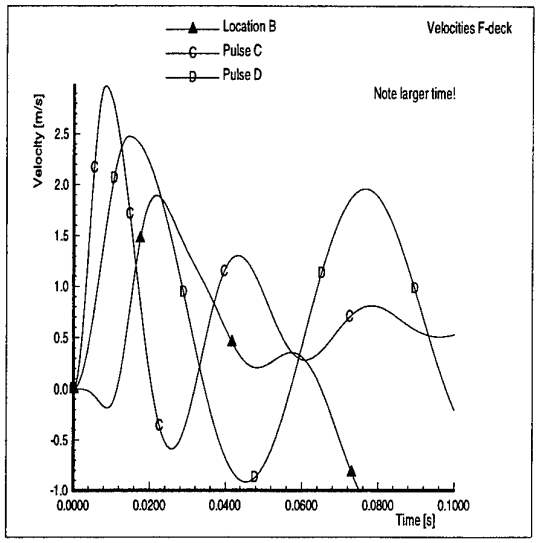

b) Velocities location B (centre of compartment)

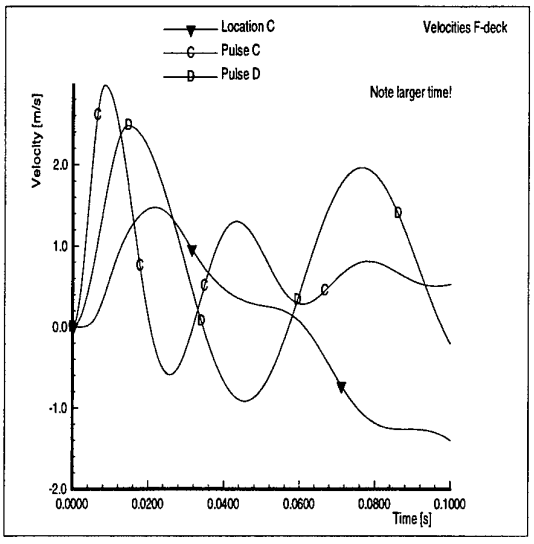

c) Velocities location C (between centreline and corrugated plate)

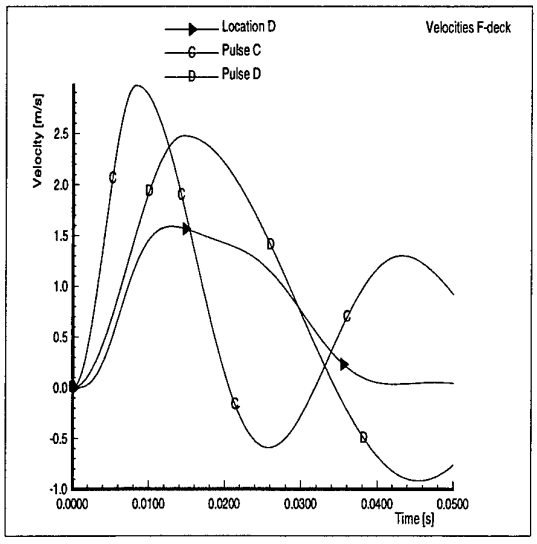

d) Velocities location D (midway compartment at corrugated plate)

Fig. 3.11 Velocities and accelerations as function of time for locations at the F-deck, modified model including Rayleigh damping, compare fig. 4.4 of ref. [2]

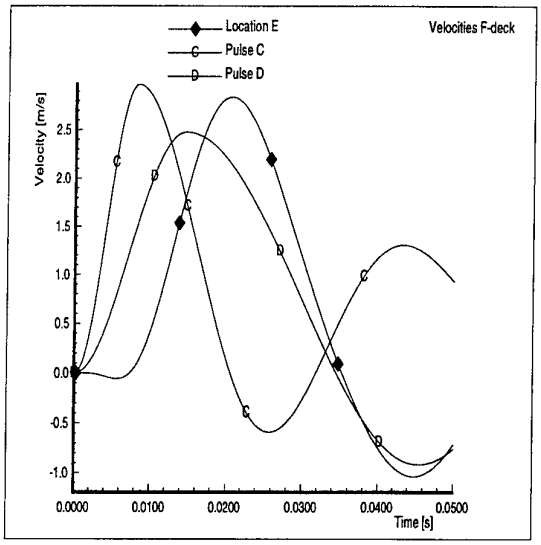

e) Velocities location E (midway between hull and corrugated plate)

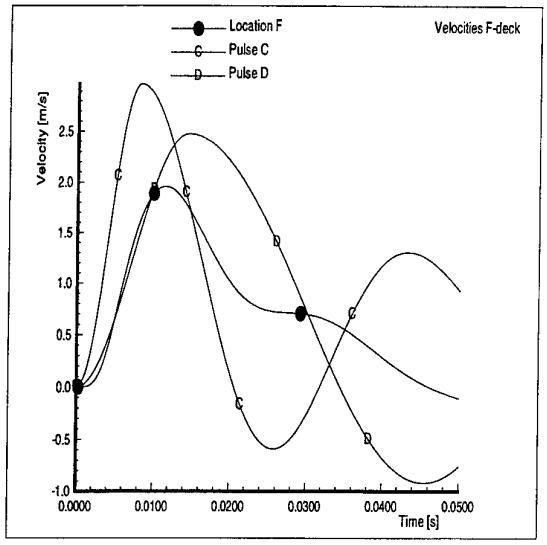

f) Velocities location F (midway compartment, at hull)

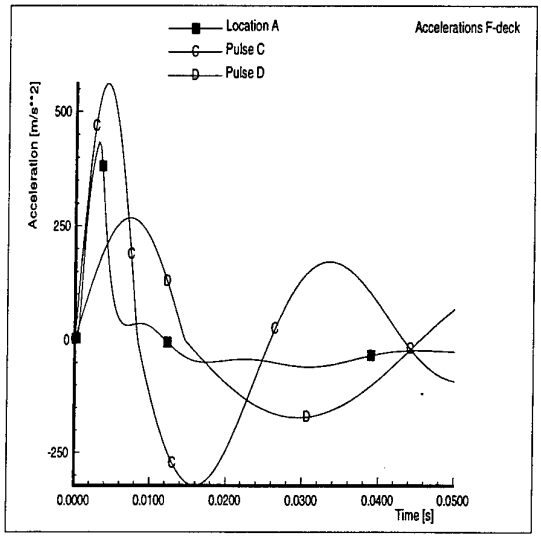

g) Accelerations location A (centreline, at bulkhead)

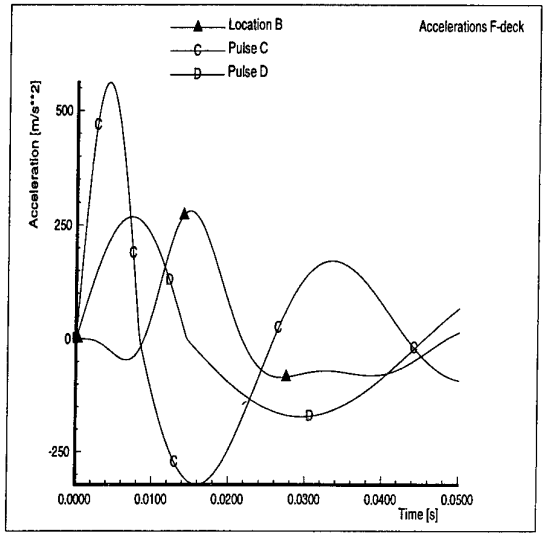

h) Accelerations location B (centre of compartment)

Fig. 3.11 Velocities and accelerations as function of time for locations at the F-deck, modified model including Rayleigh damping, compare fig. 4.4 of ref. [2]

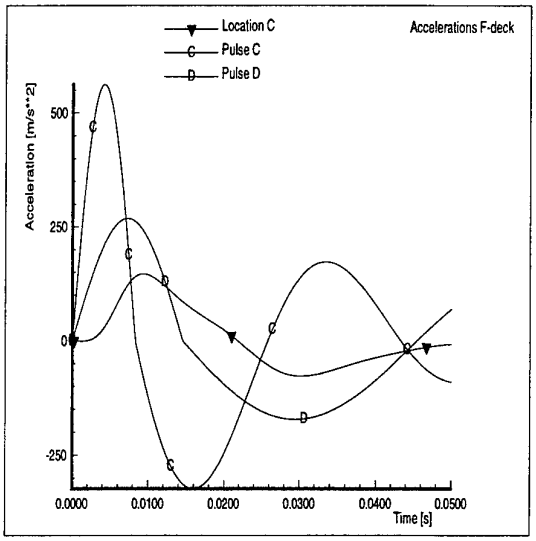

i) Accelerations location C (between centreline and corrugated plate)

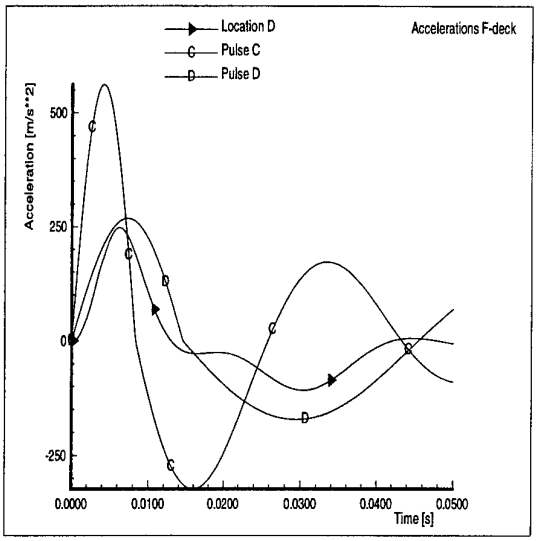

j) Accelerations location D (midway compartment at corrugated plate)

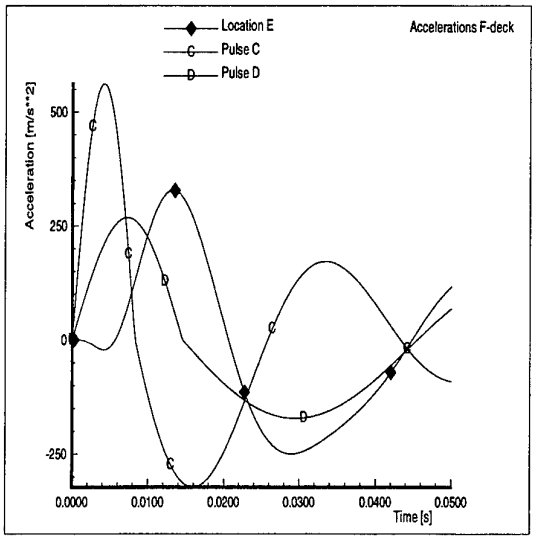

k) Accelerations location E (midway between hull and corrugated plate)

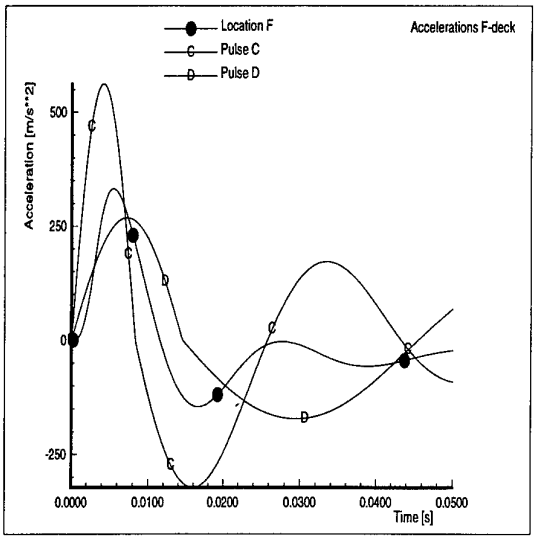

l) Accelerations location F (midway compartment, at hull)

Fig. 3.11 Velocities and accelerations as function of time for locations at the F-deck, modified model including Rayleigh damping, compare fig. 4.4 of ref. [2]

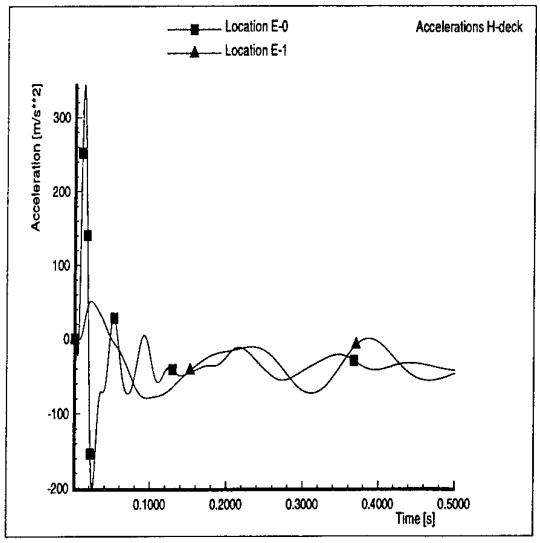

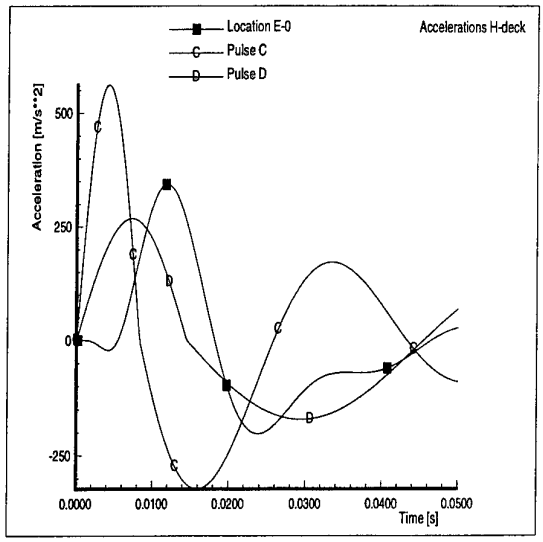

a) Location E-0, E-1, large time period b) Location E-0, short time period
(close to location E (midway hull and corrugated plate), but at discrete mass)

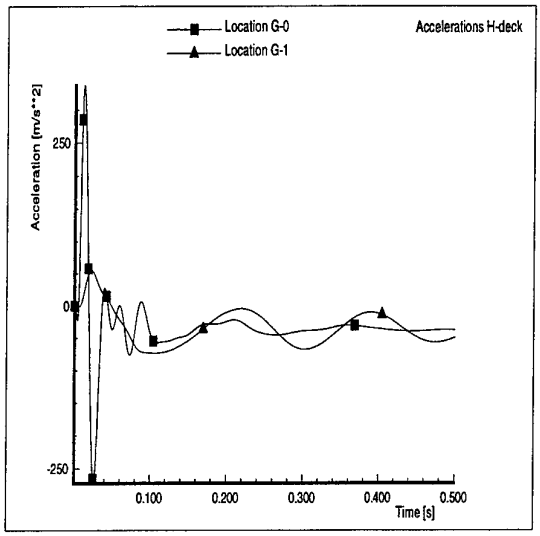

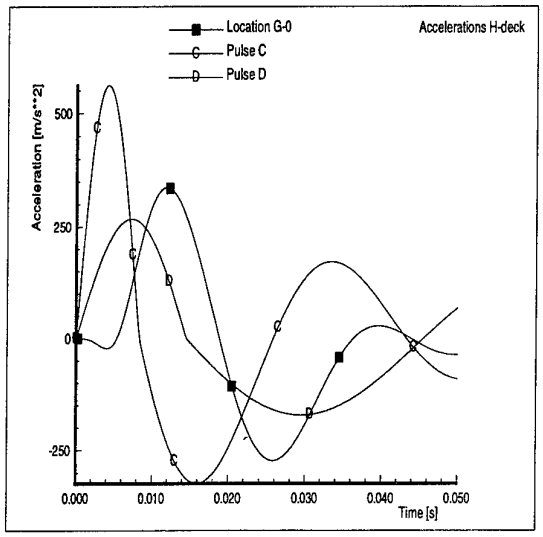

c) Location G-0, G-1, large time period d) Location G-0, short time period
(centre of large deck part between hull and corrugated plate, at discrete mass)

Fig. 3.12 Accelerations as function of time for additional locations at the H-deck (E-0, G-0 are at deck (below spring), E-1, G-1 are at discrete mass (above spring)), modified model including Rayleigh damping

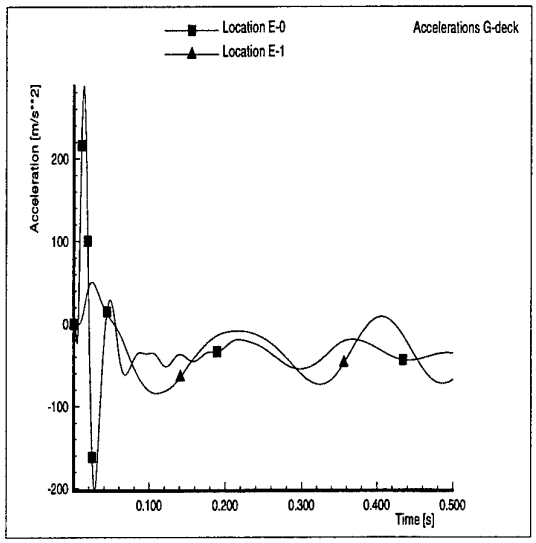

a) Location E-0, E-1, large time period

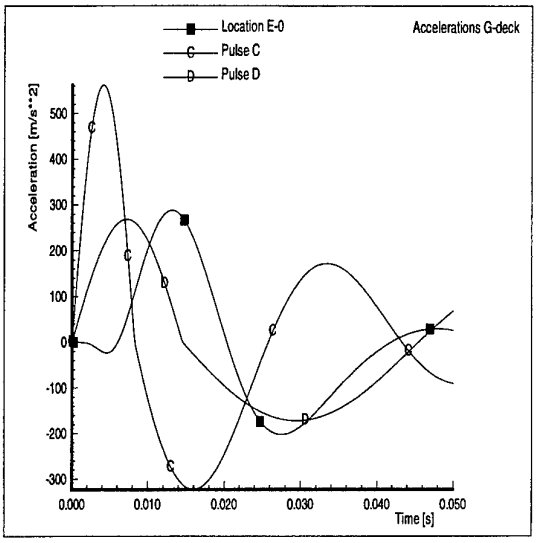

b) Location E-0, short time period
(close to location E (midway hull and corrugated plate), but at discrete mass)

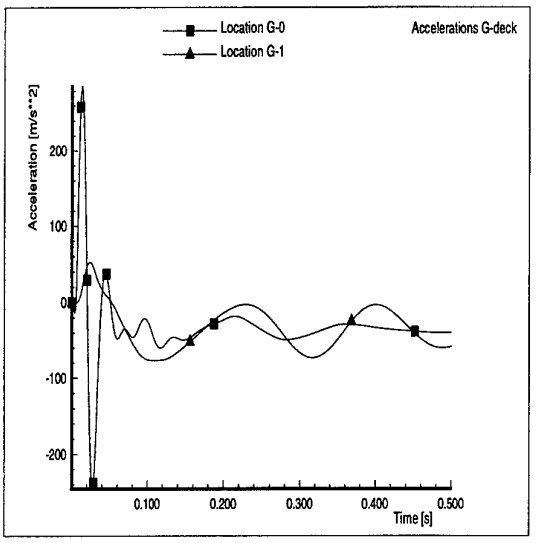

c) Location G-0, G-1, large time period

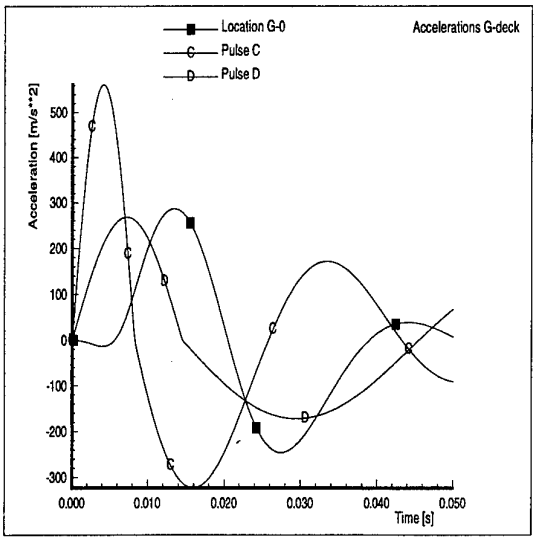

d) Location G-0, short time period
(centre of large deck part between hull and corrugated plate, at discrete mass)

Fig. 3.13 Accelerations as function of time for additional locations at the G-deck (E-0, G-0 are at deck (below spring), E-1, G-1 are at discrete mass (above spring)), modified model including Rayleigh damping

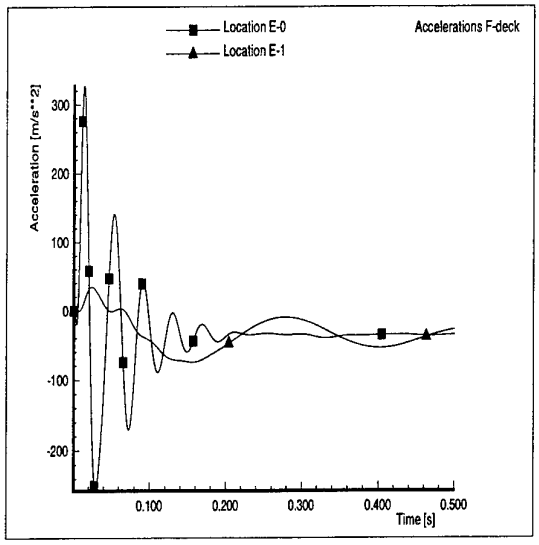

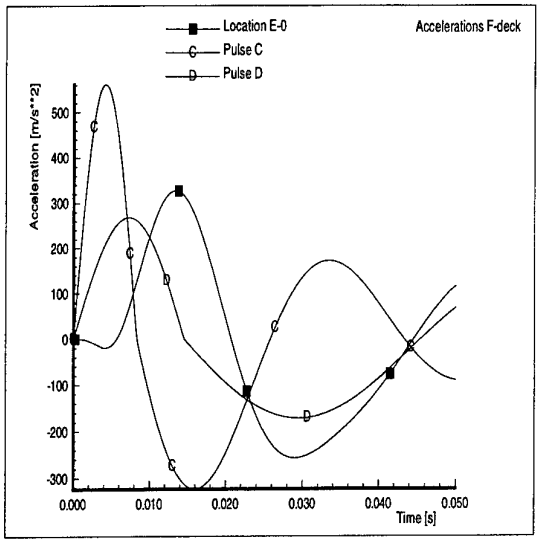

a) Location E-0, E-1, large time period b) Location E-0, short time period
(close to location E (midway hull and corrugated plate), but at discrete mass)

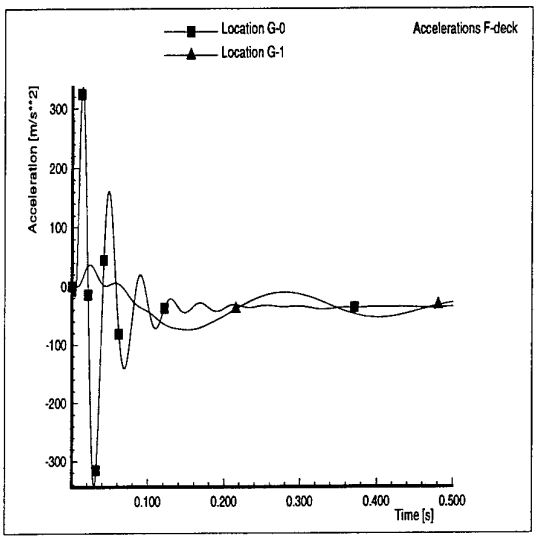

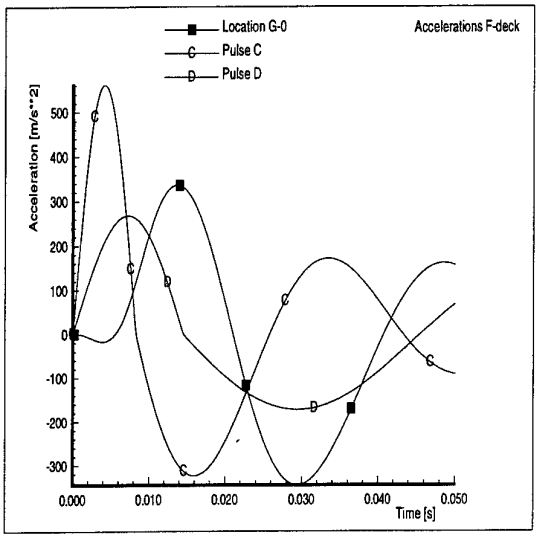

c) Location G-0, G-1, large time period d) Location G-0, short time period
(centre of large deck part between hull and corrugated plate, at discrete mass)

Fig. 3.14 Accelerations as function of time for additional locations at the F-deck (E-0, G-0 are at deck (below spring), E-1, G-1 are at discrete mass (above spring)), modified model including Rayleigh damping

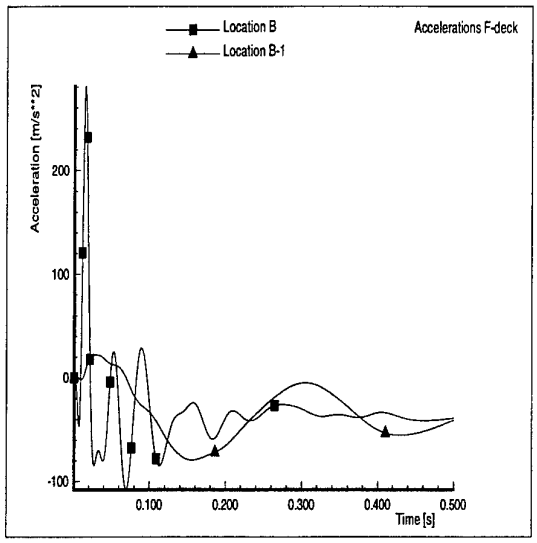

e) Location B (at deck, centre of compartment) and B-1 (above spring), at discrete mass

Fig. 3.14 Accelerations as function of time for additional locations at the F-deck (E-0, G-0 are at deck (below spring), E-1, G-1 are at discrete mass (above spring)), modified model including Rayleigh damping

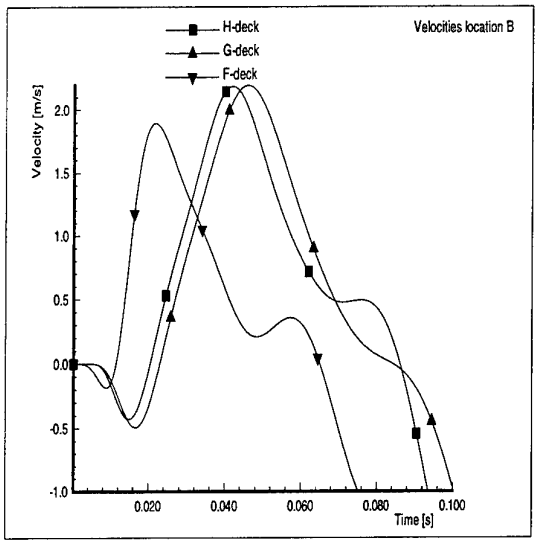

a) Velocities

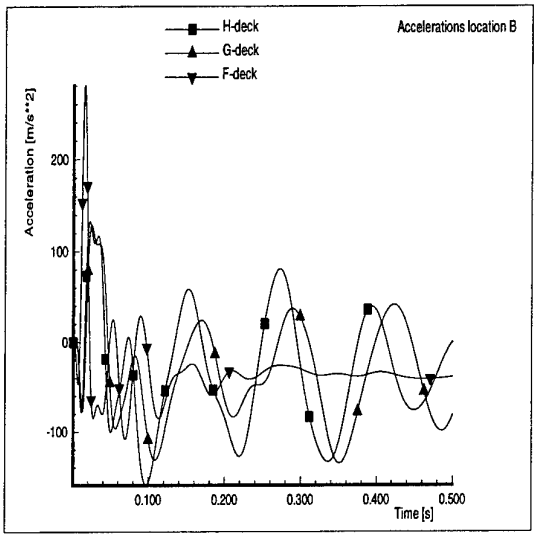

b) Accelerations, large time period

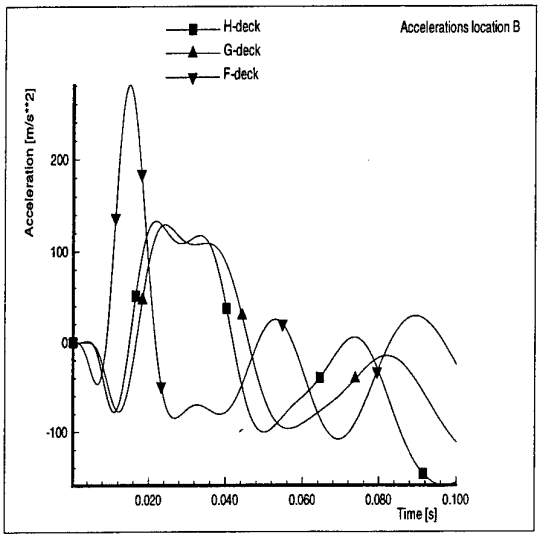

c) Accelerations, short time period

Fig. 3.15 Comparison of velocities and accelerations as function of time for location B (centre of compartment) of all decks, modified model including Rayleigh damping, compare fig. 4.6 and 4.7 of ref. [2]

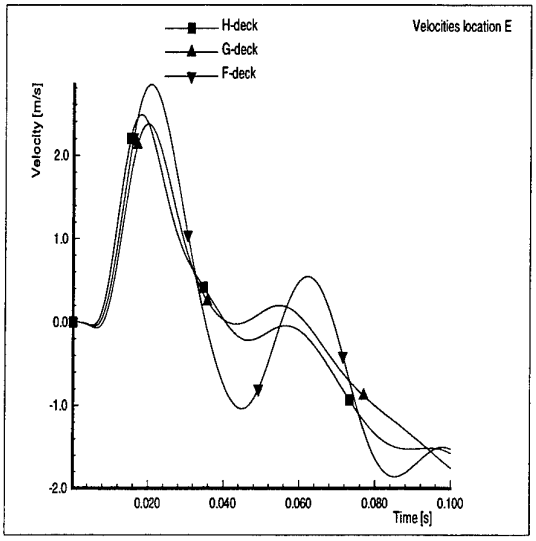

a) Velocities

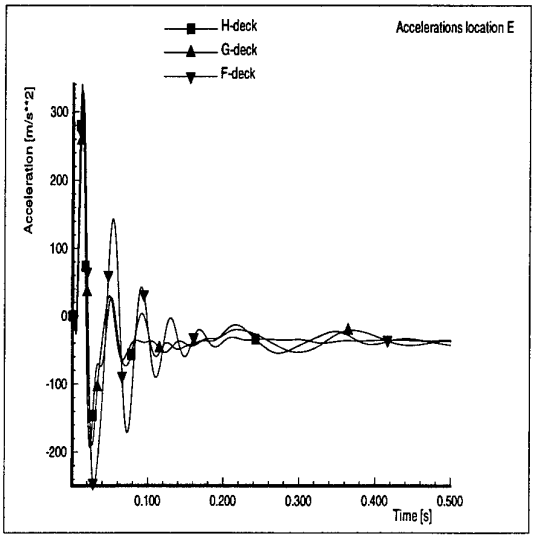

b) Accelerations, large time period

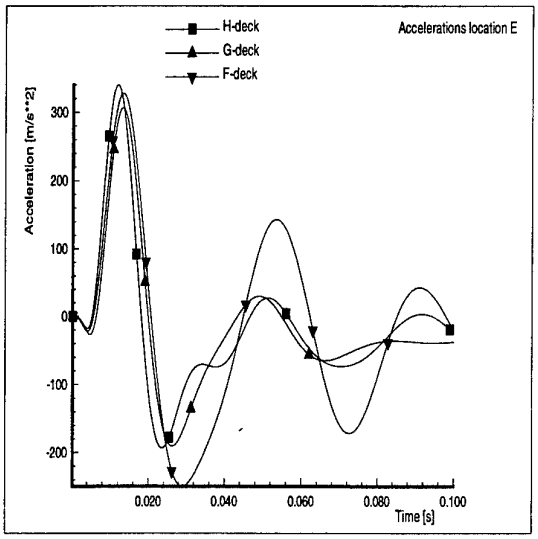

c) Accelerations, short time period

Fig. 3.16 Comparison of velocities and accelerations as function of time for location E (midway between hull and corrugated plate) of all decks, modified model including Rayleigh damping, compare fig. 4.6 and 4.7 of ref. [2]

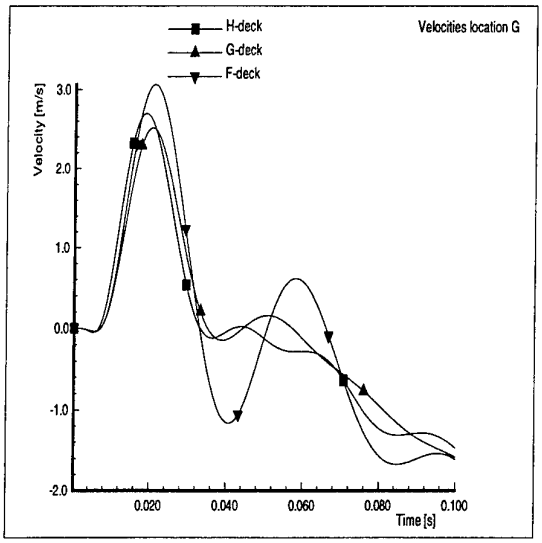

a) Velocities

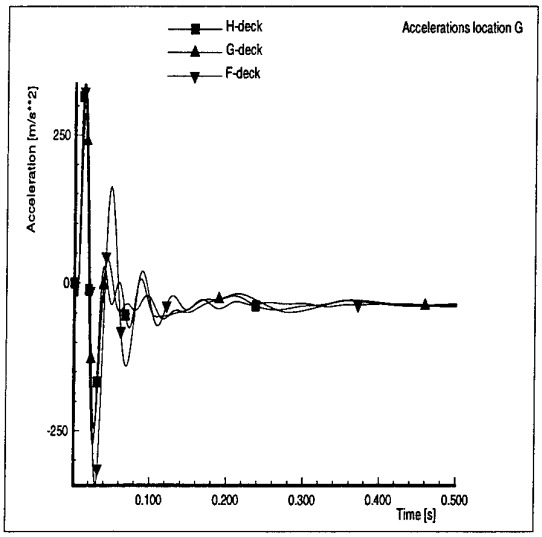

b) Accelerations, large time period

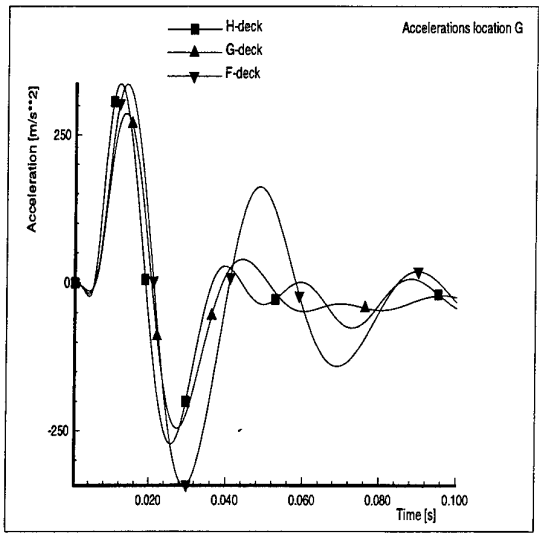

c) Accelerations, short time period

Fig. 3.17 Comparison of velocities and accelerations as function of time for location G (centre of large deck part between hull and corrugated plate) of all decks, modified model including Rayleigh damping, compare fig. 4.6 and 4.7 of ref. [2]

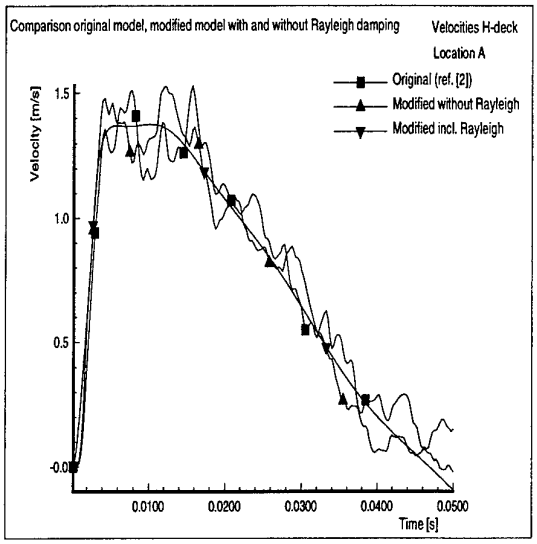

a) Location A
(centreline, at bulkhead)

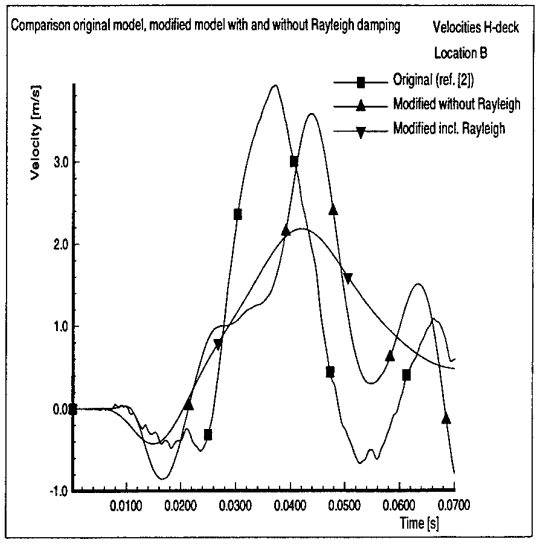

b) Location B
(centre of compartment)

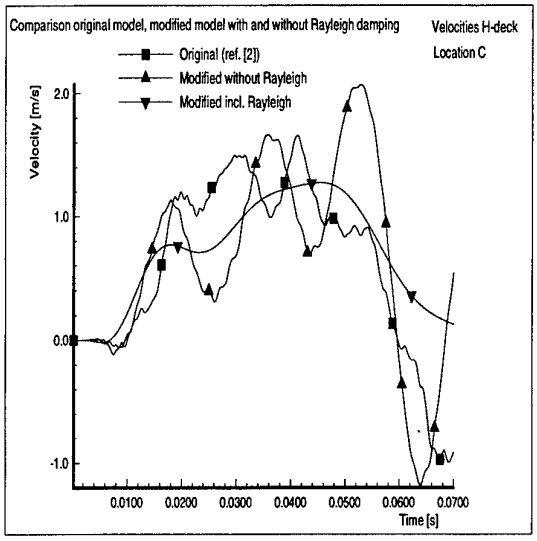

c) Location C (between
centreline and corrugated plate)

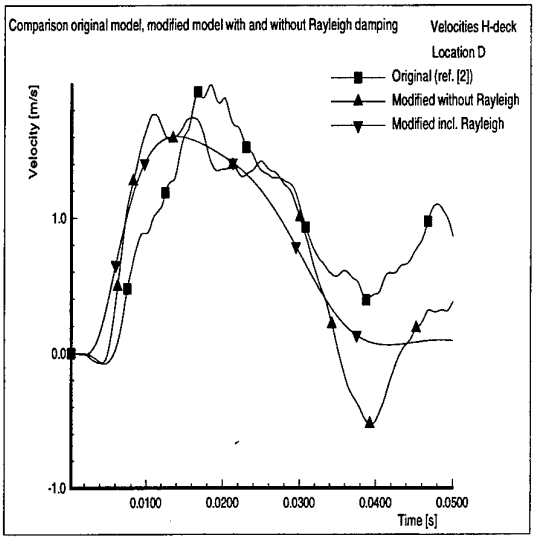

d) Location D (midway
compartment at corrugated plate)

Fig. 4.1 Comparison of velocities of H-deck of three analysis, namely original model from ref. [2] (fig. 4.2 - 4.4), modified model including Rayleigh damping, and modified model without Rayleigh damping

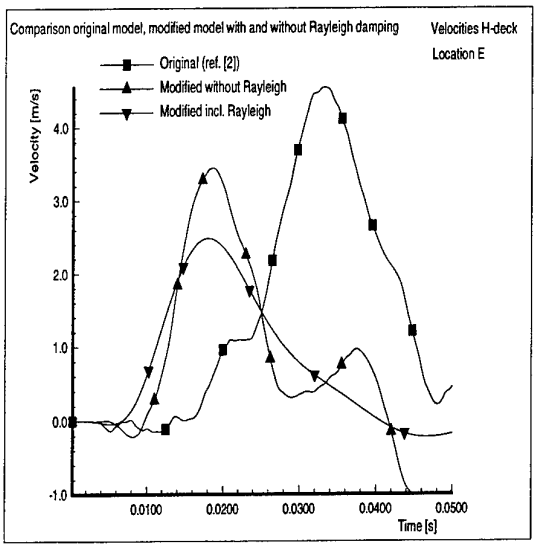

e) Location E (midway between hull and corrugated plate)

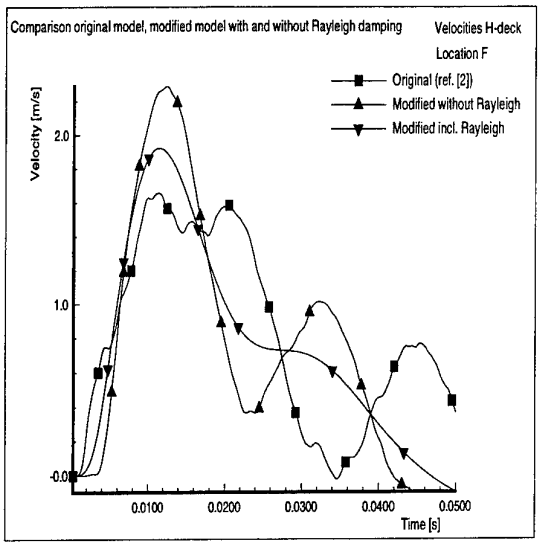

f) Location F (midway compartment, at hull)

Fig. 4.1 Comparison of velocities of H-deck of three analysis, namely original model from ref. [2] (fig. 4.2 - 4.4), modified model including Rayleigh damping, and modified model without Rayleigh damping

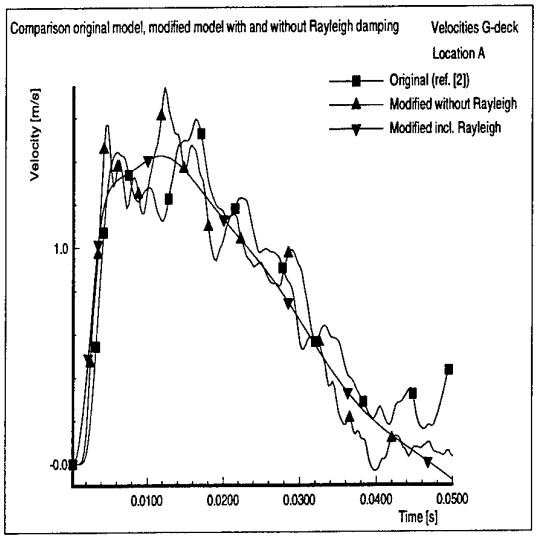

a) Location A (centreline, at bulkhead)

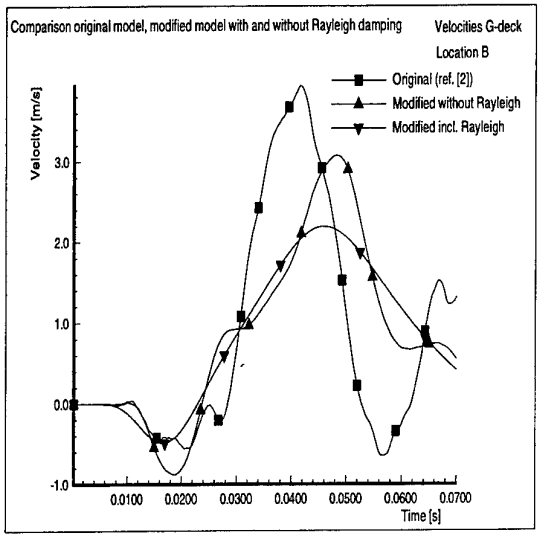

b) Location B (centre of compartment)

Fig. 4.2 Comparison of velocities of G-deck of three analysis, namely original model from ref. [2] (fig. 4.2 - 4.4), modified model including Rayleigh damping, and modified model without Rayleigh damping

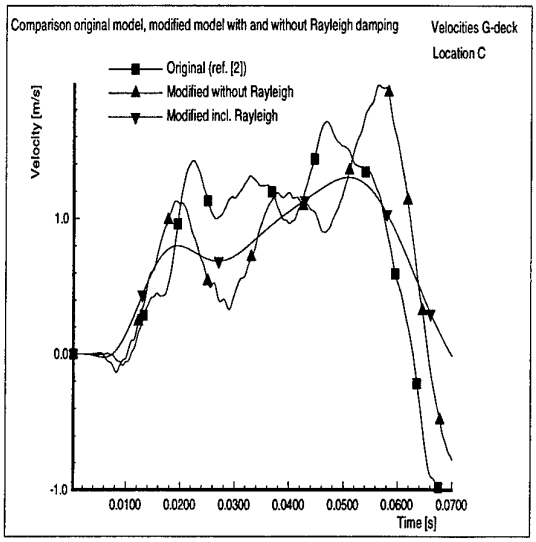

c) Location C (between centreline and corrugated plate)

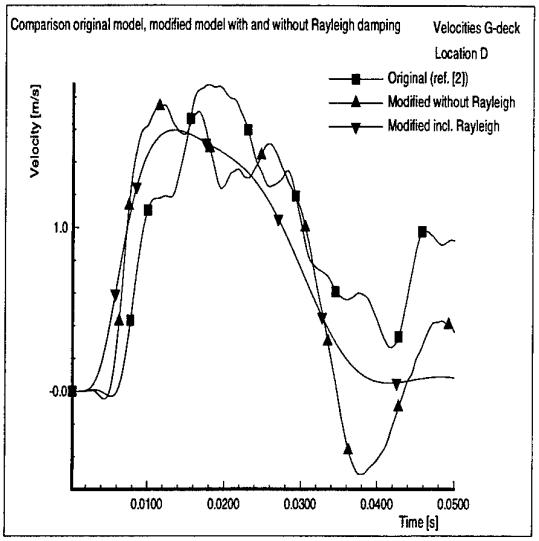

d) Location D (midway (compartment at corrugated plate)

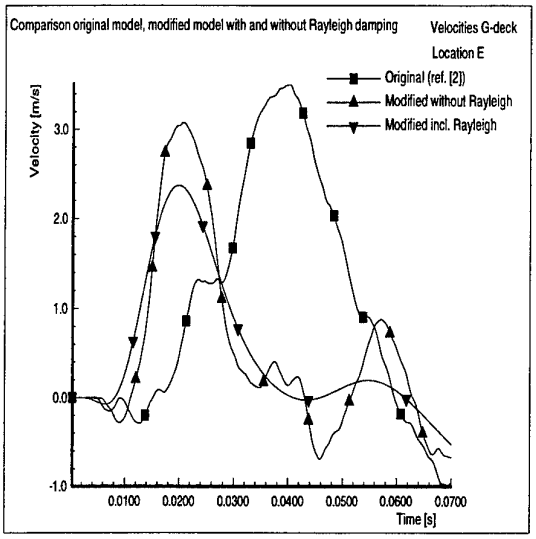

e) Location E (midway between hull and corrugated plate)

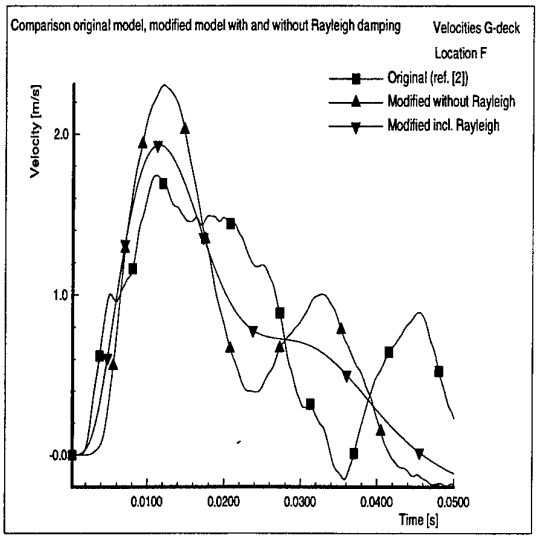

f) Location F (midway compartment, at hull)

Fig. 4.2 Comparison of velocities of G-deck of three analysis, namely original model from ref. [2] (fig. 4.2 - 4.4), modified model including Rayleigh damping, and modified model without Rayleigh damping

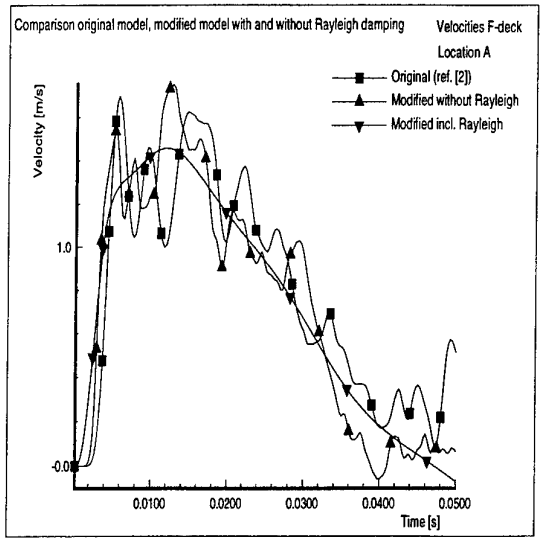

a) Location A
(centreline, at bulkhead)

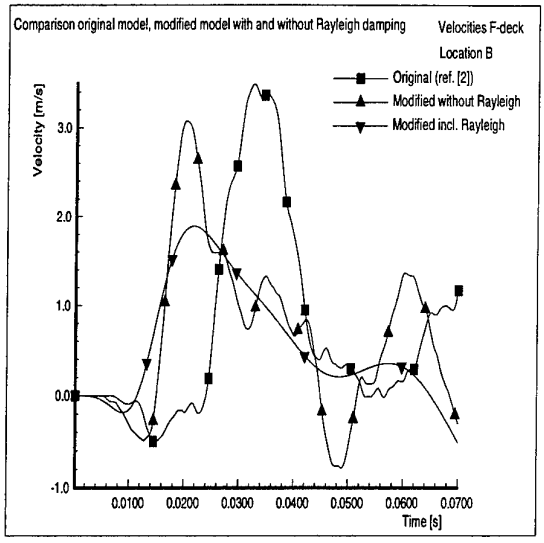

b) Location B
(centre of compartment)

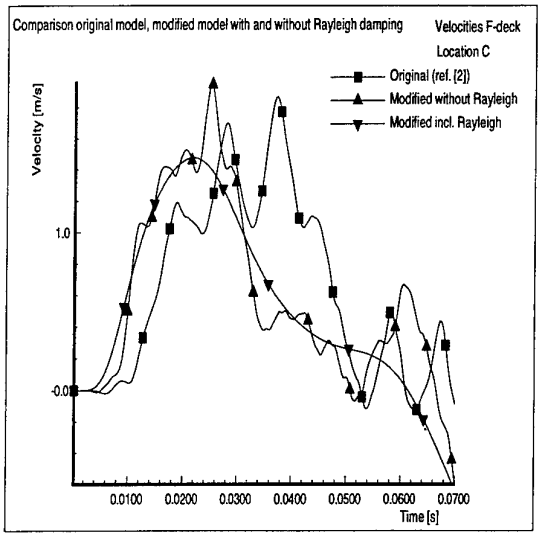

c) Location C (between
centreline and corrugated plate)

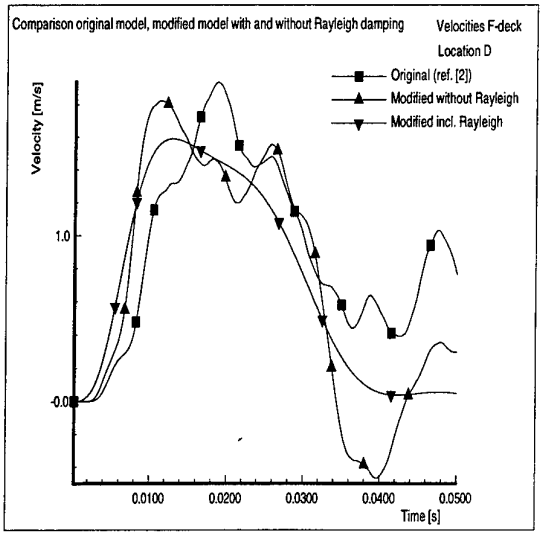

d) Location D (midway
compartment at corrugated plate)

Fig. 4.3 Comparison of velocities of F-deck of three analysis, namely original model from ref. [2] (fig. 4.2 - 4.4), modified model including Rayleigh damping, and modified model without Rayleigh damping

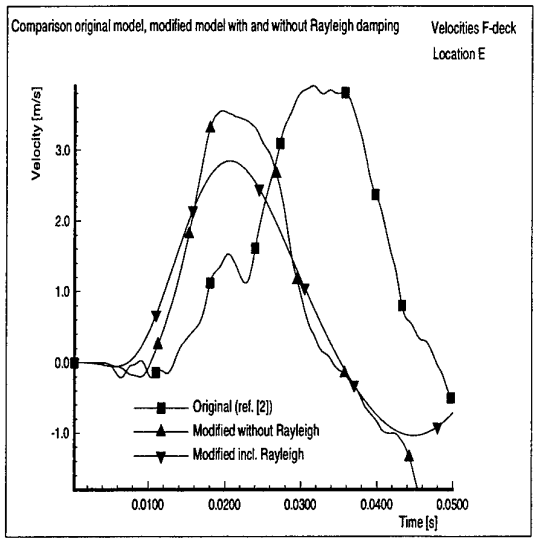

e) Location E (midway between hull and corrugated plate)

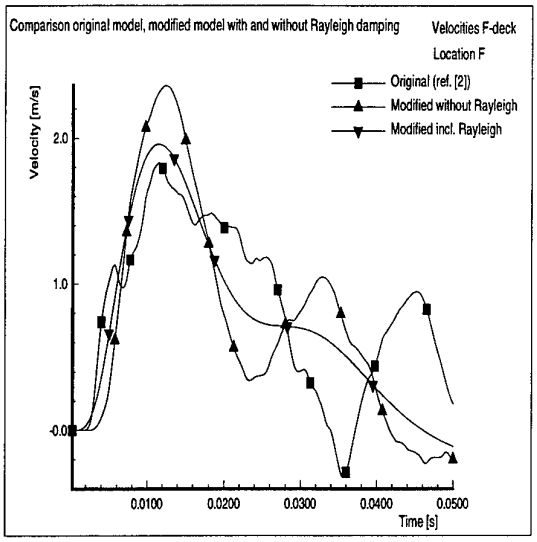

f) Location F (midway compartment, at hull)

Fig. 4.3 Comparison of velocities of F-deck of three analysis, namely original model from ref. [2] (fig. 4.2 - 4.4), modified model including Rayleigh damping, and modified model without Rayleigh damping

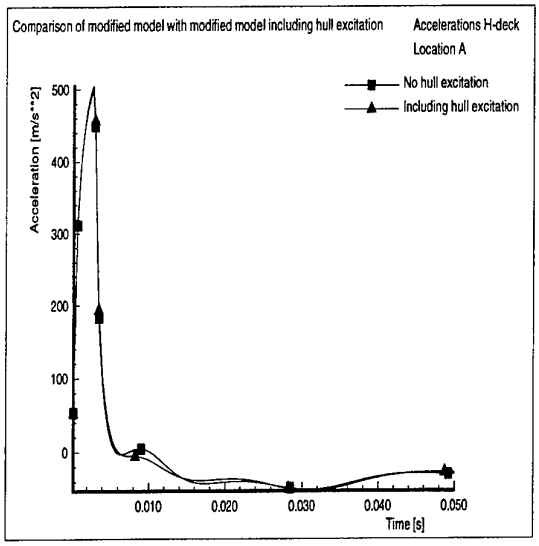

a) Location A
(centreline, at bulkhead)

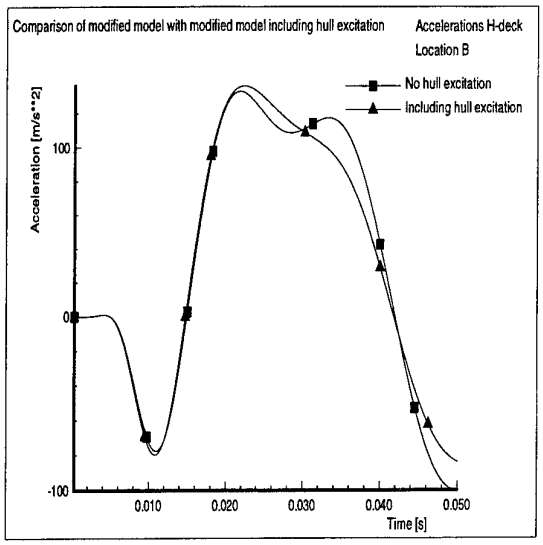

b) Location B
(centre of compartment)

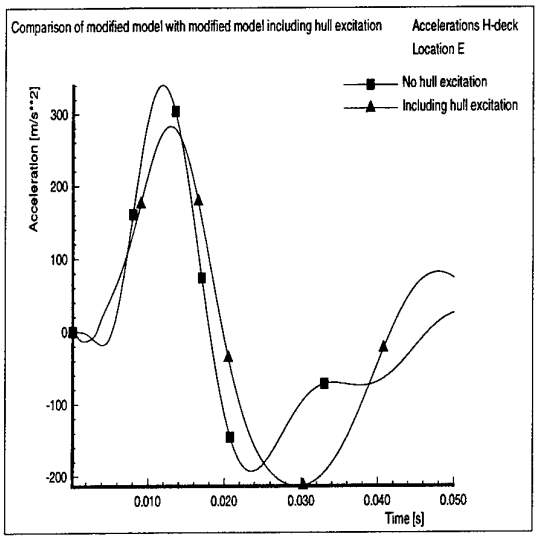

c) Location E (midway
between hull and corrugated plate)

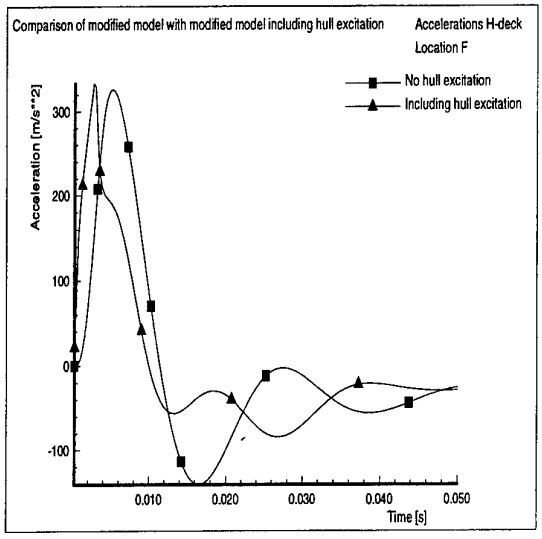

d) Location F
(midway compartment, at hull)

Fig. 4.4 Comparison of accelerations of the H-deck of two analysis, namely modified model from chapter 3 and modified model while including the kick-off pulse at the hull at Y=-11.17 m

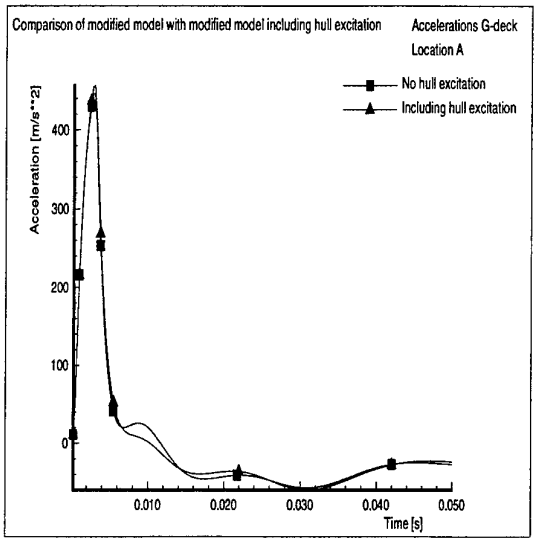

a) Location A
(centreline, at bulkhead)

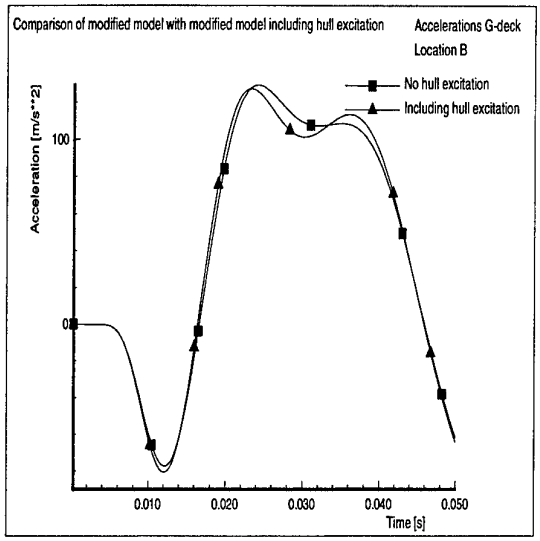

b) Location B
(centre of compartment)

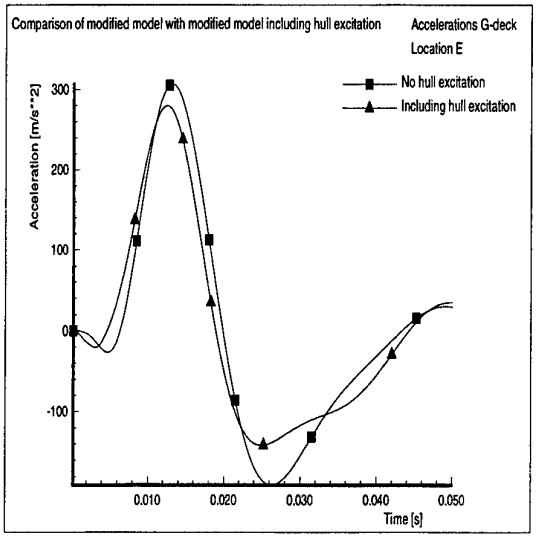

c) Location E (midway
between hull and corrugated plate)

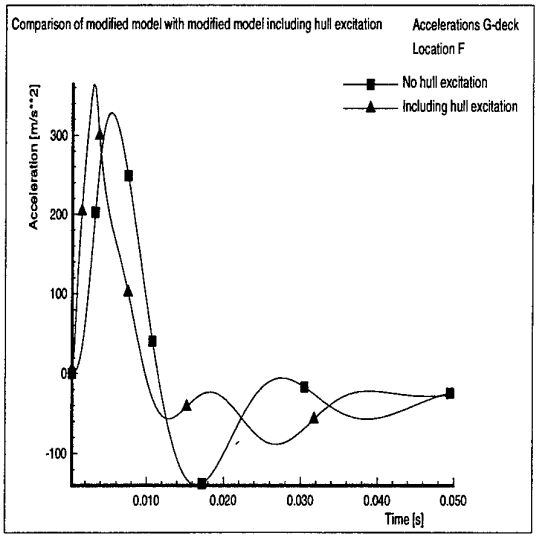

d) Location F
(midway compartment, at hull)

Fig. 4.5 Comparison of accelerations of the G-deck of two analysis, namely modified model from chapter 3 and modified model while including the kick-off pulse at the hull at Y=-11.17 m

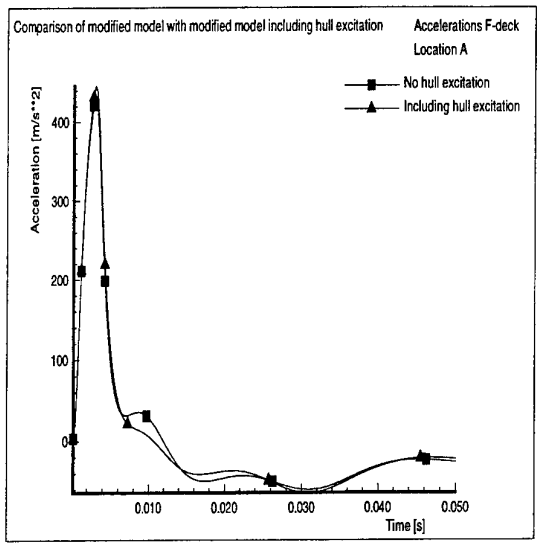

a) Location A
(centreline, at bulkhead)

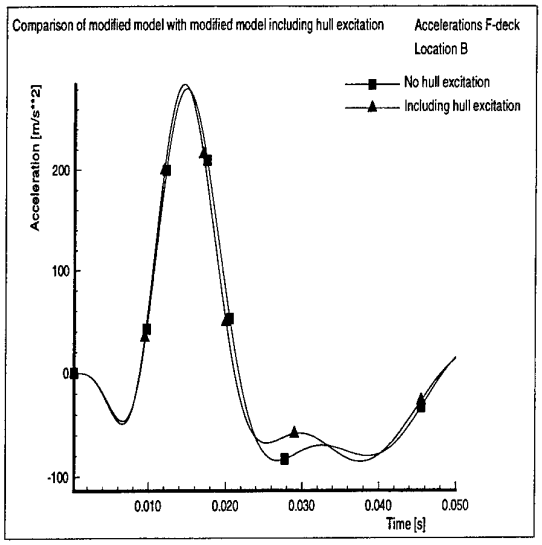

b) Location B
(centre of compartment)

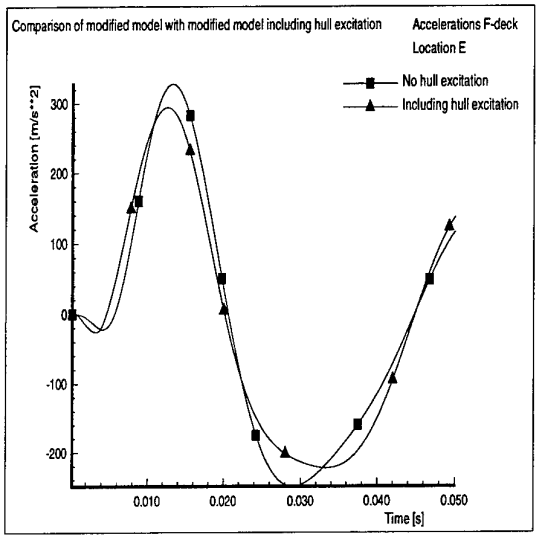

c) Location E (midway
between hull and corrugated plate)

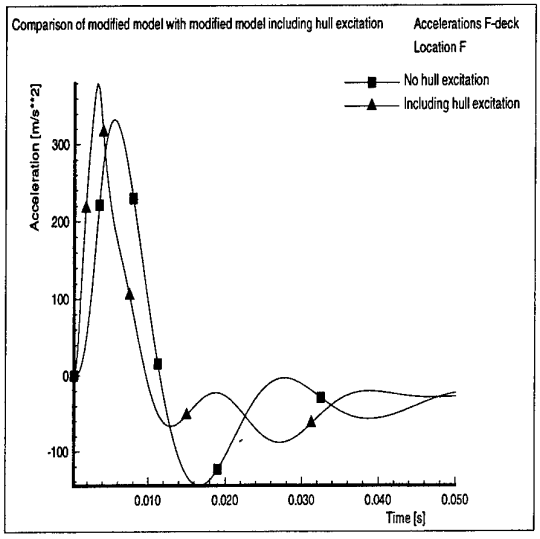

d) Location F
(midway compartment, at hull)

Fig. 4.6 Comparison of accelerations of the F-deck of two analysis, namely modified model from chapter 3 and modified model while including the kick-off pulse at the hull at Y=-11.17 m

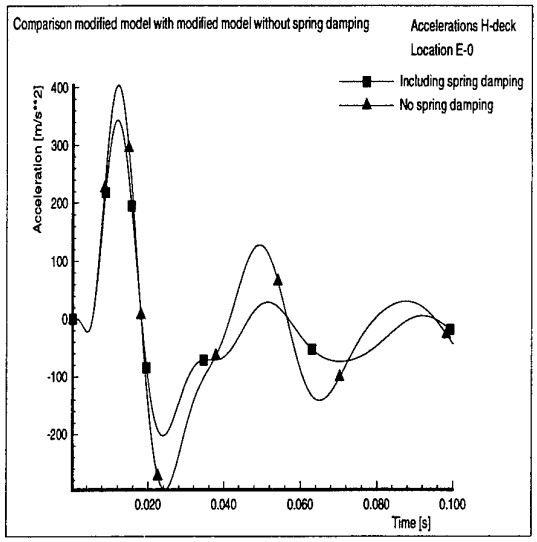

a) Location E-0 (below spring)

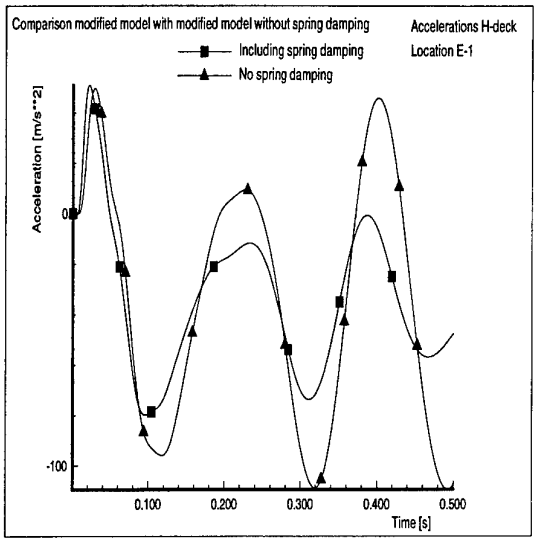

b) Location E-1 (above spring)

(close to location E (midway hull and corrugated plate), but at discrete mass)

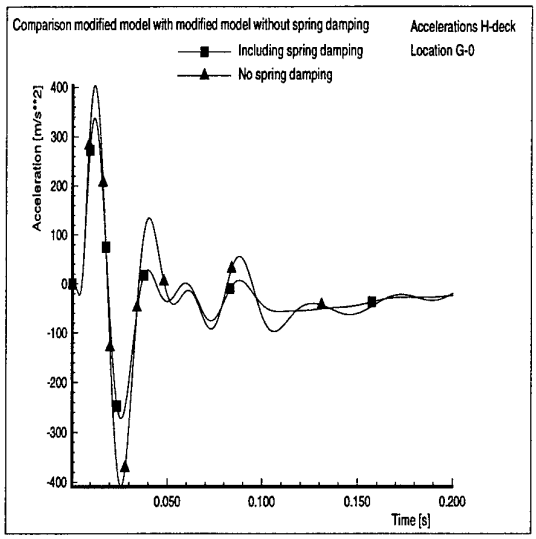

c) Location G-0 (below spring)

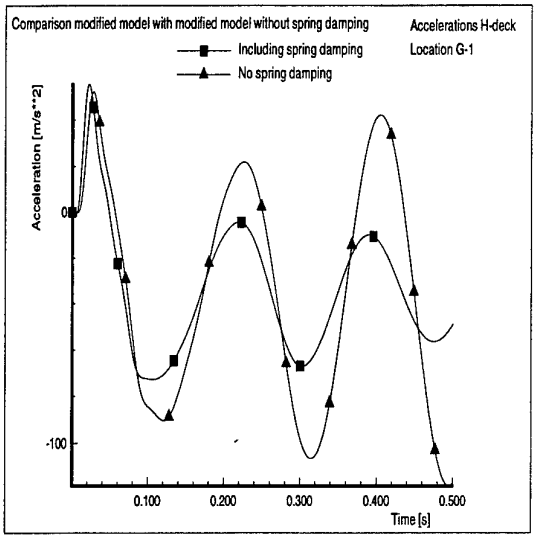

d) Location G-1 (above spring)

(centre of large deck part between hull and corrugated plate, at discrete mass)

Fig. 4.7 Comparison of accelerations of additional locations of the H-deck of two analysis, namely modified model from chapter 3 and modified model without damping for the discrete springs

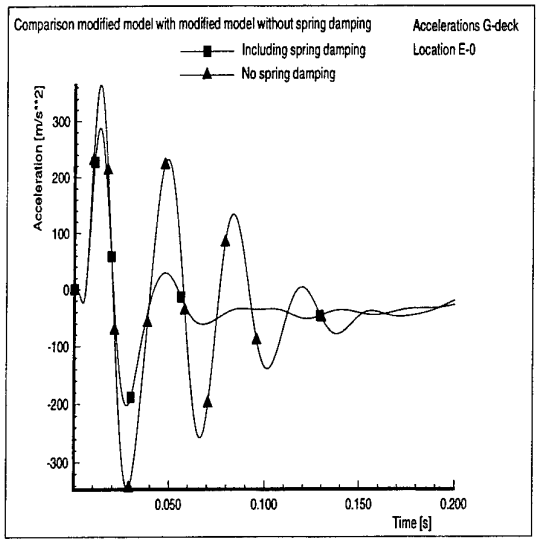

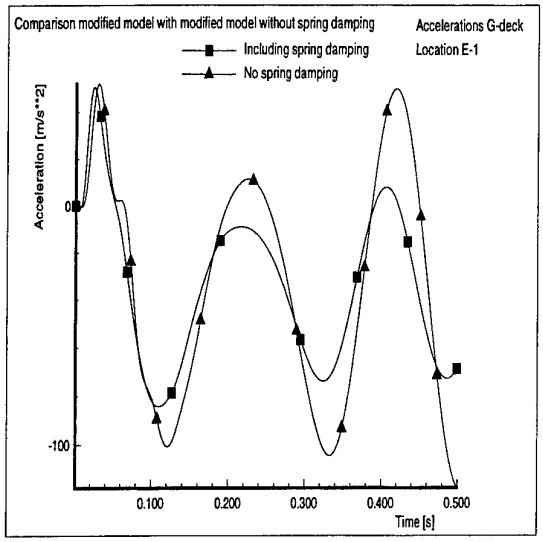

a) Location E-0 (below spring) b) Location E-1 (above spring)
(close to location E (midway hull and corrugated plate), but at discrete mass)

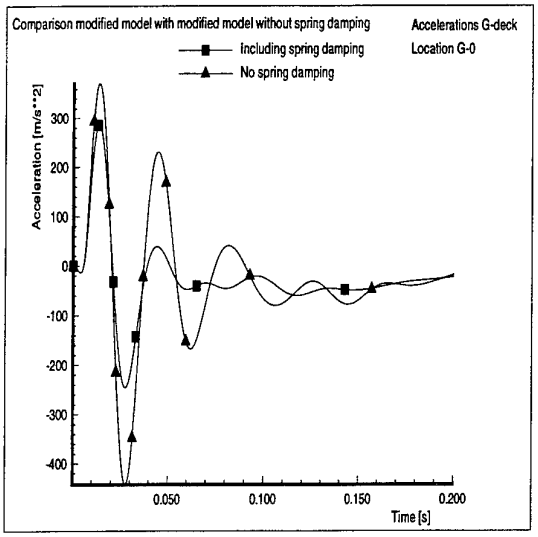

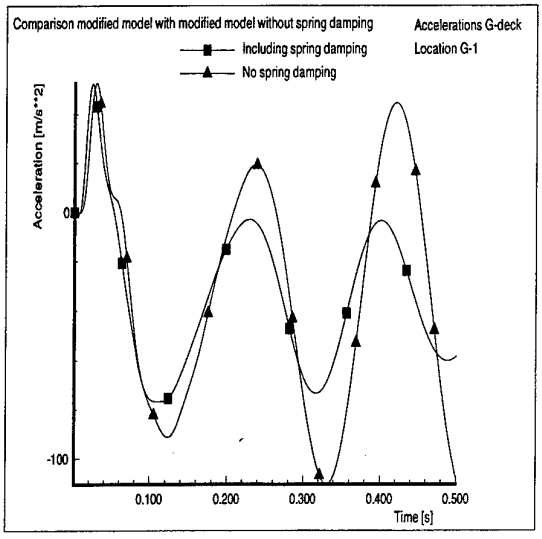

c) Location G-0 (below spring) d) Location G-1 (above spring)
(centre of large deck part between hull and corrugated plate, at discrete mass)

Fig. 4.8 Comparison of accelerations of additional locations of the G-deck of two analysis, namely modified model from chapter 3 and modified model without damping for the discrete springs

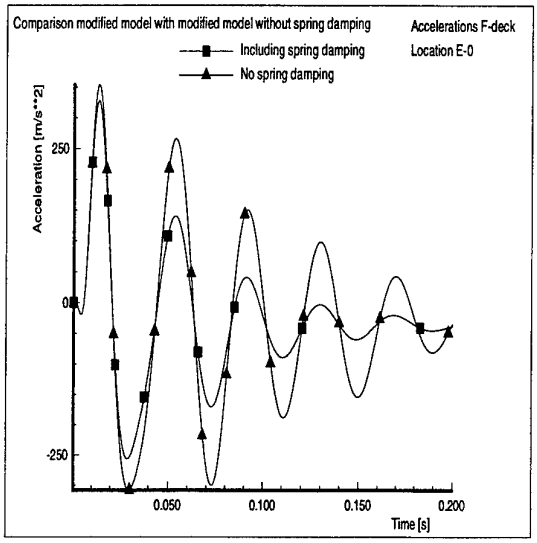

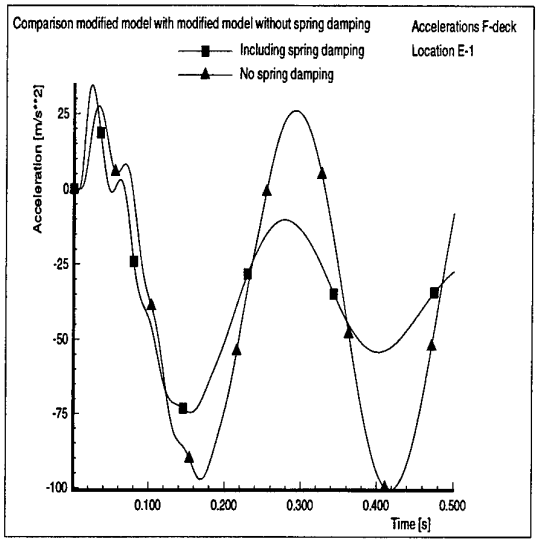

a) Location E-0 (below spring) b) Location E-1 (above spring)
(close to location E (midway hull and corrugated plate), but at discrete mass)

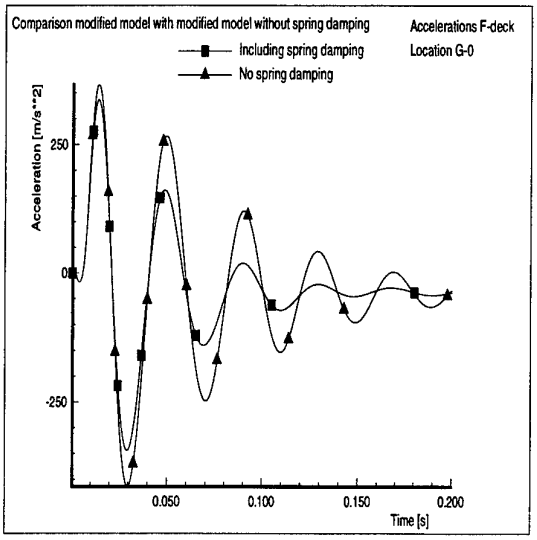

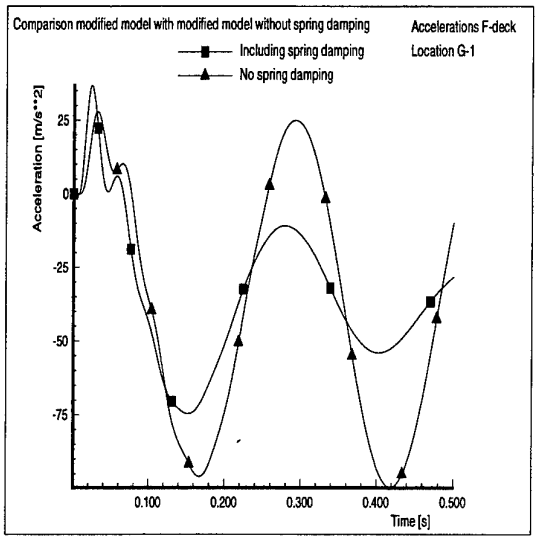

c) Location G-0 (below spring) d) Location G-1 (above spring)
(centre of large deck part between hull and corrugated plate, at discrete mass)

Fig. 4.9 Comparison of accelerations of additional locations of the F-deck of two analysis, namely modified model from chapter 3 and modified model without damping for the discrete springs

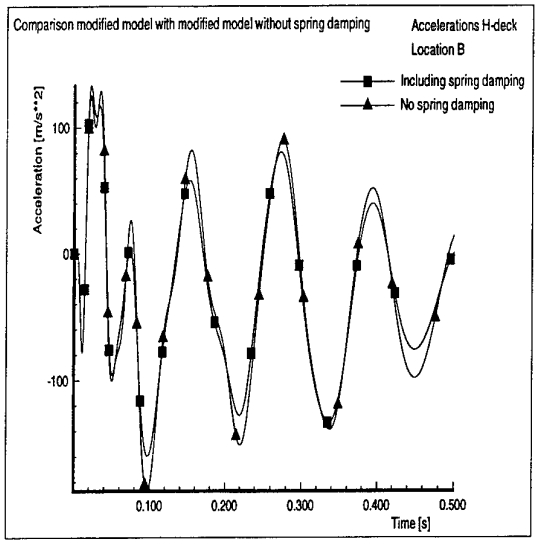

a) At H-deck (fixed discrete mass)

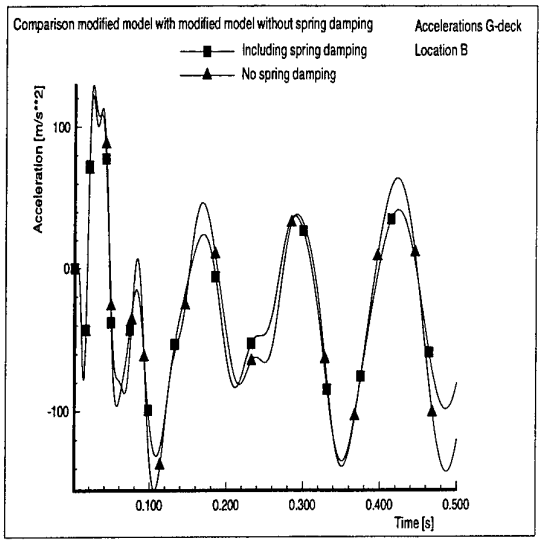

b) At G-deck (fixed discrete mass)

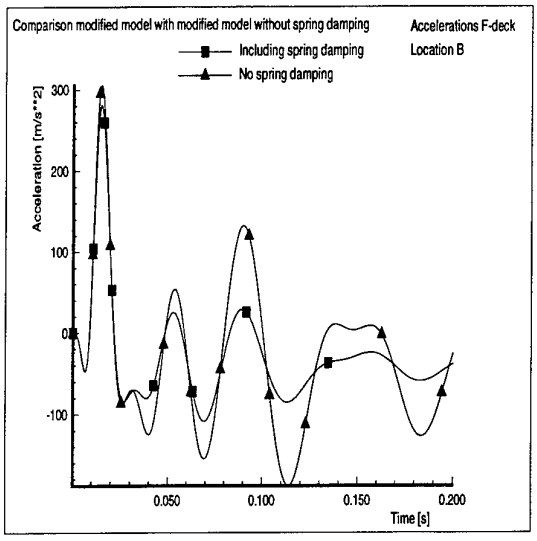

c) At F-deck (discrete mass, below spring)

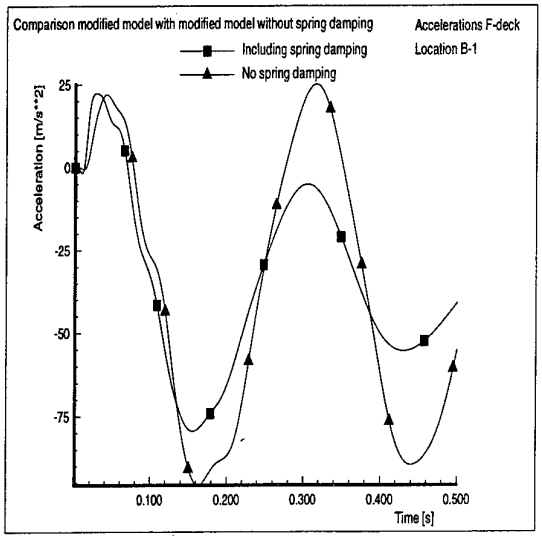

d) At F-deck (discrete mass, above spring)

Fig. 4.10 Comparison of accelerations of locations B of all decks of two analysis, namely modified model from chapter 3 and modified model without damping for the discrete springs

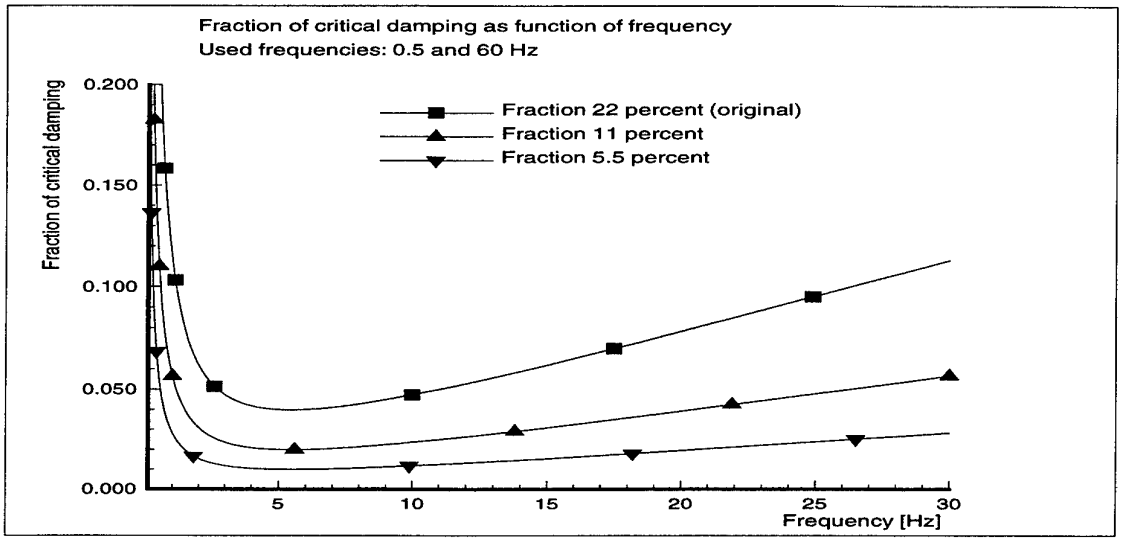

Fig. 5.1 Fraction of critical damping as function of frequency used to investigate the effect of the magnitude of the Rayleigh damping, calculated using 0.5 Hz and 60 Hz, both with 22 percent (original), 11 percent and 5.5 percent

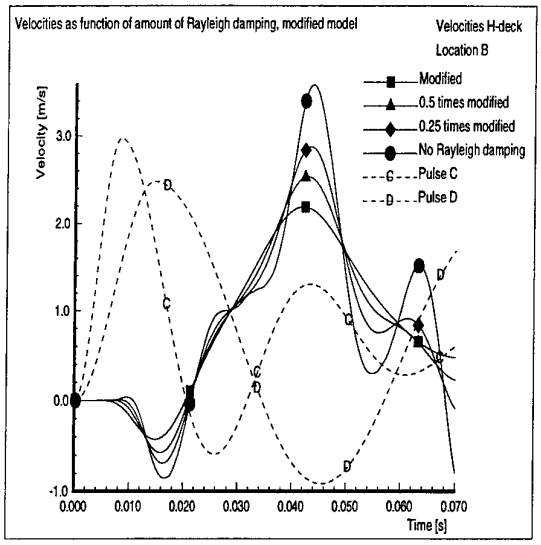

a) Location B (at fixed mass, centre of compartment)

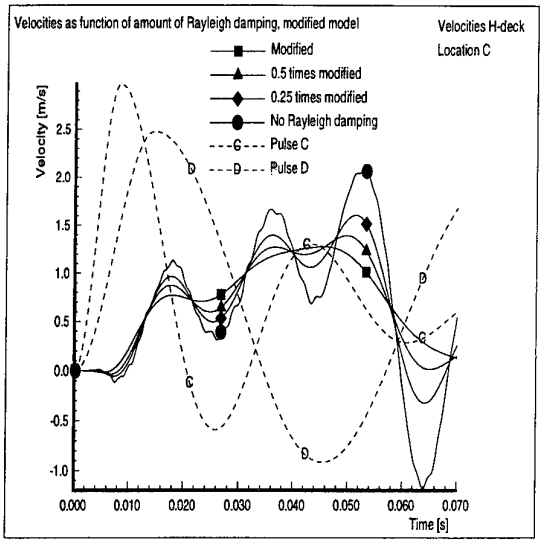

b) Location C (between fixed masses, between centreline and corrugated plate)

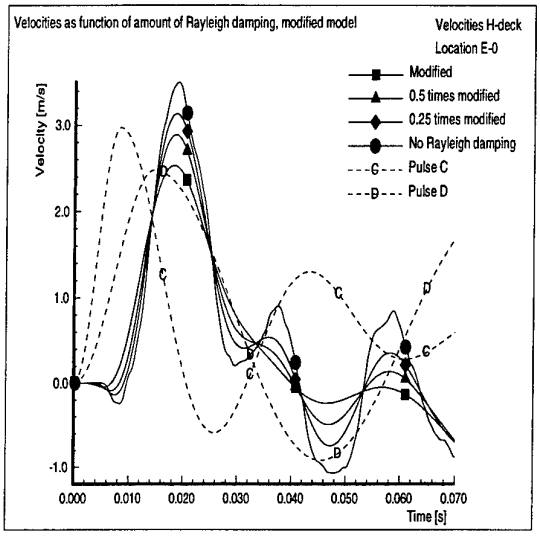

c) Location E-0 (at mass below spring, close to location E)

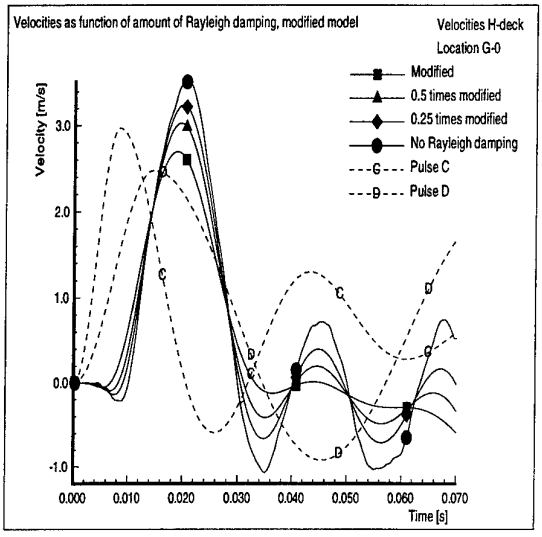

d) Location G-0 (at mass below spring, centre of large deck part)

Fig. 5.2 Comparison of velocities of H-deck for modified model with different Rayleigh damping values

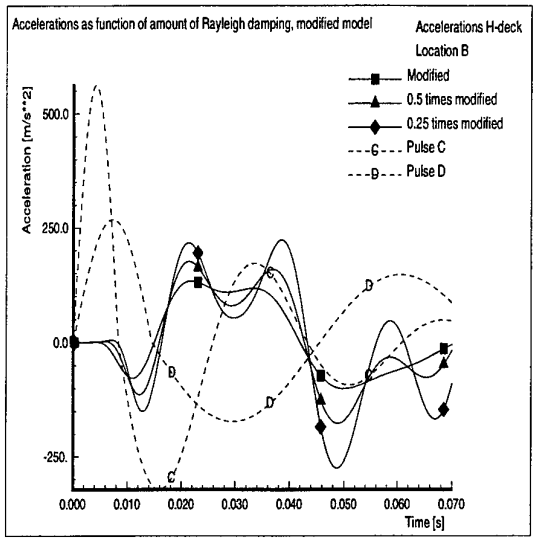

a) Location B (at fixed mass, centre of compartment)

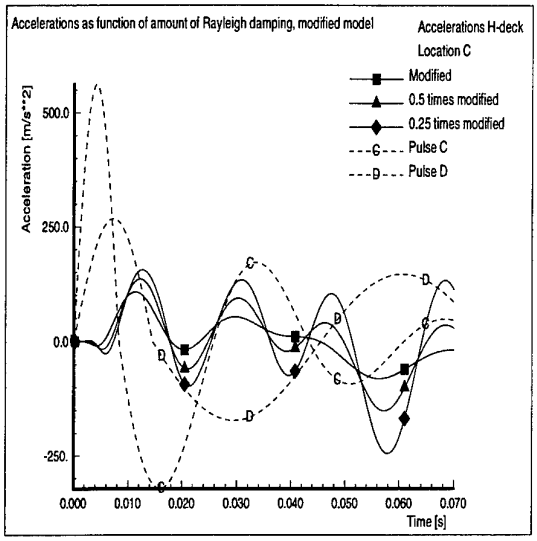

b) Location C (between fixed masses, between centreline and corrugated plate)

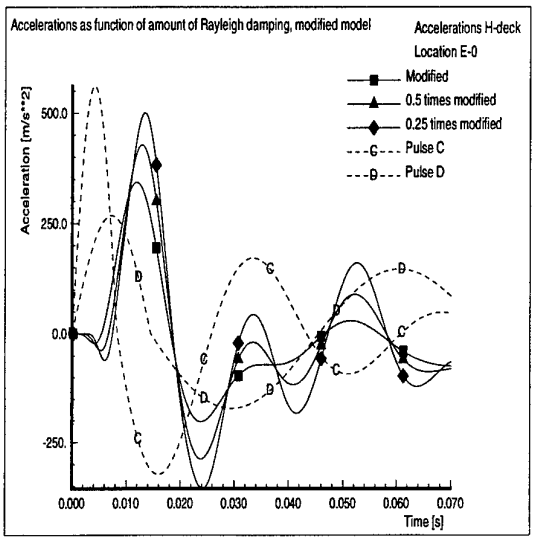

c) Location E-0 (at mass below spring, close to location E)

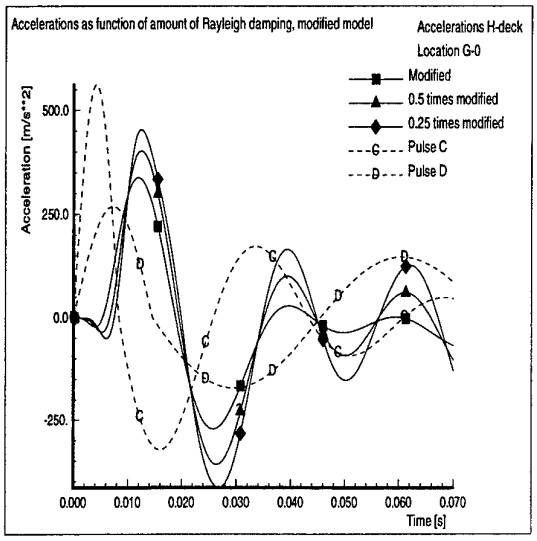

d) Location G-0 (at mass below spring, centre of large deck part)

Fig. 5.3 Comparison of accelerations of H-deck for modified model with different Rayleigh damping values

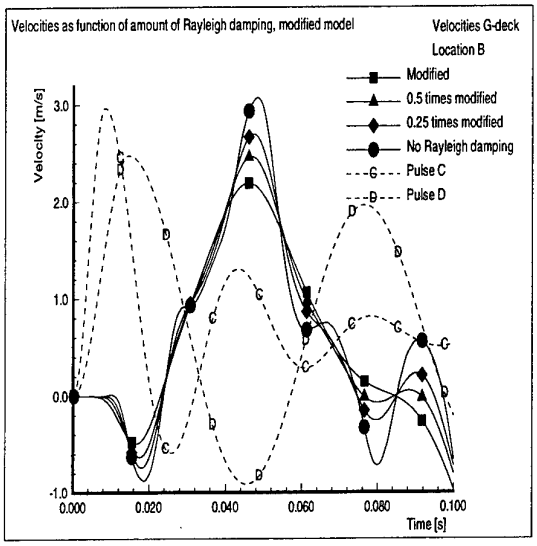

a) Location B (at fixed mass, centre of compartment)

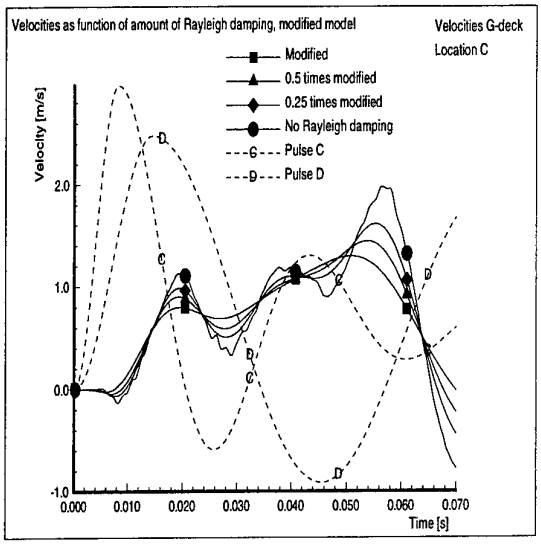

b) Location C (between fixed masses, between centreline and corrugated plate)

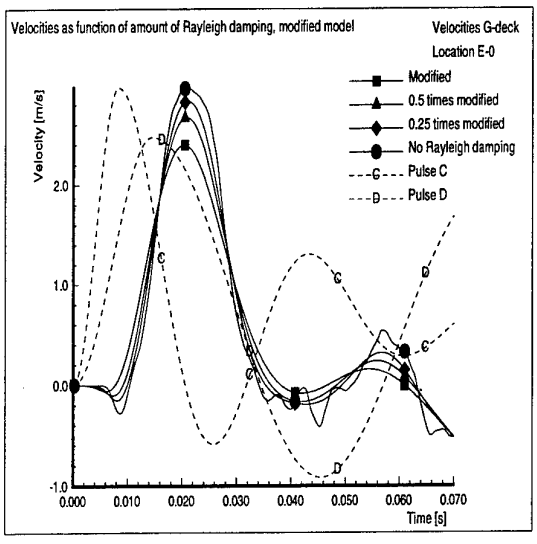

c) Location E-0 (at mass below spring, close to location E)

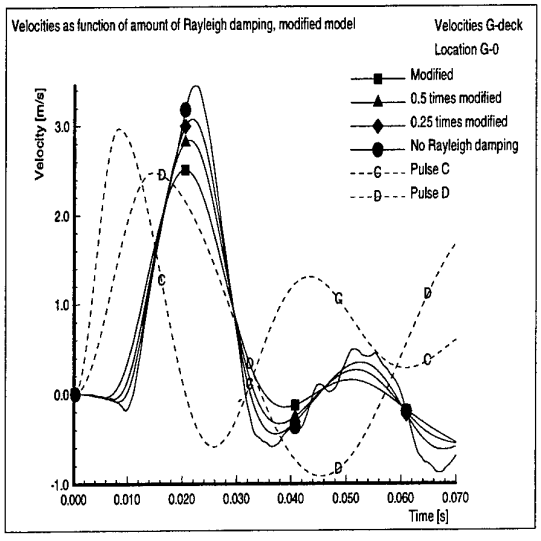

d) Location G-0 (at mass below spring, centre of large deck part)

Fig. 5.4 Comparison of velocities of G-deck for modified model with different Rayleigh damping values

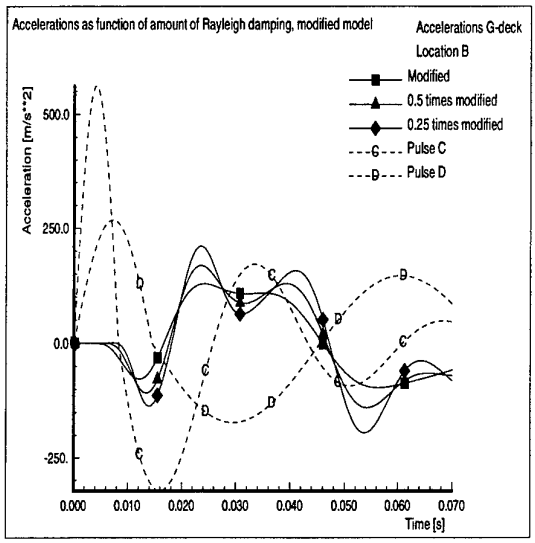

a) Location B (at fixed mass, centre of compartment)

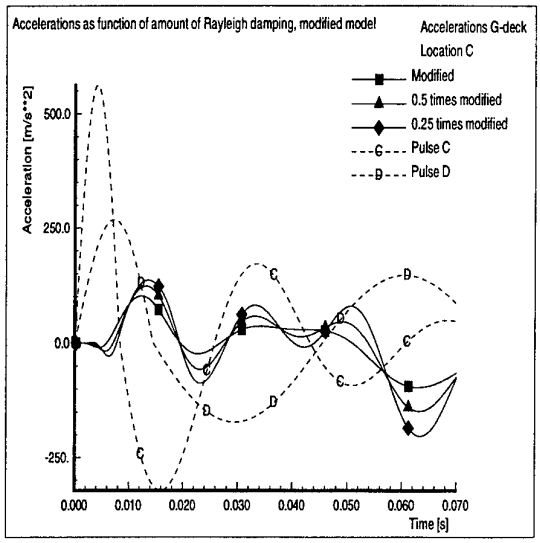

b) Location C (between fixed masses, between centreline and corrugated plate)

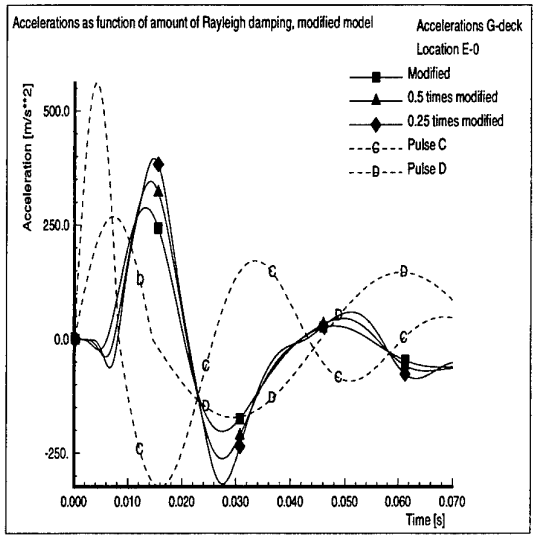

c) Location E-0 (at mass below spring, close to location E)

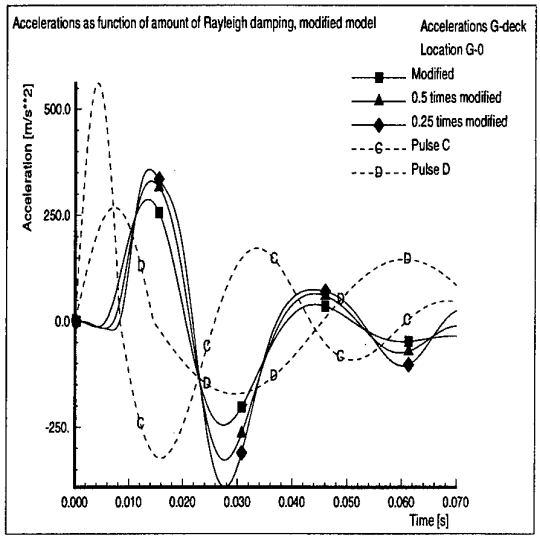

d) Location G-0 (at mass below spring, centre of large deck part)

Fig. 5.5 Comparison of accelerations of G-deck for modified model with different Rayleigh damping values

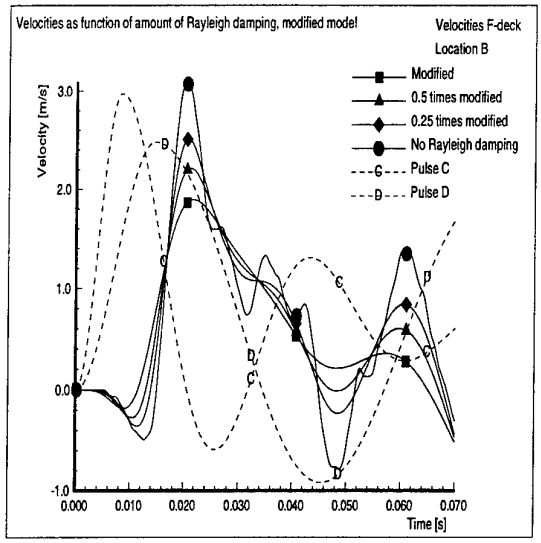

a) Location B (at mass below spring, centre of compartment)

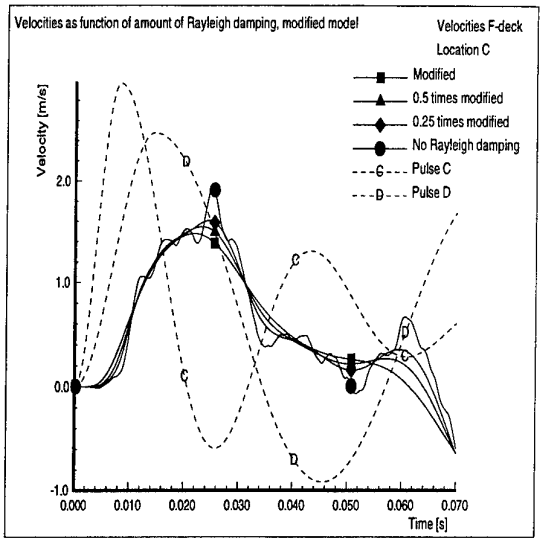

b) Location C (between masses on springs, between centreline and corrugated plate)

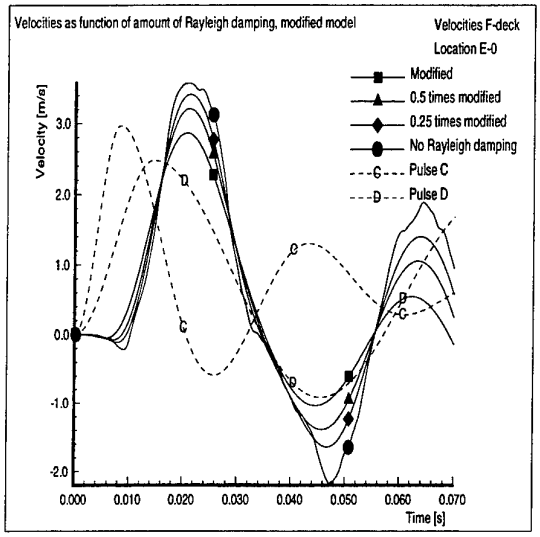

c) Location E-0 (at mass below spring, close to location E)

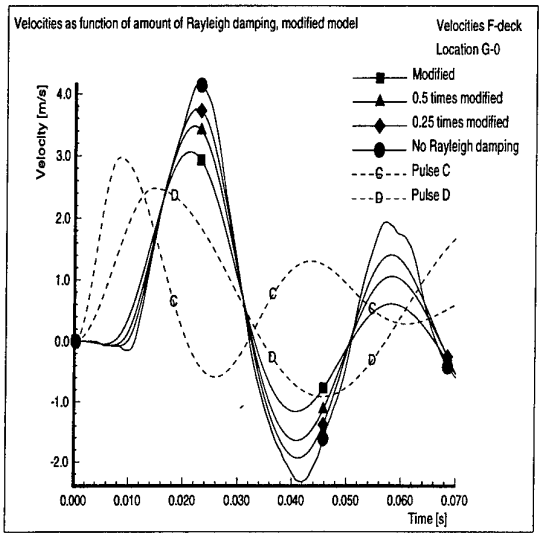

d) Location G-0 (at mass below spring, centre of large deck part)

Fig. 5.6 Comparison of velocities of F-deck for modified model with different Rayleigh damping values

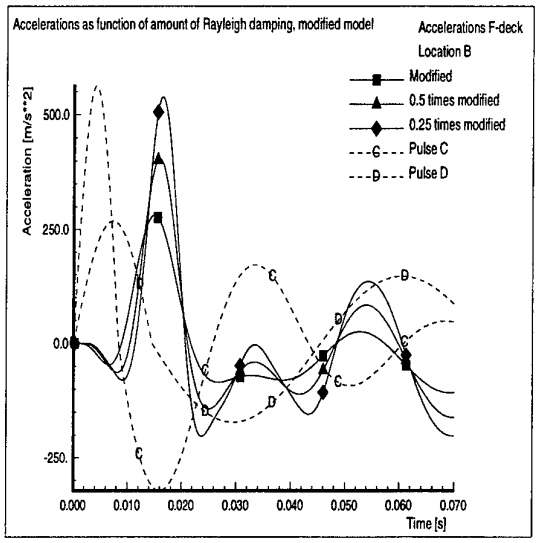

a) Location B (at mass below spring, centre of compartment)

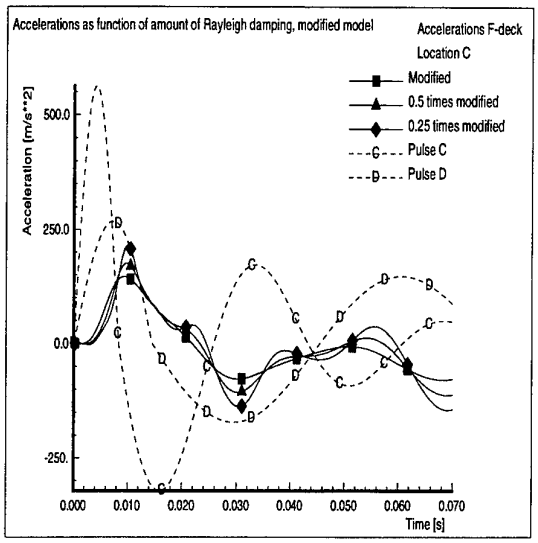

b) Location C (between masses on springs, between centreline and corrugated plate)

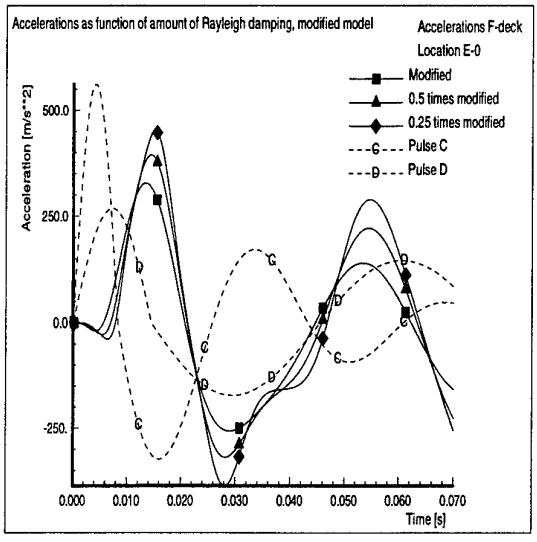

c) Location E-0 (at mass below spring, close to location E)

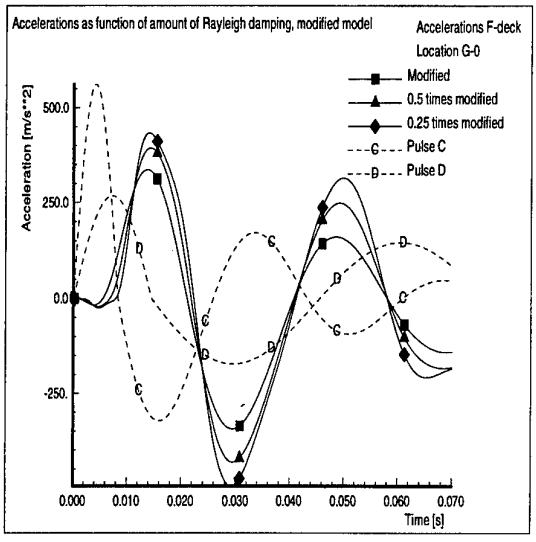

d) Location G-0 (at mass below spring, centre of large deck part)

Fig. 5.7 Comparison of accelerations of F-deck for modified model with different Rayleigh damping values

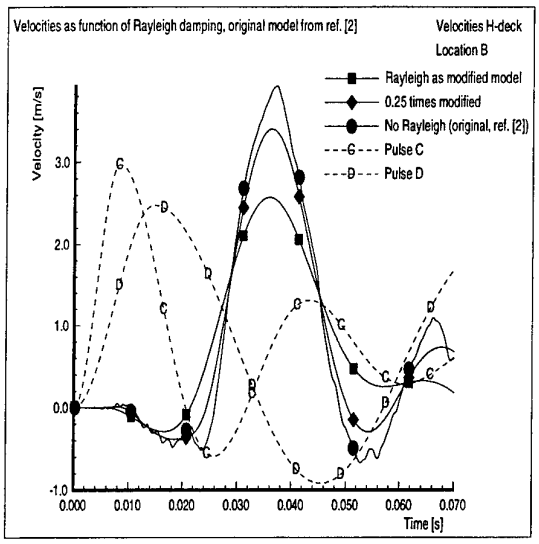

a) Location B (equally distributed mass, centre of compartment)

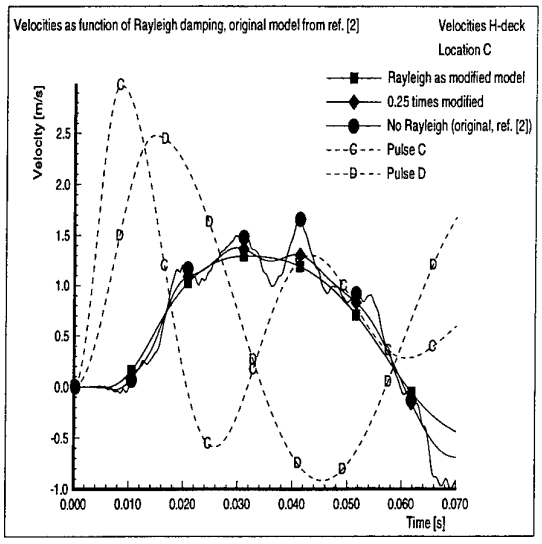

b) Location C (equally distributed mass, between centreline and corrugated plate)

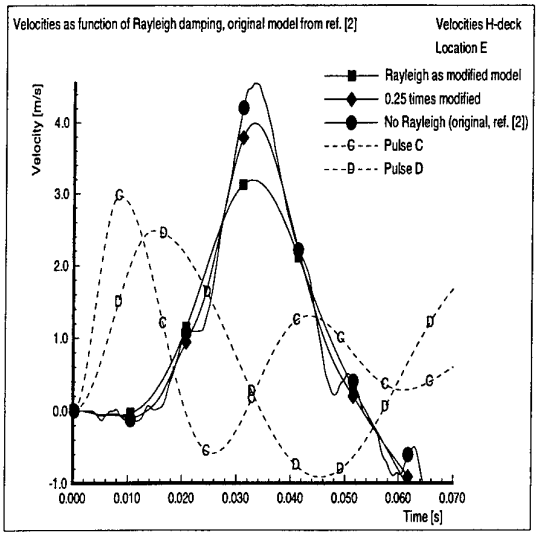

c) Location E (equally distributed mass, midway between hull and corrugated plate)

Fig. 5.8 Comparison of velocities of H-deck for original model from ref. [2], but including the effect of different Rayleigh damping values

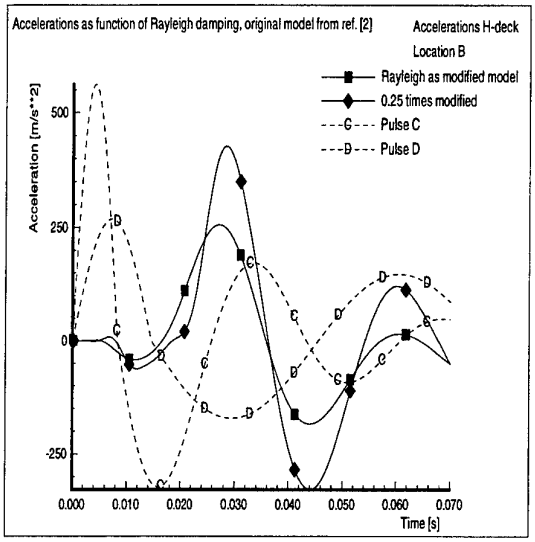

a) Location B (equally distributed mass, centre of compartment)

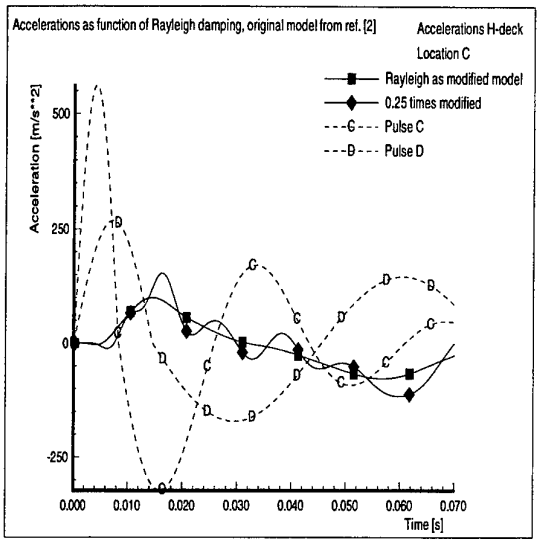

b) Location C (equally distributed mass, between centreline and corrugated plate)

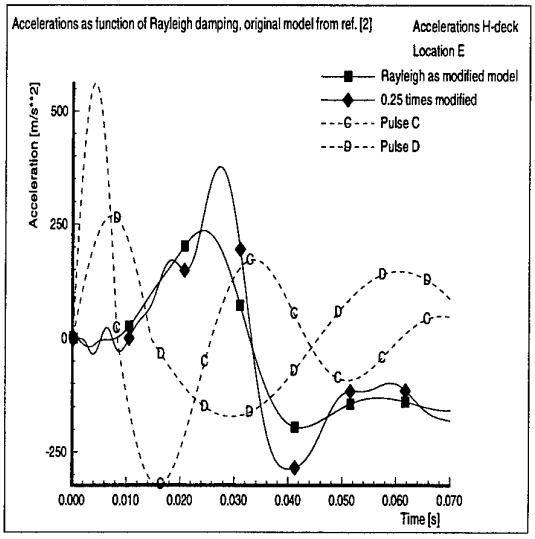

c) Location E (equally distributed mass, midway between hull and corrugated plate)

Fig. 5.9 Comparison of accelerations of H-deck for original model from ref. [2], but including the effect of different Rayleigh damping values

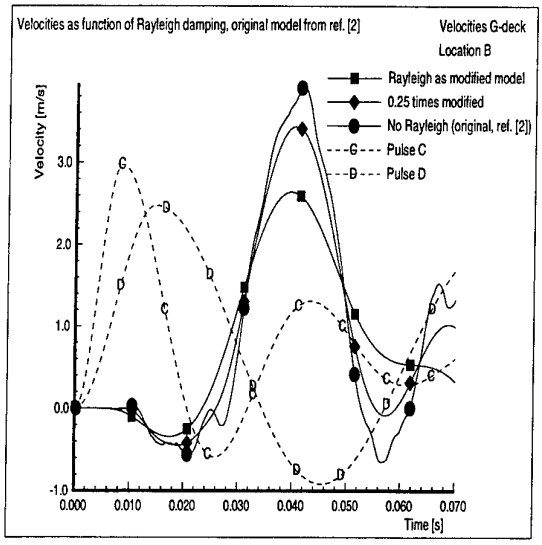

a) Location B (equally distributed mass, centre of compartment)

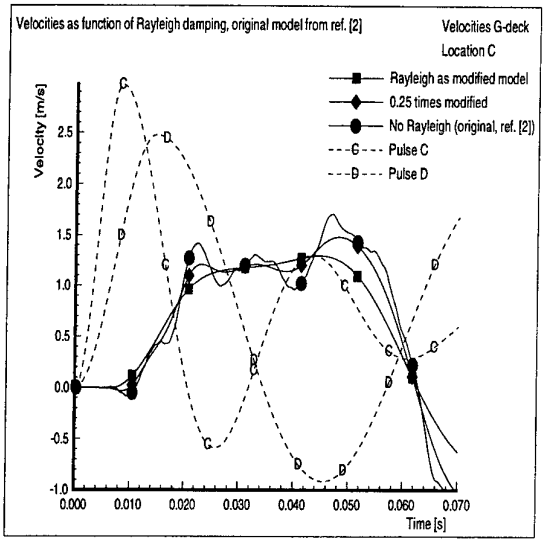

b) Location C (equally distributed mass, between centreline and corrugated plate)

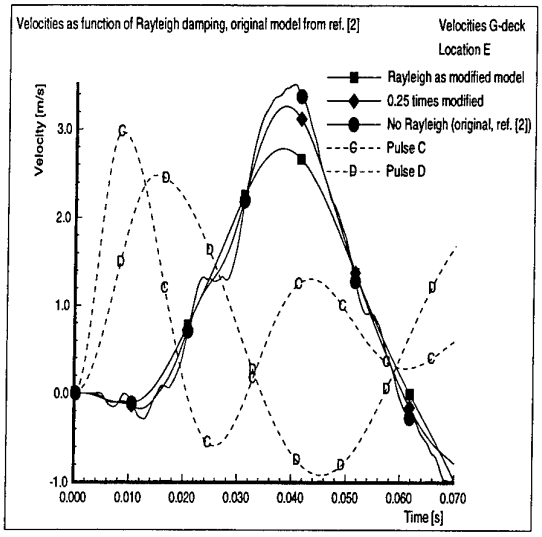

c) Location E (equally distributed mass, midway between hull and corrugated plate)

Fig. 5.10 Comparison of velocities of G-deck for original model from ref. [2], but including the effect of different Rayleigh damping values

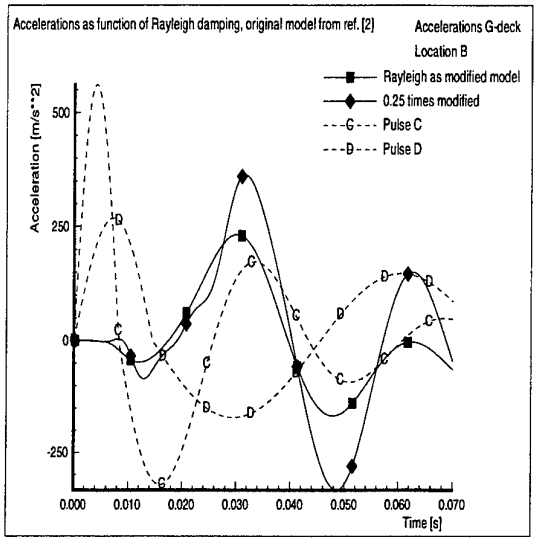

a) Location B (equally distributed mass, centre of compartment)

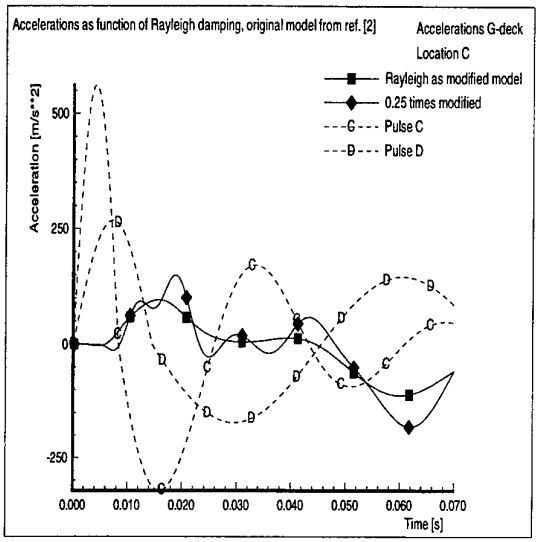

b) Location C (equally distributed mass, between centreline and corrugated plate)

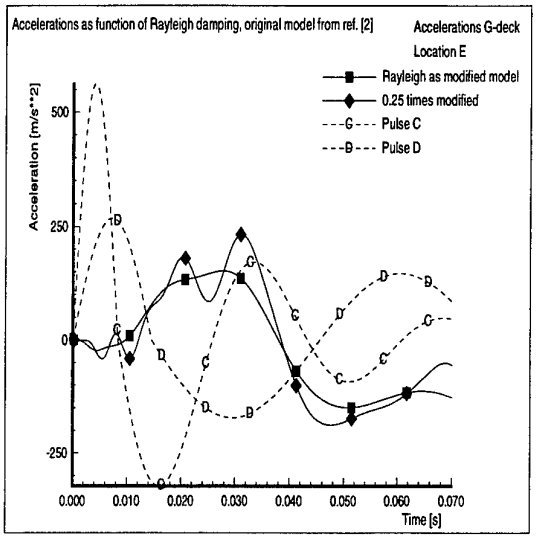

c) Location E (equally distributed mass, midway between hull and corrugated plate)

Fig. 5.11 Comparison of accelerations of G-deck for original model from ref. [2], but including the effect of different Rayleigh damping values

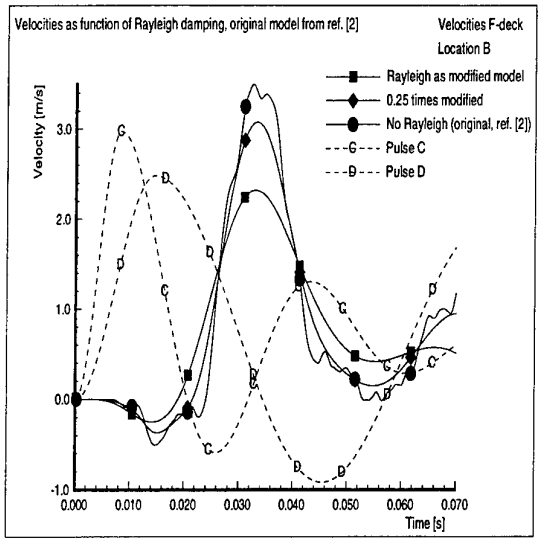

a) Location B (equally distributed mass, centre of compartment)

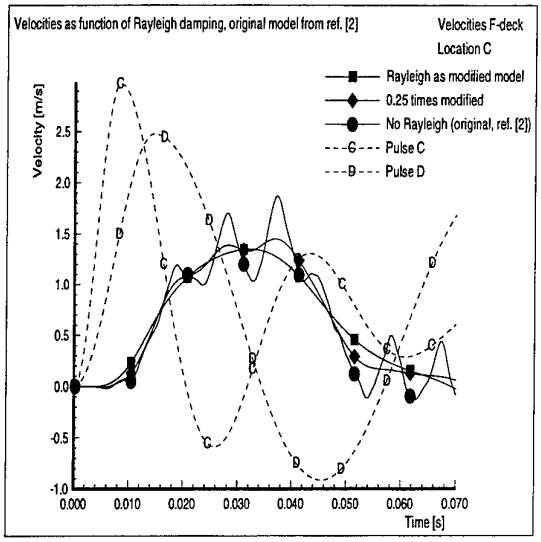

b) Location C (equally distributed mass, between centreline and corrugated plate)

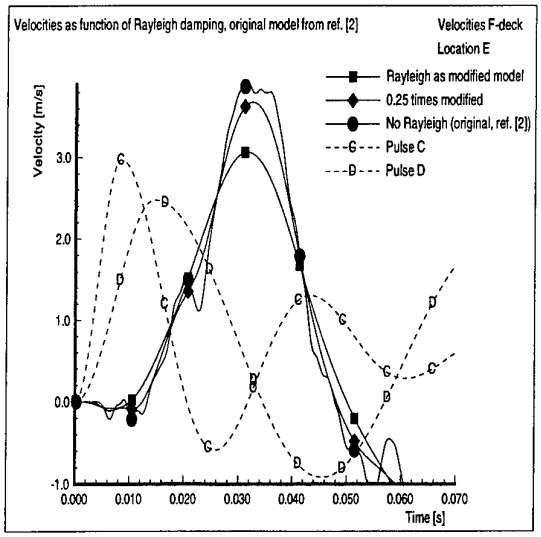

c) Location E (equally distributed mass, midway between hull and corrugated plate)

Fig. 5.12 Comparison of velocities of F-deck for original model from ref. [2], but including the effect of different Rayleigh damping values

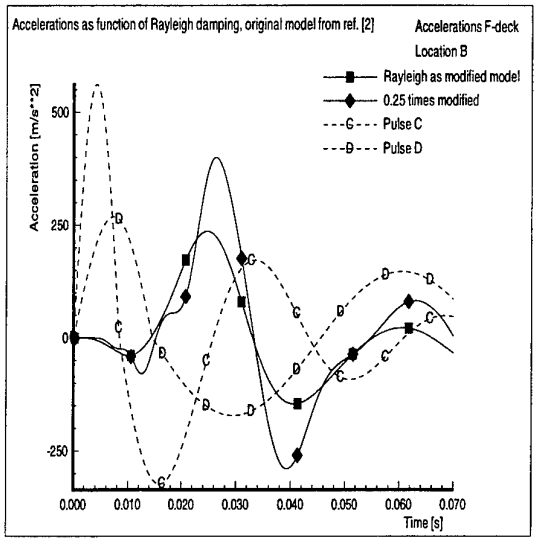

a) Location B (equally distributed mass, centre of compartment)

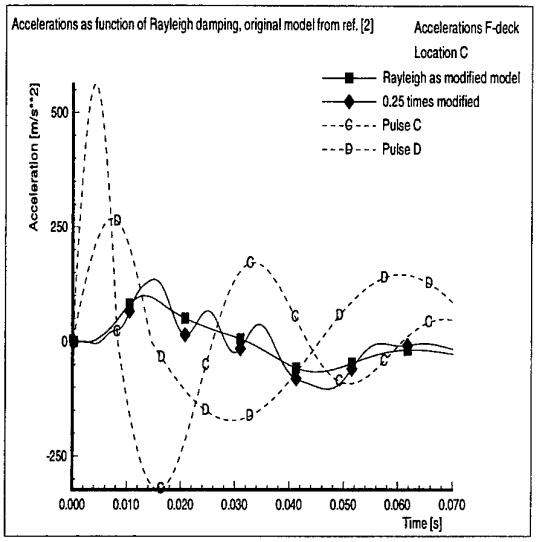

b) Location C (equally distributed mass, between centreline and corrugated plate)

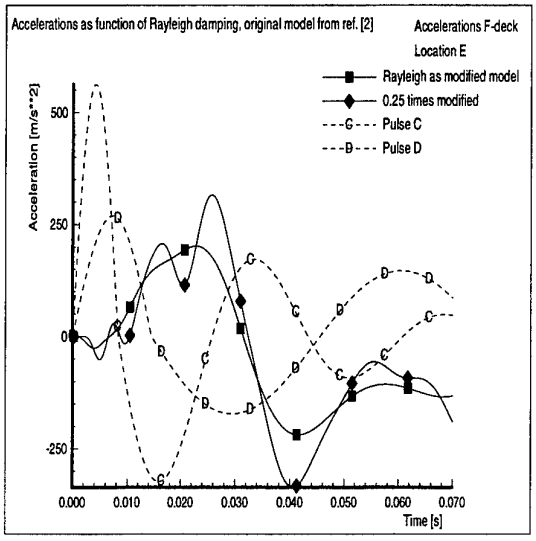

c) Location E (equally distributed mass, midway between hull and corrugated plate)

Fig. 5.13 Comparison of accelerations of F-deck for original model from ref. [2], but including the effect of different Rayleigh damping values

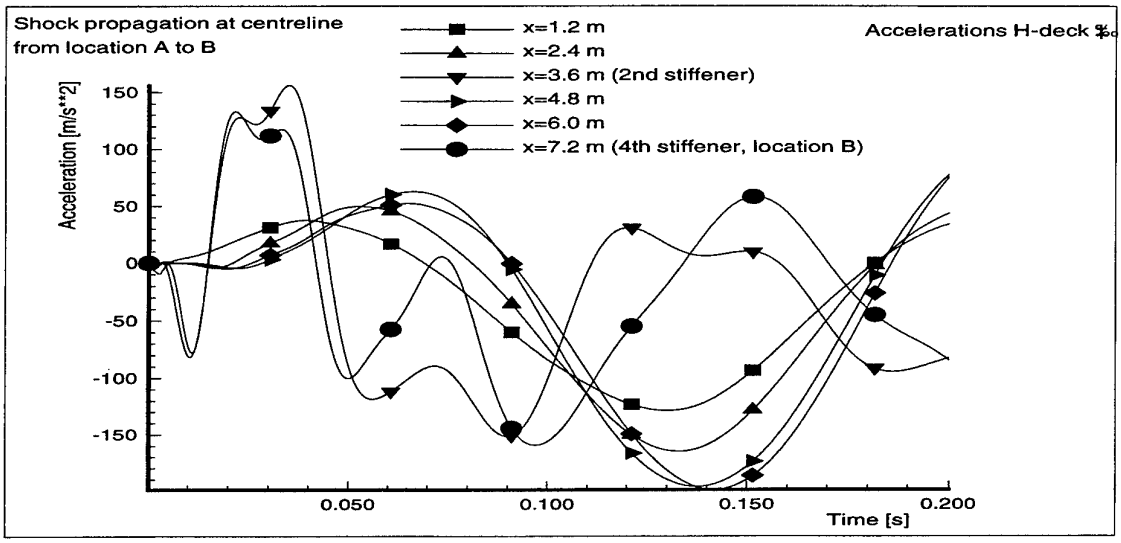

Fig. 6.1 Shock wave propagation in length direction of compartment at centreline of H-deck, so at small deck part, modified model including Rayleigh damping

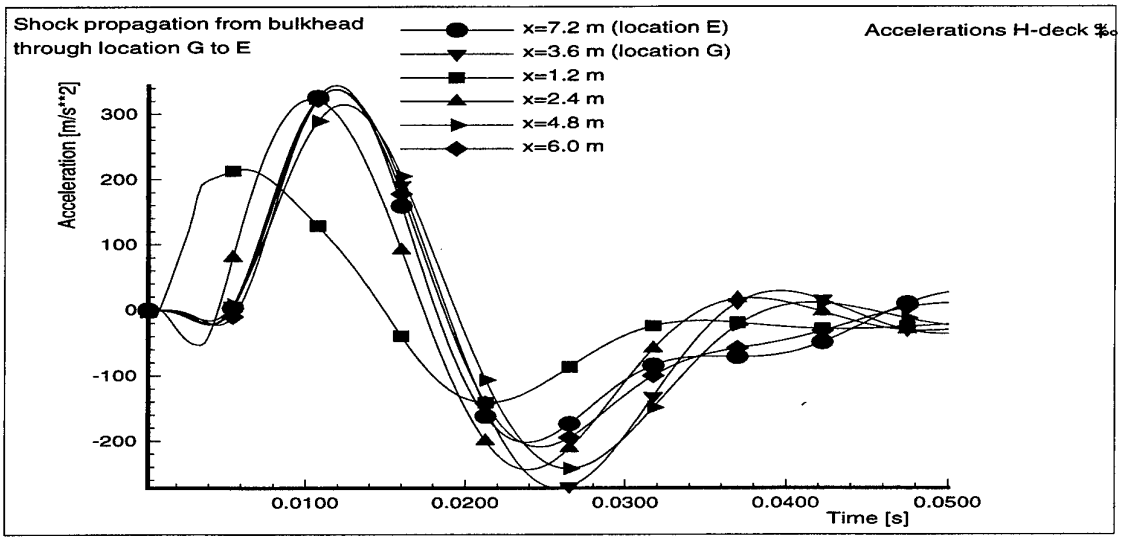

Fig. 6.2 Shock wave propagation in length direction of compartment at line through location G of H-deck, parallel to centreline, so at large deck part, modified model including Rayleigh damping

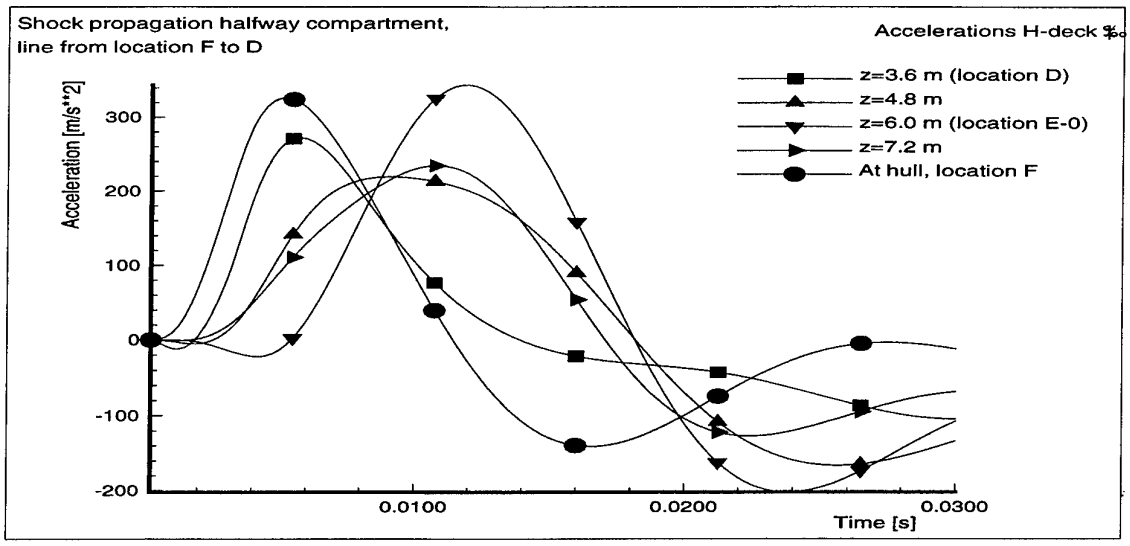

Fig. 6.3 Shock wave propagation in transverse direction of compartment, midway the compartment between locations B and F of H-deck, so at large deck part, modified model including Rayleigh damping

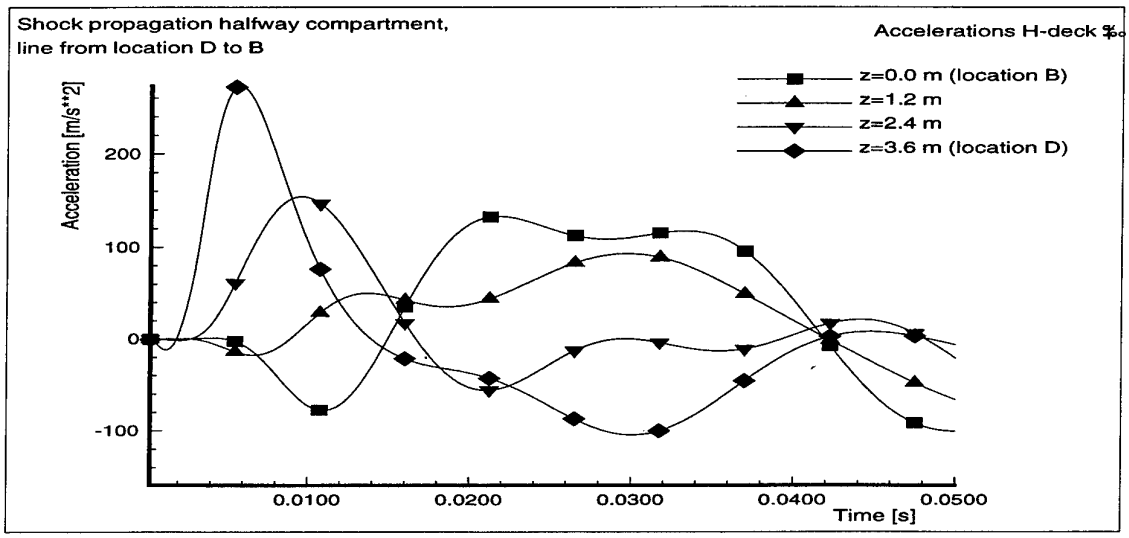

Fig. 6.4 Shock wave propagation in transverse direction of compartment, midway the compartment between locations D and B of H-deck, so at small deck part, modified model including Rayleigh damping

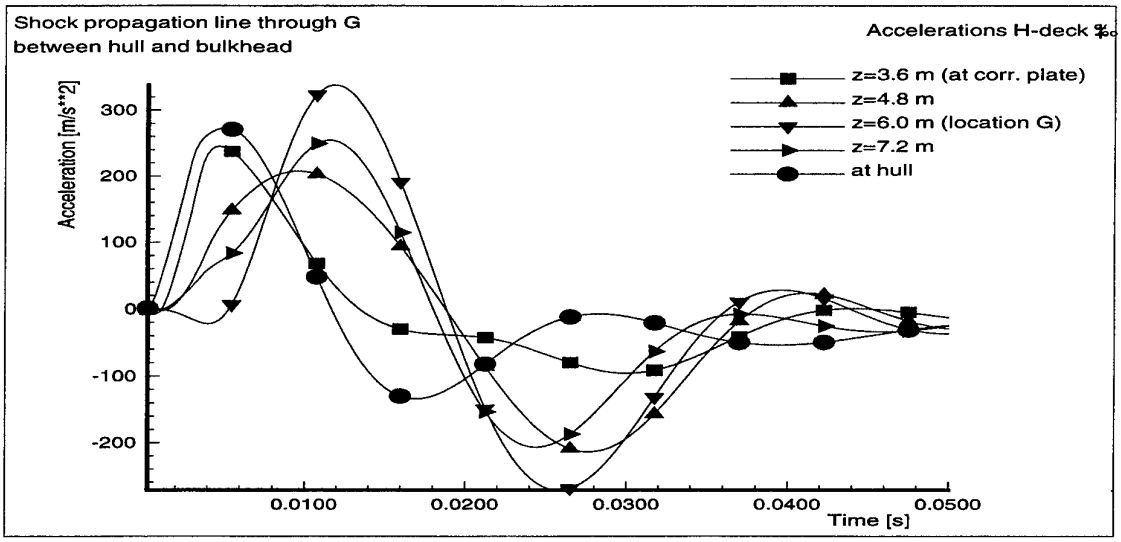

Fig. 6.5 Shock wave propagation in transverse direction of compartment, at a quarter of the compartment length through location G and between hull and bulkhead of H-deck, so at large deck part, modified model including Rayleigh damping

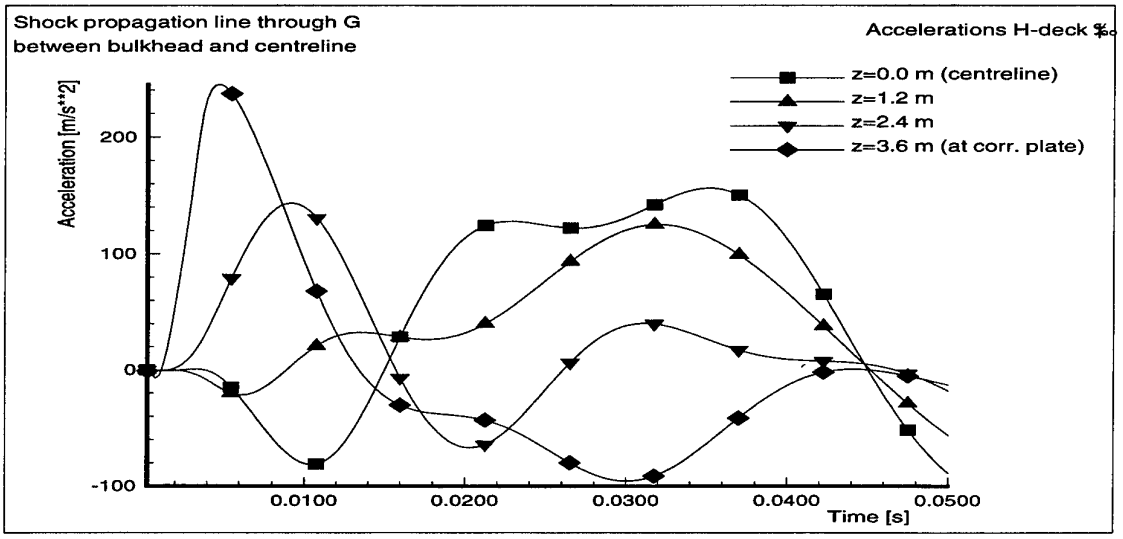

Fig. 6.6 Shock wave propagation in transverse direction of compartment, at a quarter of the compartment length and between bulkhead and centreline of H-deck, so at small deck part, modified model including Rayleigh damping

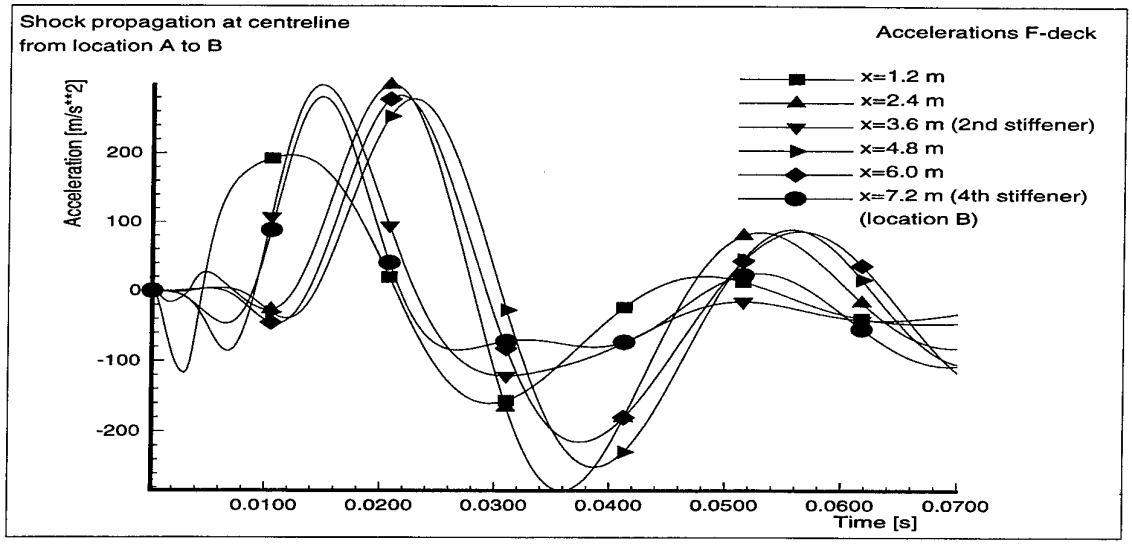

Fig. 6.7 Shock wave propagation in length direction of compartment at centreline of F-deck, so at small deck part, modified model including Rayleigh damping

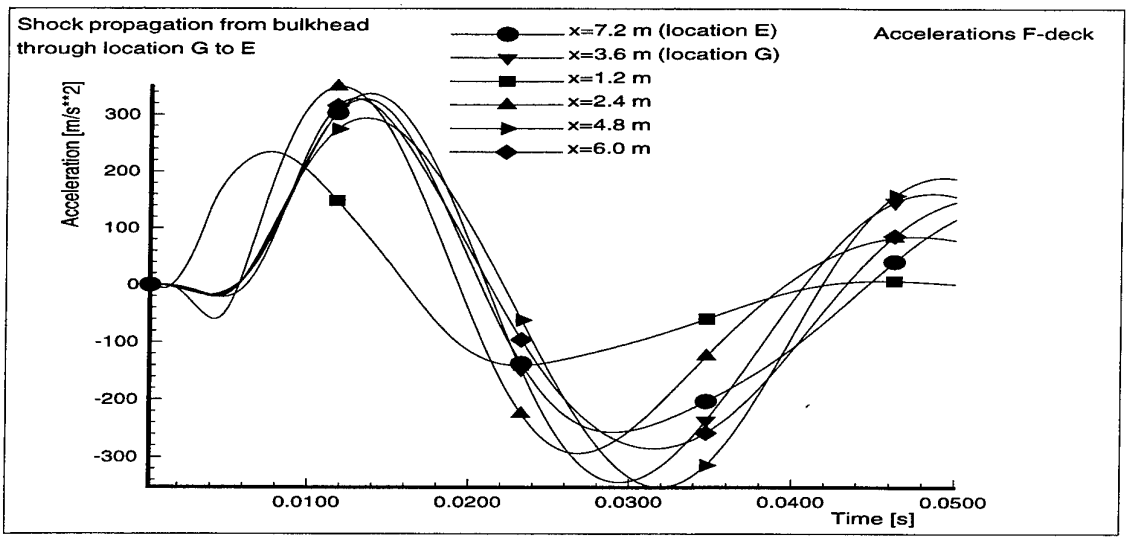

Fig. 6.8 Shock wave propagation in length direction of compartment at line through location G of F-deck, parallel to centreline, so at large deck part, modified model including Rayleigh damping

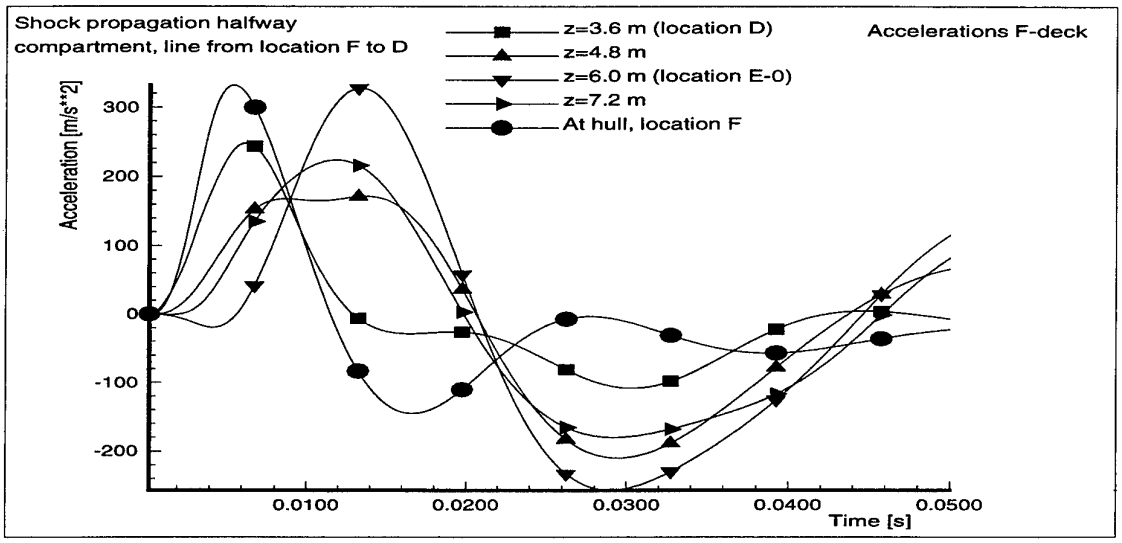

Fig. 6.9 Shock wave propagation in transverse direction of compartment, midway the compartment between locations B and F of F-deck, so at large deck part, modified model including Rayleigh damping

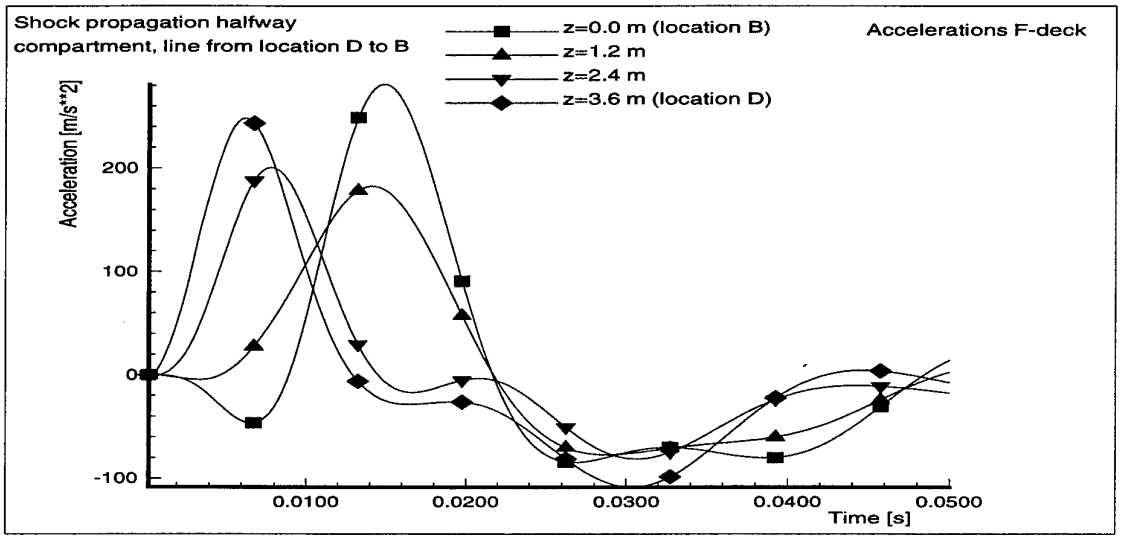

Fig. 6.10 Shock wave propagation in transverse direction of compartment, midway the compartment between locations D and B of F-deck, so at small deck part, modified model including Rayleigh damping

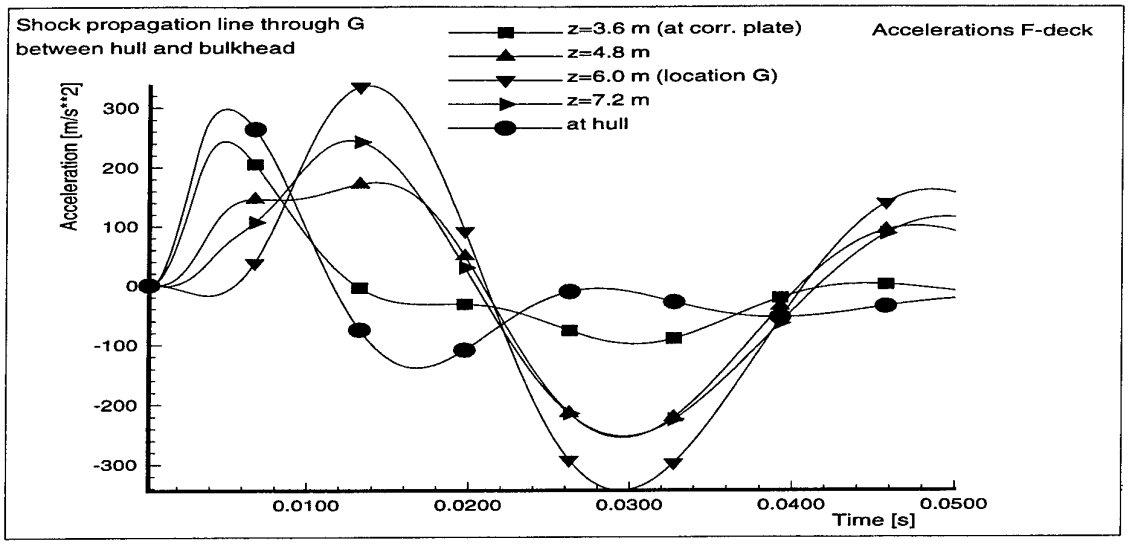

Fig. 6.11 Shock wave propagation in transverse direction of compartment, at a quarter of the compartment length through location G and between hull and bulkhead of F-deck, so at large deck part, modified model including Rayleigh damping

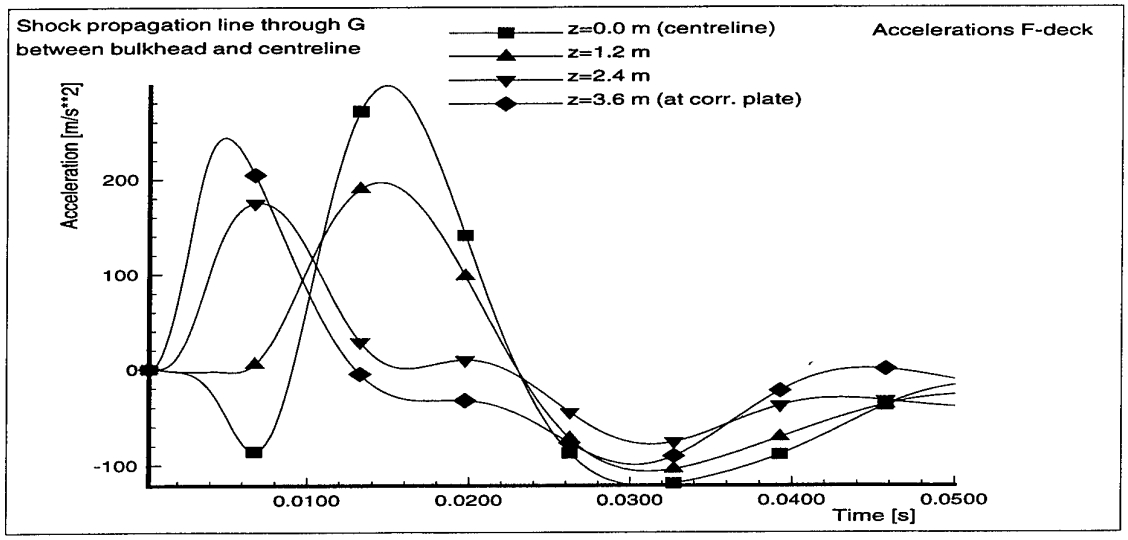

Fig. 6.12 Shock wave propagation in transverse direction of compartment, at a quarter of the compartment length and between bulkhead and centreline of F-deck, so at small deck part, modified model including Rayleigh damping

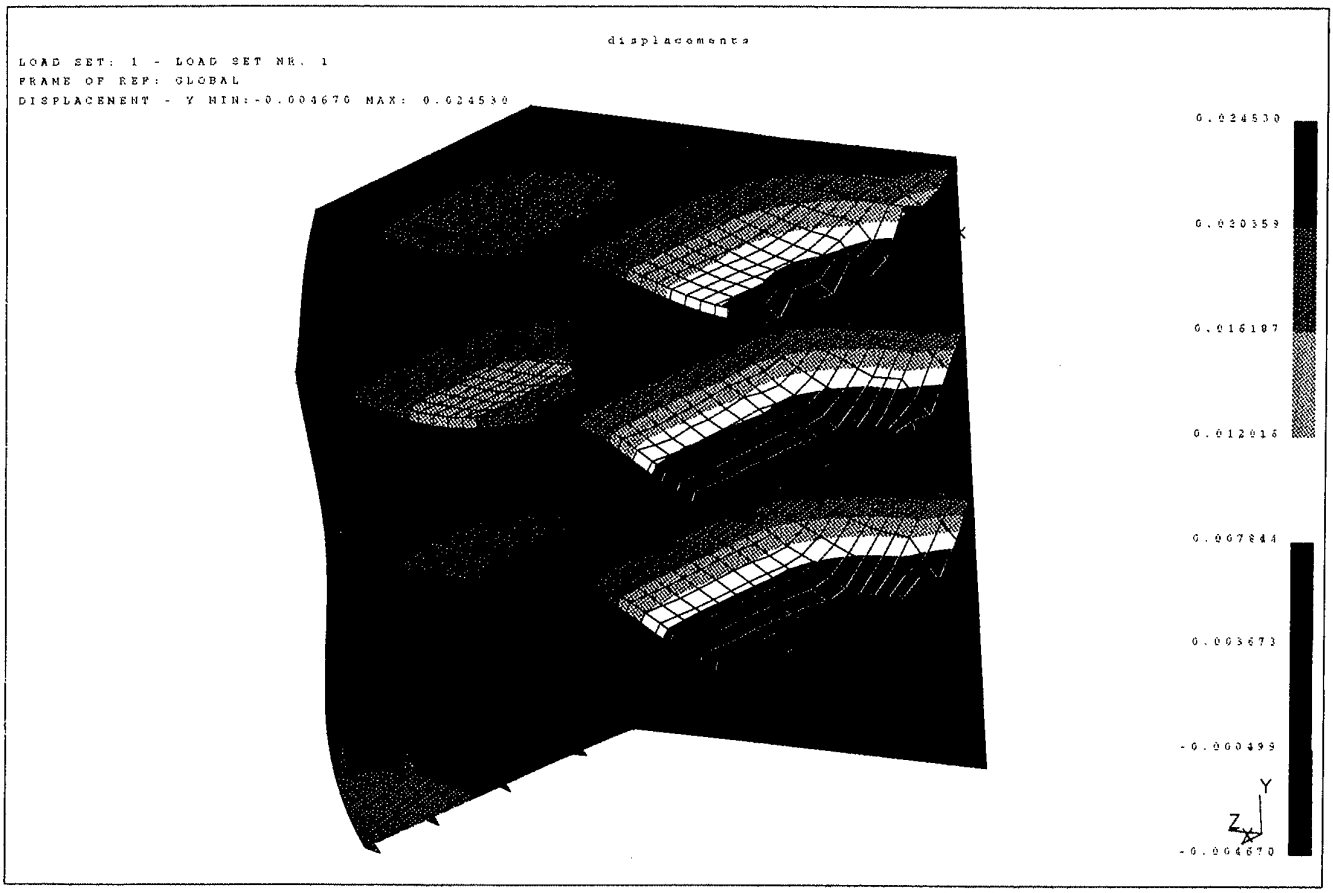

Fig. 6.13 Contour plot of vertical displacement component at deformed geometry at time = 20.0 ms, modified model including Rayleigh damping

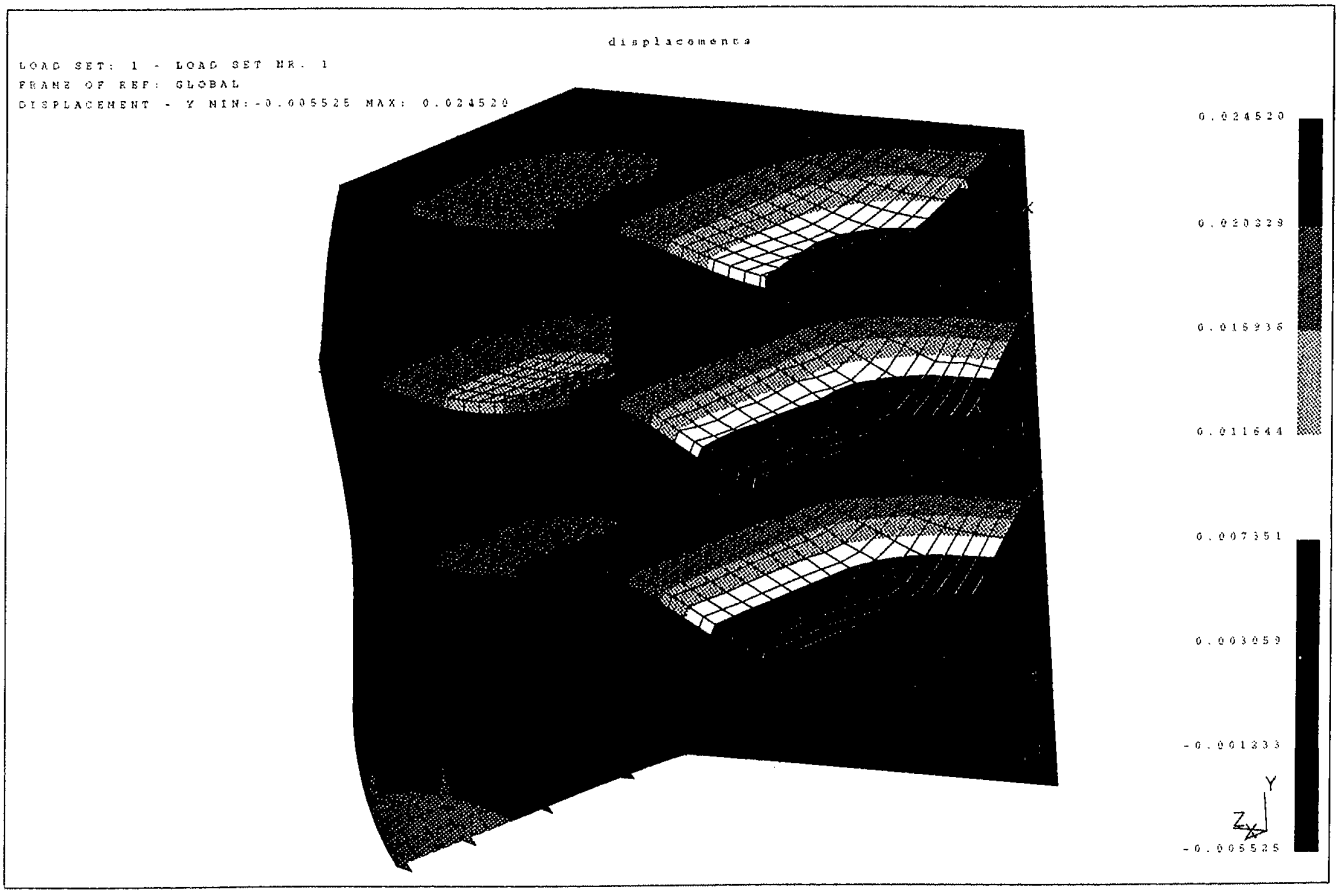

Fig. 6.14 Contour plot of vertical displacement component at deformed geometry at time = 20.0 ms, modified model including Rayleigh damping and including an additional HP100x7 profile at centreline of decks

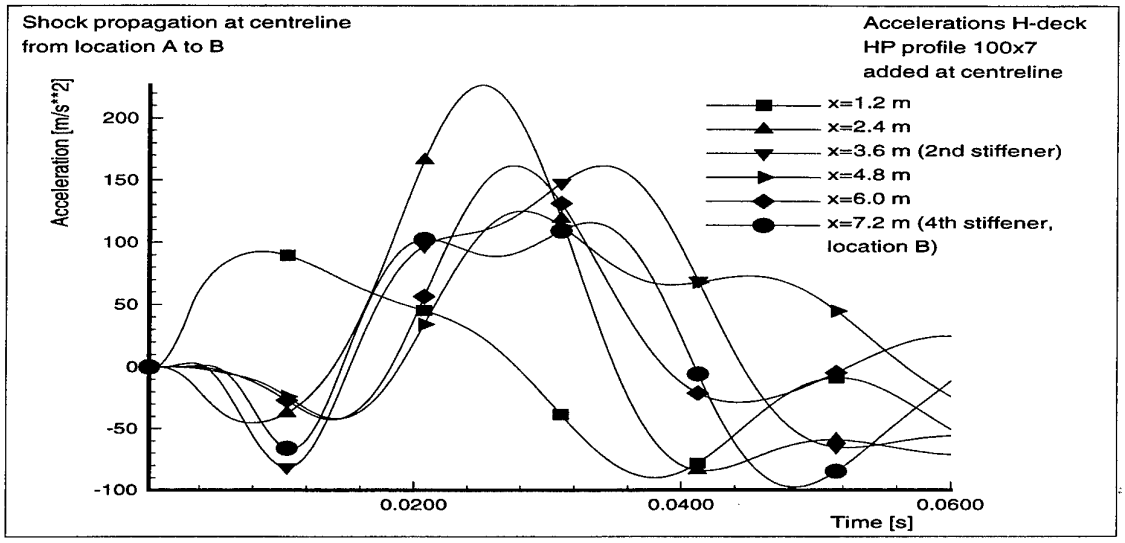

Fig. 6.15 Shock wave propagation in length direction of compartment at centreline of H-deck, so at small deck part, modified model including Rayleigh damping, including HP 100x7 at centreline

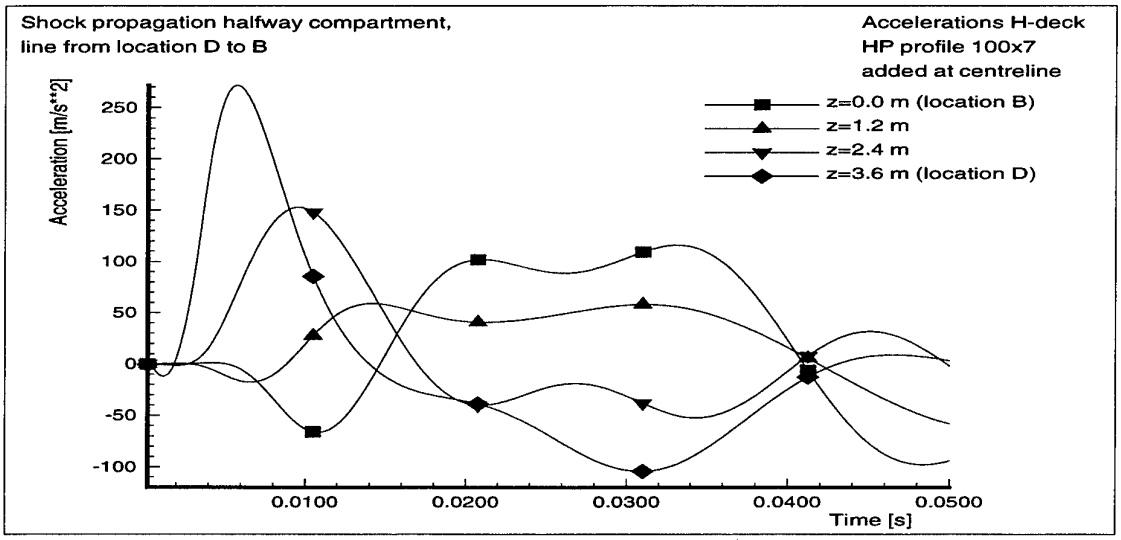

Fig. 6.16 Shock wave propagation in transverse direction of compartment, midway the compartment between locations D and B of H-deck, so at small deck part, modified model including Rayleigh damping, including HP100x7 at centreline

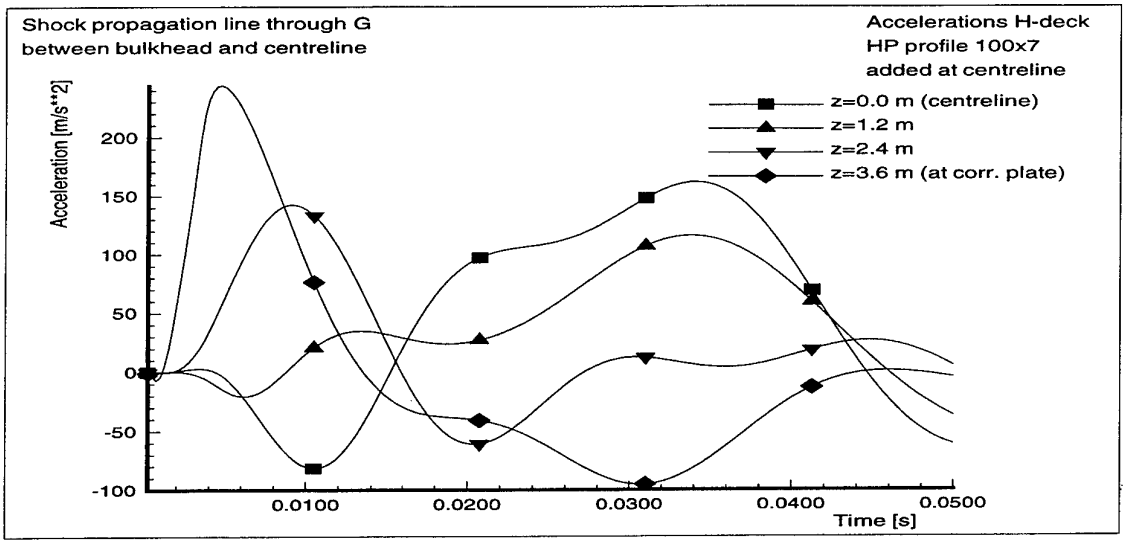

Fig. 6.17 Shock wave propagation in transverse direction of compartment, at a quarter of the compartment length and between bulkhead and centreline of H-deck, so at small deck part, modified model including Rayleigh damping, including HP100x7 at centreline

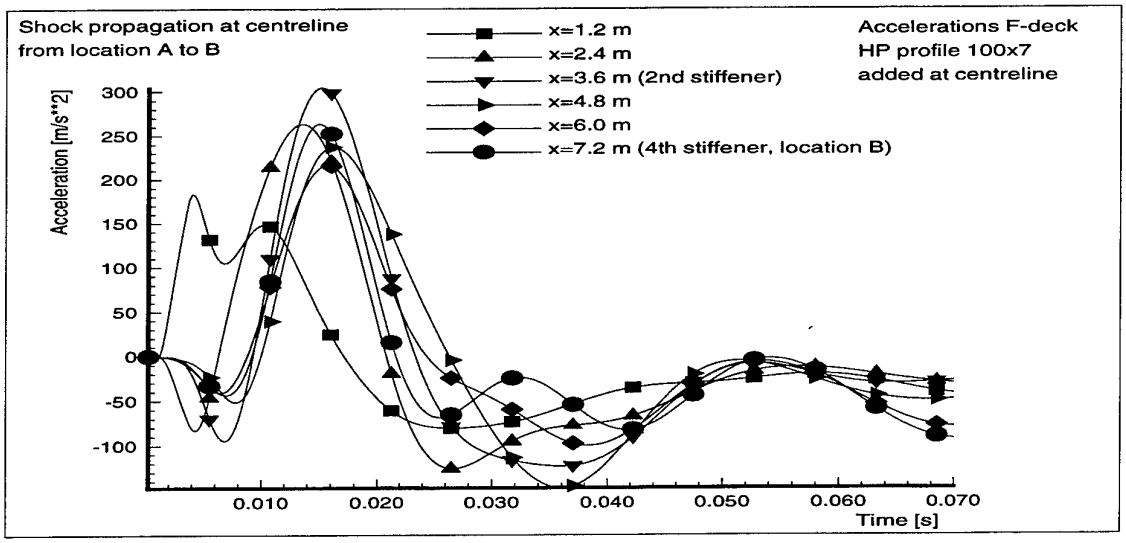

Fig. 6.18 Shock wave propagation in length direction of compartment at centreline of F-deck, so at small deck part, modified model including Rayleigh damping, including HP 100x7 at centreline

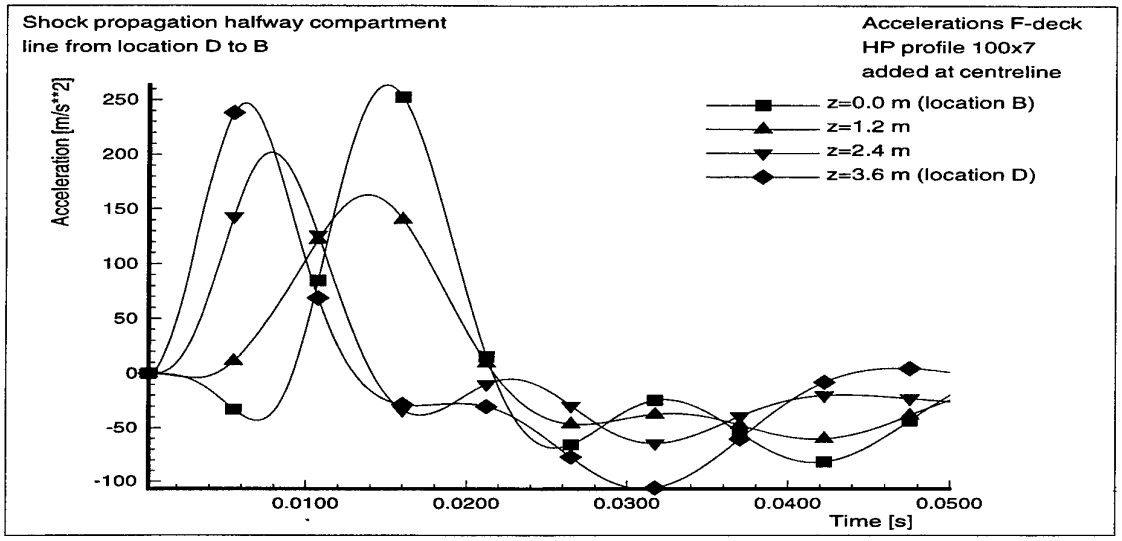

Fig. 6.19 Shock wave propagation in transverse direction of compartment, midway the compartment between locations D and B of F-deck, so at small deck part, modified model including Rayleigh damping, including HP100x7 at centreline

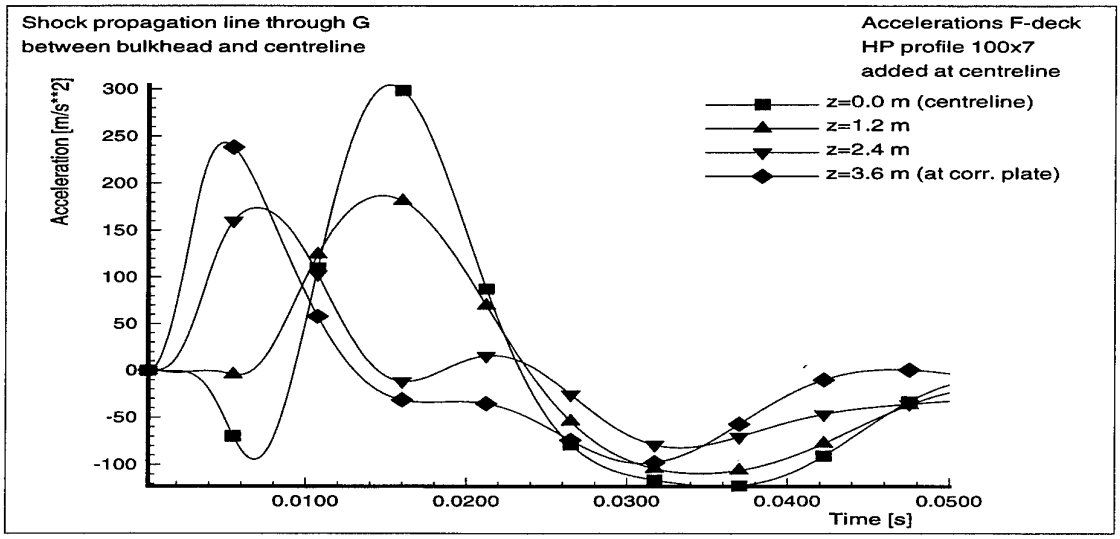

Fig. 6.20 Shock wave propagation in transverse direction of compartment, at a quarter of the compartment length and between bulkhead and centreline of F-deck, so at small deck part, modified model including Rayleigh damping, including HP100x7 at centreline

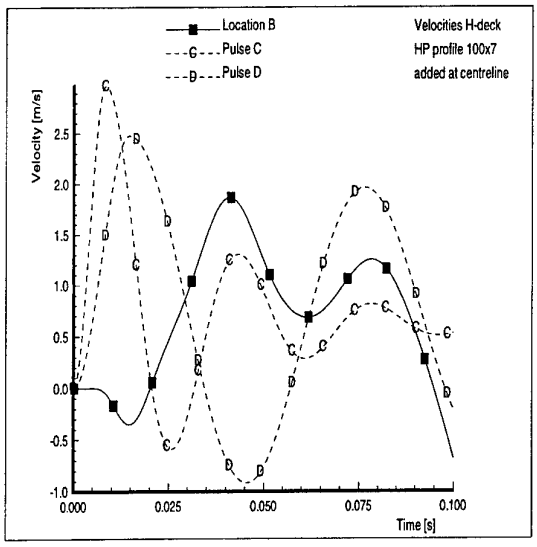

a) Velocities location B (centre of compartment)

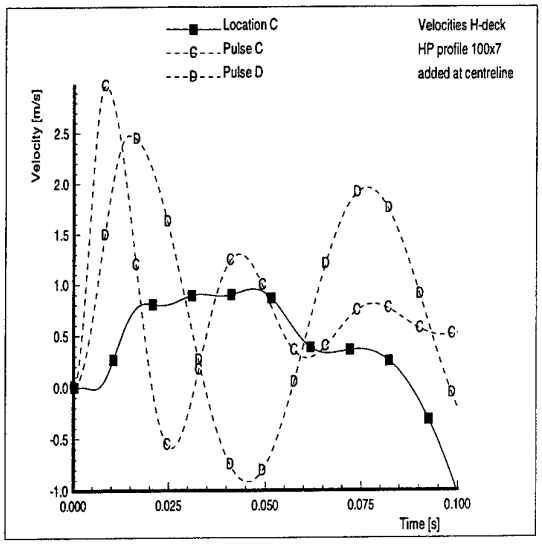

b) Velocities location C (between centreline and corrugated plate)

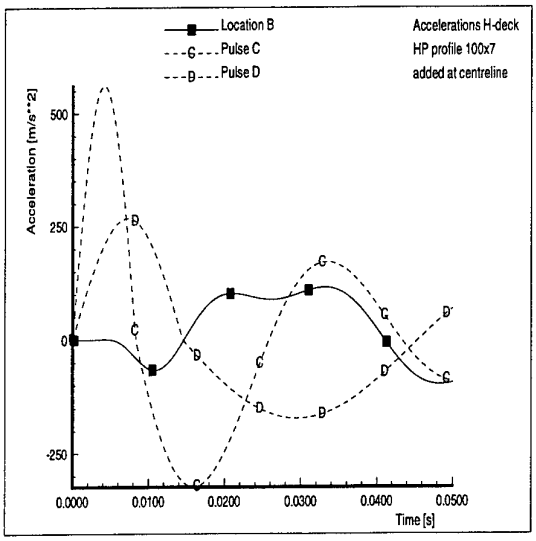

c) Accelerations location B (centre of compartment)

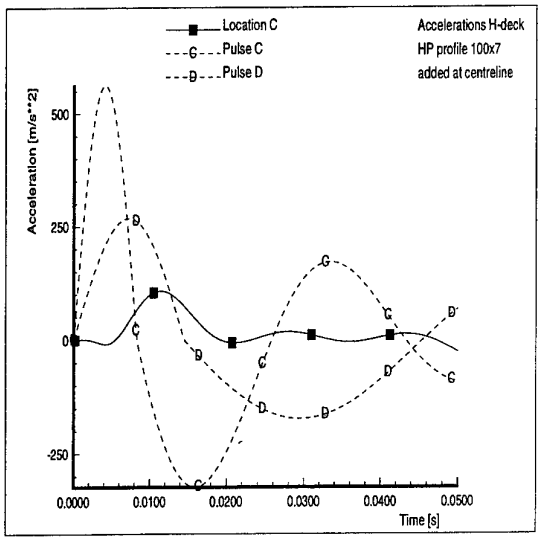

d) Accelerations location C (between centreline and corrugated plate)

Fig. 6.21 Velocities and accelerations as function of time for location B and C at the H-deck, modified model including Rayleigh damping and including an additional HP100x7 profile at the centreline of the decks, compare fig. 3.9

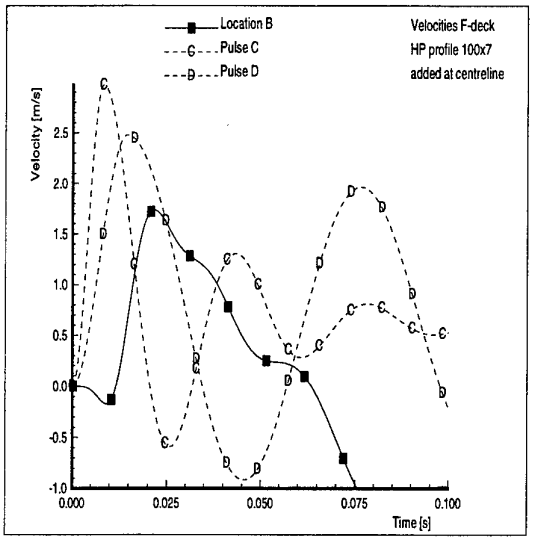

a) Velocities location B (centre of compartment)

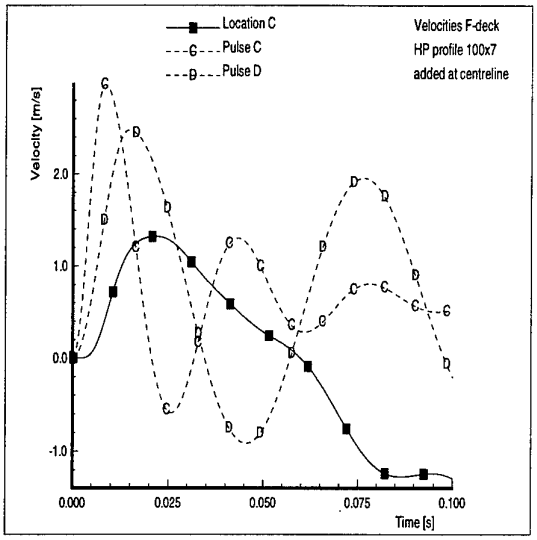

b) Velocities location C (between centreline and corrugated plate)

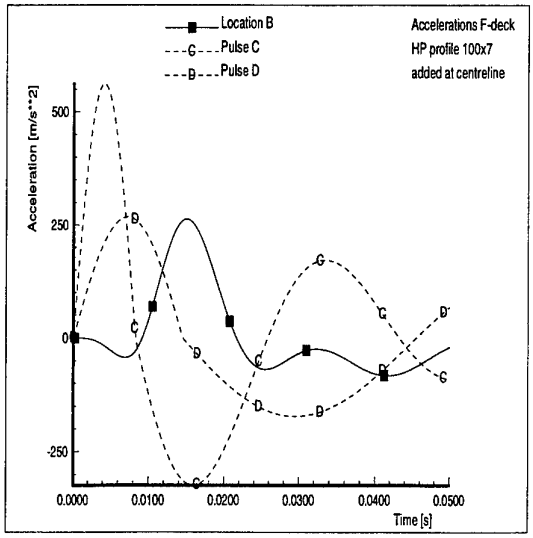

c) Accelerations location B (centre of compartment)

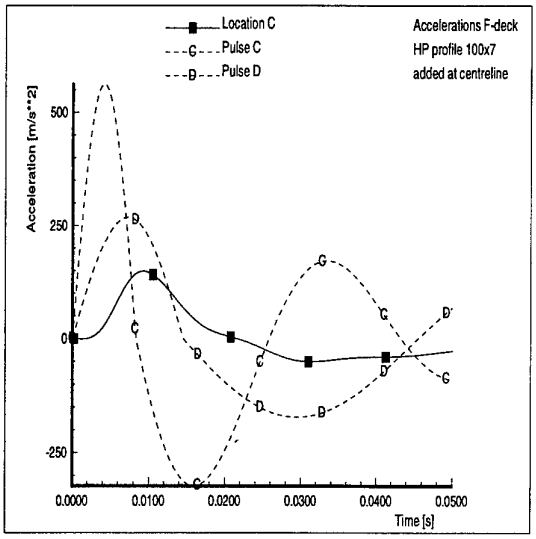

d) Accelerations location C (between centreline and corrugated plate)

Fig. 6.22 Velocities and accelerations as function of time for location B and C at the F-deck, modified model including Rayleigh damping and including an additional HP100x7 profile at the centreline of the decks, compare fig. 3.11

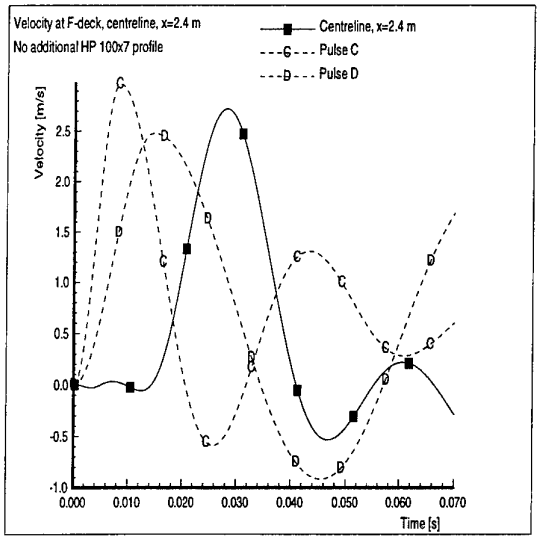

a) Velocity without HP profile

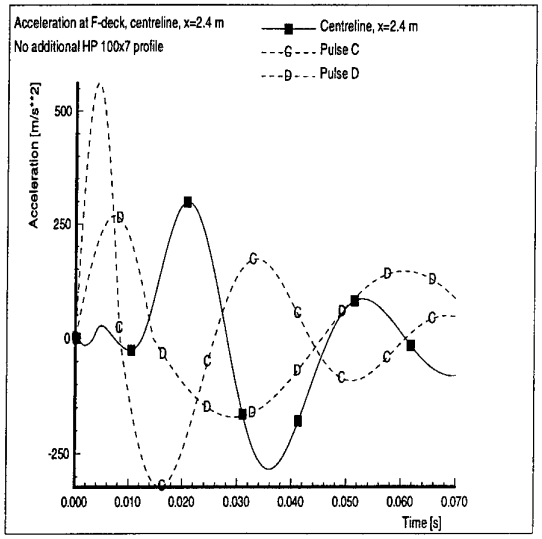

b) Acceleration without HP profile

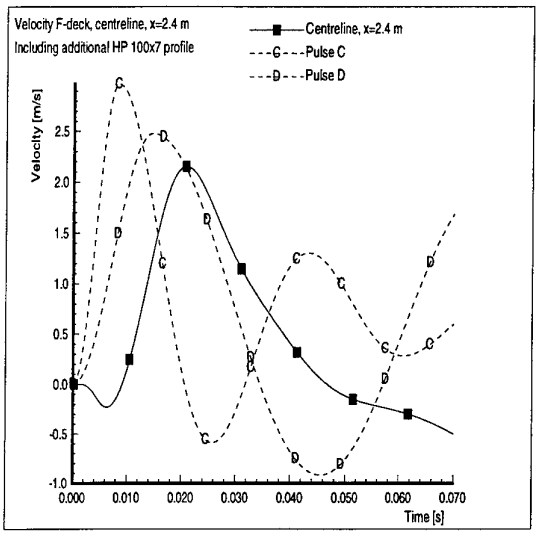

c) Velocity including HP profile

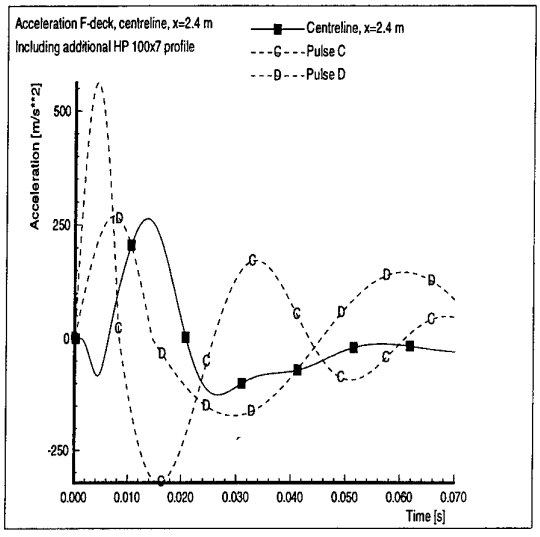

d) Acceleration including HP profile

Fig. 6.23 Effect of additional HP 100x7 profile on correspondence with standard pulse shapes; location at F-deck, at centreline, at x=2.4 m

REPORT DOCUMENTATION PAGE

1. DEFENCE REPORT NUMBER (MOD-NL)	2. RECIPIENT'S ACCESSION NUMBER	3. PERFORMING ORGANIZATION REPORT NUMBER
TD 97 - 0267		97-CMC-R0290
4. PROJECT/TASK/WORK UNIT NO.	5. CONTRACT NUMBER	6. REPORT DATE
62375617	A95/KM/117	3 July 1997
7. NUMBER OF PAGES	8. NUMBER OF REFERENCES	9. TYPE OF REPORT AND DATES COVERED
92	5	Interim report

10. TITLE AND SUBTITLE

Shock transmission, response calculation of a compartment of a frigate with discrete masses and rayleigh damping

11. AUTHOR(S)

W. Trouwborst

12. PERFORMING ORGANIZATION NAME(S) AND ADDRESS(ES)

Centre for Mechanical Engineering
Leeghwaterstraat 5
2628 CA DELFT, The Netherlands

13. SPONSORING/MONITORING AGENCY NAME(S) AND ADDRESSES(S)
Sponsor: Netherlands Ministry of Defence
Monitoring agency: TNO Defence Research, Schoemakerstraat 97, 2628 VK DELFT, The Netherlands

14. SUPPLEMENTARY NOTES

The Centre for Mechanical Engineering is part of TNO Building and Construction Research
The classification designation 'ONGERUBRICEERD' is equivalent to 'UNCLASSIFIED'.

15. ABSTRACT (MAXIMUM 200 WORDS, 1044 BYTES)

This report gives results as obtained with a finite element analysis using the finite element program DIANA of a compartment of a frigate loaded with a shock pulse based on the kick-off velocity concept. Three decks are included in the FEM model. The effects of discrete masses, either fixed at the deck or mounted at discrete springs (with and without damping), Rayleigh damping and excitation of the hull have been analysed. Responses at the decks are compared with the standard pulse shapes as defined in the Shock Handbook, which are generally used to define the shock loading of the equipment. Both the kick-off pulse and the standard pulses are based on the same underwater explosion.

16. DESCRIPTORS
Finite element methods
Frigates

IDENTIFIERS
Underwater shock
Shock wave propagation
Shock analysis

17a. SECURITY CLASSIFICATION (OF REPORT)	17b. SECURITY CLASSIFICATION (OF PAGE)	17c. SECURITY CLASSIFICATION (OF ABSTRACT)
ONGERUBRICEERD	ONGERUBRICEERD	ONGERUBRICEERD

18. DISTRIBUTION/AVAILABILITY STATEMENT	17d. SECURITY CLASSIFICATION (OF TITLES)
Unlimited availability, requests shall be referred to sponsor	ONGERUBRICEERD

Distributielijst bij rapport 97-CMC-R0290
Instituut: TNO Bouw, CMC
Project A95/KM/117

DWOO	1
HWO-Centrale Organisatie	(B)
HWO-KM	1
HWO-KL	(B)
HWO-KLu	(B)
Projectbegeleider DMKM, ir. T.N. Bosman	4
Documentatie afdeling Maritieme Techniek	1
TNO-DO	1
Bibliotheek KMA	3
Centrum voor Mechanische Constructies	3

(B) = Beperkt rapport